LOCKHEED MARTIN ENERGY RESEARCH LIBRARIES
3 4456 0446135 7

NUREG/CR-5504
(ORNL/TM-13631)

Technical Basis for an ASTM Standard on Determining the Reference Temperature, T_o, for Ferritic Steels in the Transition Range

Prepared by
J.G. Merkle, K. Wallin, D.E. McCabe

Oak Ridge National Laboratory

Prepared for
U.S. Nuclear Regulatory Commission

OAK RIDGE NATIONAL LABORATORY
CENTRAL RESEARCH LIBRARY
CIRCULATION SECTION
4500N ROOM 175
LIBRARY LOAN COPY
DO NOT TRANSFER TO ANOTHER PERSON.
if you wish someone else to see this report, send in name with report and the library will arrange a loan.
ORNL-118 (6-97)

AVAILABILITY NOTICE

Availability of Reference Materials Cited in NRC Publications

NRC publications in the NUREG series, NRC regulations, and *Title 10, Energy,* of the *Code of Federal Regulations,* may be purchased from one of the following sources:

1. The Superintendent of Documents
   U.S. Government Printing Office
   P.O. Box 37082
   Washington, DC 20402–9328
   <http://www.access.gpo.gov/su_docs>
   202–512–1800

2. The National Technical Information Service
   Springfield, VA 22161–0002
   <http://www.ntis.gov/ordernow>
   703–487–4650

The NUREG series comprises (1) technical and administrative reports, including those prepared for international agreements, (2) brochures, (3) proceedings of conferences and workshops, (4) adjudications and other issuances of the Commission and Atomic Safety and Licensing Boards, and (5) books.

A single copy of each NRC draft report is available free, to the extent of supply, upon written request as follows:

Address: Office of the Chief Information Officer
Reproduction and Distribution
Services Section
U.S. Nuclear Regulatory Commission
Washington, DC 20555–0001
E–mail: <GRW1@NRC.GOV>
Facsimile: 301–415–2289

A portion of NRC regulatory and technical information is available at NRC's World Wide Web site:

<http://www.nrc.gov>

All NRC documents released to the public are available for inspection or copying for a fee, in paper, microfiche, or, in some cases, diskette, from the Public Document Room (PDR):

NRC Public Document Room
2121 L Street, N.W., Lower Level
Washington, DC 20555–0001
<http://www.nrc.gov/NRC/PDR/pdr1.htm>
1–800–397–4209 or locally 202–634–3273

Microfiche of most NRC documents made publicly available since January 1981 may be found in the Local Public Document Rooms (LPDRs) located in the vicinity of nuclear power plants. The locations of the LPDRs may be obtained from the PDR (see previous paragraph) or through:

<http://www.nrc.gov/NRC/NUREGS/SR1350/V9/lpdr/html>

Publicly released documents include, to name a few, NUREG-series reports; *Federal Register* notices; applicant, licensee, and vendor documents and correspondence; NRC correspondence and internal memoranda; bulletins and information notices; inspection and investigation reports; licensee event reports; and Commission papers and their attachments.

Documents available from public and special technical libraries include all open literature items, such as books, journal articles, and transactions, *Federal Register* notices, Federal and State legislation, and congressional reports. Such documents as theses, dissertations, foreign reports and translations, and non-NRC conference proceedings may be purchased from their sponsoring organization.

Copies of industry codes and standards used in a substantive manner in the NRC regulatory process are maintained at the NRC Library, Two White Flint North, 11545 Rockville Pike, Rockville, MD 20852–2738. These standards are available in the library for reference use by the public. Codes and standards are usually copyrighted and may be purchased from the originating organization or, if they are American National Standards, from—

American National Standards Institute
11 West 42nd Street
New York, NY 10036–8002
<http://www.ansi.org>
212–642–4900

DISCLAIMER

This report was prepared as an account of work sponsored by an agency of the United States Government. Neither the United States Government nor any agency thereof, nor any of their employees, makes any warranty, expressed or implied, or assumes any legal liability or responsibility for any third party's use, or the results of such use, of any information, apparatus, product, or process disclosed in this report, or represents that its use by such third party would not infringe privately owned rights.

NUREG/CR-5504
ORNL/TM-13631

Technical Basis for an ASTM Standard on Determining the Reference Temperature, T_0, for Ferritic Steels in the Transition Range

Manuscript Completed: October 1998
Date Published: November 1998

Prepared by
J.G. Merkle, K. Wallin, D.E. McCabe

Oak Ridge National Laboratory
Managed by Lockheed Martin Energy Research Corporation
Oak Ridge, TN 37831-6151

S.N. Malik, NRC Project Manager

Prepared for
Division of Engineering Technology
Office of Nuclear Regulatory Research
U.S. Nuclear Regulatory Commission
Washington, DC 20555-0001
NRC Job Code B0119

LOCKHEED MARTIN ENERGY RESEARCH LIBRARIES
3 4456 0446135 7

ABSTRACT

This report documents the technical bases for the new ASTM standard, E1921-97, "Test Method for the Determination of Reference Temperature, T_o, for Ferritic Steels in the Transition Range." Reference temperature, T_o, is the temperature at which the median static initiation fracture toughness for 1T specimens equals 100 MPa $\sqrt{m}$. Derivations are presented for the three-parameter Weibull statistical model of data scatter used in the standard. The basis for the observed existence of a common Master Curve of median fracture toughness for 1T specimens versus normalized temperature is presented. Methods for dealing with uncertainty in T_o due to test temperatures less than T_o, and sample size, are explained. Test specifications and recommendations regarding stable crack growth, constraint, popins, and side-grooving are discussed. Experimental data supporting the procedures of E1921-97 are given for 26 different materials. Potential issues requiring further study for application of the standard are discussed. These issues include strain rate and high fluence effects, relation between Charpy temperature and T_o shifts due to embrittlement, low upper-shelf materials, local toughness variations of metallurgical origin, limits of the weakest-link hypothesis, use of the precracked Charpy specimen, and the use of surrogate materials in the absence of material-specific specimens.

CONTENTS

ABSTRACT iii

FIGURES vii

TABLES xi

EXECUTIVE SUMMARY xiii

ACKNOWLEDGMENTS xix

1. MASTER CURVE: THEORETICAL BASIS FOR SCATTER AND "SIZE EFFECT," AND BACKGROUND OF TEMPERATURE DEPENDENCE 1-1
   1.1 Theoretical Basis for Master Curve Scatter and "Size Effect" 1-1
      1.1.1 Unconditional Probability of Cleavage Initiation 1-5
      1.1.2 Conditional Cleavage Propagation 1-10
      1.1.3 Lower Shelf Toughness 1-16
      1.1.4 Conclusions 1-19
   1.2 Background of the Master Curve Temperature Dependence 1-21
      1.2.1 Background 1-21
      1.2.2 The Master Curve 1-24
   1.3 References 1-26

2. EXPERIMENTAL CONFIRMATION OF THE MASTER CURVE APPROACH 2-1
   2.1 Master Curve for Engineering Applications 2-1
   2.2 Appendices Attached to the Method 2-4
   2.3 Problems Associated with Low Upper-Shelf Materials 2-6
   2.4 References 2-8

3. TEST METHOD 3-1
   3.1 Specimen Designs 3-1
   3.2 Specimen Preparation 3-1
   3.3 Alternate Measurement Locations 3-2
   3.4 Test Temperature Estimation 3-2
   3.5 Replicate Specimen Requirements 3-3
   3.6 K_{Jc} Calculation 3-4
   3.7 Side Groove Effects 3-5
   3.8 References 3-8

4. VALIDITY REQUIREMENTS 4-1
   4.1 Selection of a Numerical Value, M, for Controlling Constraint 4-1
   4.2 Rationale for Setting Crack Growth Limits 4-6
   4.3 Impact of Low Upper-Shelf Materials on Establishment of Master Curve 4-7
   4.4 Pop-ins 4-9
   4.5 References 4-11

5. MASTER CURVE PARAMETER ESTIMATION 5-1
5.1 Applied Statistical Methods 5-1
5.2 Standard Deviation 5-1
5.3 Small Sample Statistics 5-2
5.4 Least Squares Estimation 5-3
5.5 Method of Maximum Likelihood (MML) 5-6
5.6 References 5-13

6. PRECISION AND BIAS 6-1
6.1 Weibull Parameters 6-1
6.2 References 6-5

7. CONSIDERATIONS FOR APPLICATIONS OF THE MASTER CURVE APPROACH 7-1
7.1 References 7-9

APPENDIX A A-1

APPENDIX B B-1

APPENDIX C C-1

APPENDIX D D-1

FIGURES

1.1 An example of a cleavage fracture initiation process 1-2

1.2 Typical cleavage fracture surfaces for specimens with cracks 1-3

1.3 Basis of the general statistical model 1-3

1.4 Probability tree for a single potential cleavage initiator in a reference volume element 1-4

1.5 Several independent volume elements 1-7

1.6 Stress distribution in front of a crack showing definitions of $\Delta\theta$, θ, x and Δx 1-8

1.7 Steepness of stress distribution in front of crack 1-12

1.8 Comparison of the different possible conditional propagation probability functions [Eqs. (1.18) and (1.20)] using A = 0.5 as the limiting propagation probability 1-14

1.9 Comparison of different possible cumulative failure probability expressions, Eqs. (1.21a) through (1.21d) 1-16

1.10 Comparison of different possible cumulative failure probability expressions for lower shelf behavior, Eqs. (1.23a) to (1.23d) 1-19

1.11 Relation between fracture toughness and yield strength for unirradiated and irradiated material 1-22

1.12 Relation between fracture toughness and temperature for unirradiated and irradiated material 1-22

1.13 Temperature dependence of yield strength for ferritic steels 1-23

1.14 Relation between fracture toughness and thermal part of yield strength for unirradiated and irradiated material 1-24

1.15 Fracture toughness "Master Curve" for ferritic steels and welds 1-25

2.1 Correlation between T_o temperature and drop-weight NDT 2-3

2.2 Master curve positioned by T_o determined from precracked Charpy specimens 2-5

2.3 Fracture toughness trends for size effect as predicted by weakest-link theory 2-6

2.4 Illustration of the difficulties of proving the master curve with low upper-shelf steels 2-7

2.5 Prediction of ductile instability K_{Jc} for a 1T C(T) specimen of a low upper-shelf steel. 2-7

3.1 Data from side-groove study of Moreland 3-7

3.2 R-curves of a low upper-shelf weld metal, comparing straight-side and side-grooved specimens 3-7

4.1 Weibull plot of K_{Jc} data obtained from precracked Charpy specimens of irradiated WF-70 weld metal 4-4

4.2 Weibull plot of K_{Jc} data obtained from precracked Charpy specimens of as-received WF-70 weld metal 4-5

4.3 Weibull plot of K_{Jc} data on A 36 steel 4-5

4.4 Range of valid data for two test specimen sizes, 1/2T and 4T 4-7

4.5 Theoretical limitations on K_{Jc} data based on K_J ductile instability behavior of low upper-shelf steels 4-8

4.6 Effect of side grooving practice on the ductile tearing resistance of a low upper-shelf weld metal 4-8

4.7 K_{Jc} at pop-in versus K_{Jc} at full cleavage for irradiated compact specimens from the ORNL HSSI Fifth Irradiation Series 4-10

4.8 Schematic of pop-in magnitude. Construction lines $\overline{AO}$ and $\overline{BO}$ are used to calculate crack advance 4-11

5.1 Reliability of small sample data sets of size n, when expressed in cumulative probability coordinates 5-2

5.2 Comparison of different estimates of median rank probability (lines) with binomial theory estimate (circles) 5-5

5.3 Comparison of mean and median bias corrections for maximum likelihood estimate of K_o 5-9

5.4 Confidence bounds of 5 and 95% for maximum likelihood estimate of K_o expressed in terms of corrections to the calculated value of T_o 5-11

5.5 Confidence bounds of 5 and 95% for maximum likelihood estimate of K_o expressed in terms of corrections to the calculated value of T_o, for r = 6 5-11

5.6 Bias correction for maximum likelihood estimate of T_o 5-13

6.1 Comparison of the distribution of Weibull slopes calculated from small data sets 6-1

7.1 Comparison of fracture toughness data from shallow-cracked, biaxial specimen tests, a/W = 0.1, of Heat-Treated Plate 14 with master curve for the material, an associated estimated lower tolerance bound curve shifted for margin, and the ASME lower-bound K_{IC} curve 7-1

7.2 Comparison of fracture toughness data from specimens of various sizes for an A533B, Class 1, steel with the ASME lower-bound K_{IC} curve 7-2

7.3 Plot of RT_{NDT} versus T_o for various steels and weld metals, showing the uncertainty in the relationship between the two parameters 7-3

7.4 Experimentally determined values of T_o versus loading rate for A515 steel, and values estimated by Barsom's method 7-4

7.5 Experimentally based values of T_o versus loading rate for A533B steel, and fitted line representing values estimated by Wallin's method 7-6

7.6 Comparison of fracture toughness data, adjusted to 1T specimen size, for several irradiated base and weld metals, with the master curve and its estimated 3 and 97 percent tolerance bounds, showing that irradiation has no significant effect on the shape of the master curve or its tolerance bounds 7-6

7.7 Comparison of the master curve based on data from precracked Charpy specimens of HSST Plate 02, and the associated estimated 5 and 95 percent tolerance bounds, with the ASME K_{IC} database adjusted to 1T specimen size 7-8

A.1 ORNL HSST Plate 14A, A 533 grade B (heat treated) A-4

A.2 ORNL HSST Plate 02, A 533 grade B A-4

A.3 ORNL HSSI Fifth Irradiation Series, submerged-arc Welds 72W and 73W A-5

A.4 ORNL HSSI Fifth Irradiation Series, irradiated submerged-arc Welds 72W and 73W A-5

A.5 ORNL HSSI Tenth Irradiation Series, Weld WF-70 (No. 1) and irradiated WF-70 (No. 1) . . . A-6

A.6 ORNL HSSI Tenth Irradiation Series, Weld WF-70 (No. 2) and irradiated WF-70 (No. 2) . . . A-6

A.7 ORNL HSST Plate 13A, A 533 grade B A-7

A.8 GKSS Report 93/E/81, 20MnMoNi55 and irradiated 20MnMoNi55 . . . . . A-7

A.9 Iwadate (ASTM STP 803, Vol. II), A 508 class 3 . . . . . A-8

A.10 Sorem (WRC Bulletin 351), A 36 steel A-8

A.11 Morland [NRL-R-1006(R)], A 533 grade B class 1 . . . . . A-9

TABLES

1.1 Relation between different possible cumulative failure probability parameters 1-15

2.1 Examples of reference temperatures, T_o, and predictions of T_o from nonfracture mechanics test methods 2-2

3.1 Monte Carlo simulation (100 trials; population, 50 1T C(T) A 508 class 1, three specimens; –100°C test temperature) 3-4

3.2 Monte Carlo simulation (100 trials; population, 50 1T C(T) A 508 class 1, three specimens; –75°C test temperature) 3-4

3.3 Comparison of K_{Jc} (MPa√m) for 1T compact specimens with and without side grooves 3-6

4.1 Adjustments to Nevalainen-Dodds M_{ND} values for single-edge-notched bend specimens (a/W = 0.5) 4-2

4.2 Examples of material yield strength and median n values 4-3

6.1 Analysis of MPC/JSPS round-robin data by linear regression for best slope, maximum likelihood for K_o and T_o 6-3

6.2 Best slopes for data sets with 20 or more duplicate tests 6-4

B.1 Table of coefficients from Eqs. (B.7) and (B.8) B-5

B.2 Tabulation of modifications for test temperatures that approach lower shelf B-8

B.3 Precracked Charpy specimen requirements B-9

C.1 Ramburg Osgood work-hardening exponents, n C-3

C.2 η_p solutions for a/W = 0.5, W/B = 2 Ramburg Osgood work-hardening exponents, n C-4

C.3 η_p solutions for n = 10, variable a/W C-4

EXECUTIVE SUMMARY

This project has been undertaken to provide both the theoretical basis and supporting data development that has made possible the development of the American Society for Testing and Materials (ASTM) E 1921-97, Test Method for the Determination of Reference Temperature, T_o, for Ferritic Steels in the Transition Range. There are seven chapters that have been subdivided between the three authors. Hence, the reader will occasionally find information duplicated among chapters. In spite of this, the general continuity of the document has been maintained.

Chapter 1, Section 1.1, develops the background theory using a weakest-link model to explain why ferritic steels have rather substantial data scatter when tested in the transition range. Statistical evaluations have indicated that the three-parameter Weibull model can be theoretically justified as the most correct one for fitting data scatter patterns that have been experimentally observed. The theory also supports the experimentally demonstrated observation that two of the three Weibull parameters can in fact be justified for use as deterministic parameters of the statistical model.

Chapter 1, Section 1.2, describes the development of the master curve concept as originally proposed, namely, keyed to the scale parameter of the three-parameter Weibull model, K_o. The rationale is presented that explains why the master curve shape tends to be relatively independent of material strength, and, as such, behaves as a universal curve for a wide range of steels and covers material-hardening mechanisms. As a result, the universal curve concept originally demonstrated experimentally is also defended in theory.

Chapter 2 documents T_o reference temperatures determined for 26 steels of varying types and conditions of embrittlement. A number of these data sets were also documented with Charpy curves and/or drop-weight nil-ductility transition (NDT) temperatures, thus providing an opportunity to check some proposed correlations used in the method. One of these uses the Charpy transition curve to predict an optimum test temperature for 1T size specimens, ostensibly near to temperature T_o. This comparison worked sufficiently well. NDT temperature to T_o temperature comparisons were made to check a postulate that NDT and T_o are close to being the same. The reality was that, of 15 comparisons, only six showed equal temperatures. Hence, the anticipated one-to-one correlation was not demonstrated. Along with this vanishes the possibility that T_o reference temperatures can simply replace reference temperature NDT (RT_{NDT}) for placement of the American Society of Mechanical Engineers (ASME) lower-bound K_{Ic} curve. Because two of the three Weibull parameters are known a priori, standard deviation on data scatter can be directly calculated using gamma functions, the use of which is described in Appendix B. Tolerance bounds can be estimated without having to evaluate data scatter on a

case-by-case basis. Tolerance bounds attach statistical significance to lower bounds placed on data scatter. However, in the use of T_o to set tolerance bounds, there is residual uncertainty that is carried along due to the fact that only six replicate tests are required to establish the T_o temperature. Margin adjustment can be added to lower-bound curves to cover this error potential. The description of tolerance bound curves and margin calculations is also covered in Appendix B.

There can be problems in attempting to verify the existence of the universal master curve when using low upper-shelf materials. Material taken from a plate of normalized A 302 grade B steel provided an obvious example. The material had only 79-J upper-shelf energy and the NDT temperature was 75°C. The upper-shelf fracture toughness corresponding to ductile instability was 125 MPa√m, meaning that the temperature spread between T_o at 100 MPa√m and onset of upper-shelf behavior was too small to demonstrate conformance to the master curve shape. Data distributions at temperatures just above T_o were being truncated by ductile K_{Jc} instabilities, and median K_{Jc} values determined from such data were considered to be in error.

Chapter 3 explains the rationale used to arrive at certain test practice requirements. Specimen geometries recommended are only the types that have dominant bend stresses. Constraint is more easily controlled in this type of specimen. The precracking practice applied is more rigorously controlled than it is in other ASTM standard methods because warm prestress effects from precracking can easily bias transition-range data. Users of the method are urged to select a test temperature where $K_{Jc(med)} \cong 100$ MPa√m. This represents an optimum test temperature choice for accuracy of T_o determination and a fracture toughness level where data loss due to invalidity problems are very unlikely to develop. If the investigator has no prior knowledge of what this optimum test temperature might be, a method is offered that uses the Charpy transition curve for assistance.

Monte Carlo simulations were used to decide on the minimum number of replicate tests to be required. It was decided that six specimens would be the best compromise for acceptable accuracy while at the same time using the least number of specimens. It is accepted, however, that there will be residual error in T_o as a result. For critical applications, margin adjustment can be added to T_o using the expected standard deviation on T_o variability.

J-integral is calculated at the point of onset of cleavage fracture. Measurement of slow-stable crack growth, Δa_p, during a test is not required and, if crack growth has occurred, J is ***not*** corrected for such growth. However, the post-test fracture surface is to be examined, and, if stable growth is found to be less than 0.05 b_o, the correction to J is negligible.

Side grooving is an optional decision allowed by the method. If the recommended test temperature is used, side grooving will not alter K_{Jc} values. However, if the test temperature choice approaches the upper shelf, side grooving could become an issue. R-curve effects will develop, and side grooving affects an R-curve controlled path of fracture toughness development.

Chapter 4 deals with the decision process that was applied to define specimen toughness measurement capabilities. Control of constraint is critical to accurate Weibull modeling of statistical distributions. The M value used in the following equation is the controlling parameter used to set specimen toughness capacity limits:

$$K_{Jc(limit)} = \left(E b_o \sigma_{ys} / M\right)^{1/2} .$$

Three-dimensional finite-element (FE) analysis is used to find a minimum specimen size, controlled by the value of M, for which the finite body value of J required to attain a specified fracture criterion exceeds the small-scale yield value of J by no more than a certain percentage estimated stochastically. This approach has resulted in a suggested limit value of M = 50. Alternative considerations supported by experimental data suggested a less restrictive value of M = 30. The latter M value was selected to be used in the method for lack of experimental verification in support of the FE-derived M value.

Crack pop-ins are most commonly encountered in transition range tests, and a policy position on their significance relevant to K_{Jc} data distributions had to be decided. In addition, small jumps in load-displacement records have the potential of being caused by events other than a genuine burst of crack extension. The resolution made was that pop-in events have most likely happened when the effective crack size increase, calculated from the test record evidence, is greater than 0.01 b_o. Larger test record discontinuities are regarded to be likely pop-ins, and fractographic proof is recommended. The crack initiation mechanism of a pop-in is identical to that of full-fracture events, and the initiation K_{Jc} is to be considered a part of the data distribution.

Chapter 5 presents applied statistical theory to show the influence of sample size on the accuracy of data population recognition and to demonstrate the rationale that was applied for selecting the maximum-likelihood data analysis method over the more commonly used rank method.

Confidence limits on rank order probabilities can be calculated using the binomial distribution function. This was applied to demonstrate why it is necessary to test at least 30 or more specimens to have even a reasonable estimate of the true Weibull slope of a data population.

Scale parameter, K_o, of the three-parameter Weibull model can be determined either by rank ordering of the data followed by least-squares fitting of the Weibull formatted data or by the maximum likelihood estimation method. The least-squares method suffers weakness from the use of rank probability estimates, P_{rank}, and the fact that the methodology was originally intended to be used on symmetric distributions. In addition, data censoring can only be applied to the upper end of the data sampling.

The maximum-likelihood method to determine K_o has the advantage of not using rank probability estimates. Data censoring makes use of the survival distribution function, thereby allowing random data censoring. Hence, all test results, regardless of censoring rationale, provide usable statistical information.

Clearly, from noting the shape of the master curve and assuming fixed proportional error in K_o at all test temperatures will not ensure fixed uncertainty in T_o determination. Uncertainty depends upon the position along the master curve. Plots are presented with 5 and 95% confidence limits on ΔT_o that demonstrate the potential for error. Test temperatures more than 50°C below the T_o temperature show severely degenerated accuracy of T_o determination. It is recommended that the best range to test is $T_o \pm 50$°C for least error in T_o.

An expression is introduced showing how data from multiple test temperatures can be analyzed by maximum likelihood. Data censoring is incorporated. Since the unknown value of T_o cannot be isolated, the solution is made through an iterative process.

Chapter 6 presents experimental data in support of the precision and bias statements in the method. With six duplicate tests, the median K_{Jc} value should be within 20% of the true median of the data population. T_o determinations are expected to be within 20°C of the true T_o value of the population. Note again, that with experimental data, small data samples cannot be expected to accurately represent the Weibull slope of the data population.

Data from a Materials Properties Council/Japanese Society for the Promotion of Science round-robin activity were used to support the statistical assertions. Eighteen laboratories participated in this round robin, using A 508 class 3 1T C(T) specimens, with sampling consisting of five specimens each. Although these tests were not controlled by ASTM E 1921-97, the results were usable in support of the method.

In another study, 11 data sets were found for which 20 or more replicate tests were made. These data were evaluated for Weibull slopes; the lowest slope was 3 and the highest was 5.8. All were within a predicted 95% confidence band for 20 replicate tests.

Chapter 7 is a synopsis of the potential uses for the master curve concept; pointing out the verification work needed to make these uses acceptable.

Two example cases are presented for which the ASME universal K_{Ic} lower-bound curve completely misrepresents the fracture mechanics transition range data. This is not so much a problem with the universal curve concept as it is a demonstration of the inadequacy of RT_{NDT} as a reference temperature. The master curve methodology, applied to individual materials, can substantially reduce such errors. However, both methods share the postulate that transition range fracture toughness follows a universal curve shape. The postulates associated with the master curve cover a much broader range of variables, some of which remain to be adequately proved. The following questions are raised:

1. Will tests at high strain rates alter the shape of the master curve?
2. Will irradiation to fluence levels above 1×10^{20} n/cm^2 alter the shape of the master curve?
3. What is the relationship between the Charpy V-notch 41-J ΔTT_{41J} shift from irradiation damage and the ΔT_o shift?
4. Is it safe to evaluate low upper-shelf materials by the master curve method?
5. Can master curve methods be applied to the evaluation of materials that have through-thickness fracture toughness gradients?
6. What are the limits on the weakest-link size effect relationship?
7. Is the precracked Charpy specimen of viable fracture mechanics size for T_o determinations?

The issue of testing surrogate materials and then using these properties to represent the properties of an ostensibly equally prepared material remains to be resolved. Here the refinement of the master curve methodology can be utilized in concert with adequately defined qualifying criteria. For generic representation on all heats of specific grades of steel plate, the precision advantage of the master curve concept would be wasted when metallurgical circumstances are not under sufficient control.

ACKNOWLEDGMENTS

This project was sponsored by the Office of Nuclear Regulatory Research, U.S. Nuclear Regulatory Commission, under Interagency Agreement DOE 1886-N109-8L with the U.S. Department of Energy under contract DE-AC05-96OR22464 with Lockheed Martin Energy Research Corporation. The authors are very grateful to the ORNL staff that worked hard to assemble this report: Ms. J. Bishop of the Fracture Mechanics Group, Mr. D. Cottrell and Ms. Reneé Balogh of ORNL Graphics Services, Mr. W. Koncinski and Ms. S. C. Lyttle of ORNL Publishing Services. This report is designated HSST Program Technical Report 163.

TECHNICAL BASIS FOR AN ASTM STANDARD ON DETERMINING THE REFERENCE TEMPERATURE, T_0, FOR FERRITIC STEELS IN THE TRANSITION RANGE

1. MASTER CURVE: THEORETICAL BASIS FOR SCATTER AND "SIZE EFFECT," AND BACKGROUND OF TEMPERATURE DEPENDENCE

1.1 Theoretical Basis for Master Curve Scatter and "Size Effect"

The different possible mechanisms of slip-induced cleavage fracture initiation have been well documented in the literature. Early work by McMahon and Cohen[1] on low carbon steels containing grain boundary iron carbides illustrated the importance of carbide cracks as fracture nucleation sites in such materials, while a number of other investigators have similarly demonstrated that brittle carbides and/or inclusions, as well as grain sized micro-cracks, provide potent fracture nucleation sites in a variety of low carbon steels,[1–5] ultralow carbon steels,[6] euatectoid steels,[7–9] and refractory metal[10–12] body centered cubic systems. The experimental results in all of the studies listed reveal that fracture initiation, regardless of the site (i.e., carbide, inclusion, grain), appears to require some amount of plastic deformation/strain to locally nucleate the crack in such a region. While it is clear from various experimental investigations that some amount of local strain is necessary for crack nucleation, the local tensile fracture stress of the particle must be exceeded in order to start the process. In the case of cleavage fracture initiation from a carbide or inclusion, the magnitude of the critical local tensile stress required to provide the crack at the initiation site depends on the "strength" of the particle, which is a statistical quantity that depends on the size, shape, and characteristics of the particle, as well as any local residual stresses, as has been modeled by a variety of investigators.[5,13–16] An example of typical cleavage fracture initiation sources is presented schematically in Fig. 1.1. These are local stress that produces a dislocation pile-up, cracking of the carbides, and advancing microcracks that encounter the first large angle boundary.

The critical steps for cleavage fracture are:

I. initiation of a microcrack, for example, fracturing of a second phase particle or grain boundary,

II. propagation of this microcrack into the surrounding grains, and

III. further propagation of the propagating microcrack into other adjacent grains.

ORNL 98-5359

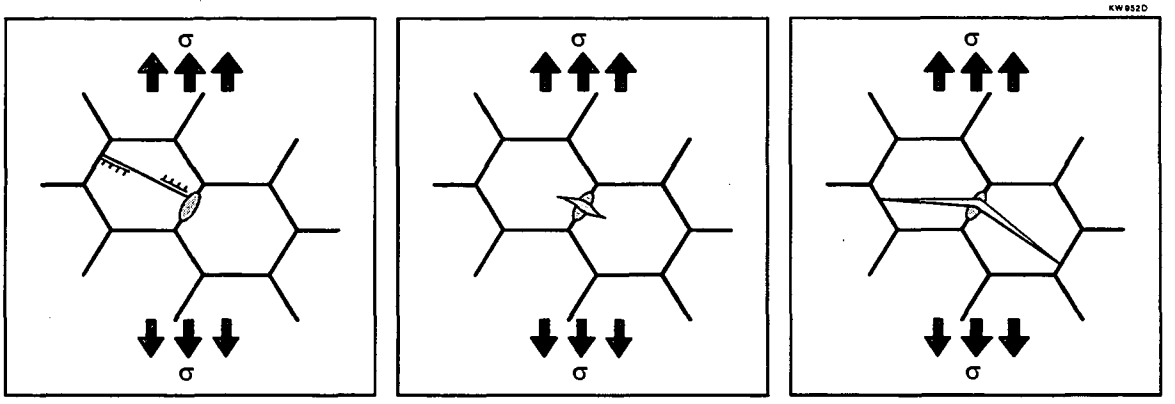

Fig. 1.1. An example of a cleavage fracture initiation process.

Depending on loading geometry, temperature, loading rate, and material, different steps are more likely to be most critical in the case of a crack. For structural steels at lower shelf temperatures, and ceramics, where the stress distribution near the crack tip is very steep, steps II and III (propagation) are more difficult than initiation and they tend to control the fracture toughness. At higher temperatures, where the steepness of the stress distribution is lower, propagation becomes easier in relation to initiation, and step I becomes more dominant in the fracture initiation process. The temperature region where step I dominates is the transition region. In a specimen with a fatigue crack, the number of initiation sites visible on the fracture surface (Fig. 1.2) varies with temperature. At lower shelf temperatures, numerous initiation sites are visible, whereas at higher temperatures, corresponding to the transition region, only one or two initiation sites are seen. In the case of notched or plain specimens, only a few initiation sites are seen even on the lower shelf. This is due to the fact that, for cracks, the peak stresses are very high virtually from the beginning of loading, whereas for notched and plain specimens, the peak stresses increase gradually during loading. Because no materials are fully uniform on a microscale, cleavage fracture initiation is a statistical event, and this fact has implications upon the macroscopic nature of brittle fracture. A statistical model is thus needed to describe the probability of cleavage fracture.

The basis of a general statistical model is presented in Fig. 1.3.[17] It is assumed that the material in front of the crack contains a distribution of possible cleavage fracture initiation sites (i.e., cleavage initiators). The probability for a single initiator being critical can be expressed as Pr{ I}, and it is a complex function of factors such as the initiator size distribution, stress, strain, grain size, temperature, and stress and strain rate. The shape

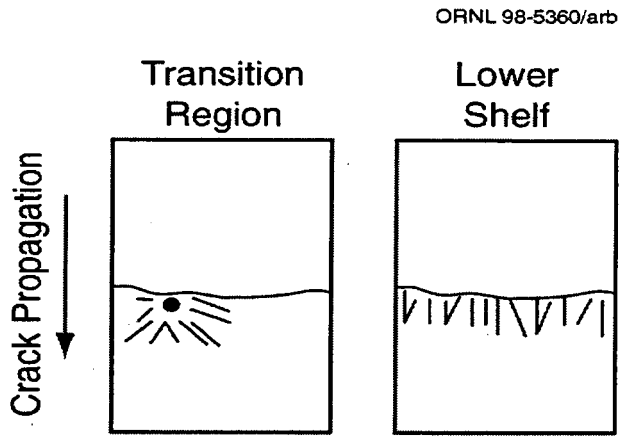

Fig. 1.2. Typical cleavage fracture surfaces for specimens with cracks. Lower shelf conditions produce numerous initiation sites, whereas in the transition region, only one or two initiation sites are visible.

and origin of the initiator distribution is not important in the case of a "sharp" crack. The only necessary assumption is that no global interaction occurs between initiators. This means that interactions on a local scale, in the region of the crack front, are permitted. Thus a cluster of cleavage initiators may be required for macroscopic initiation. As long as the cluster is local in nature, it can be interpreted as being a single initiator. All the above factors can be implemented into the initiator distribution and they are not significant as long as no attempt is made to determine the shape and specific nature of the distribution.

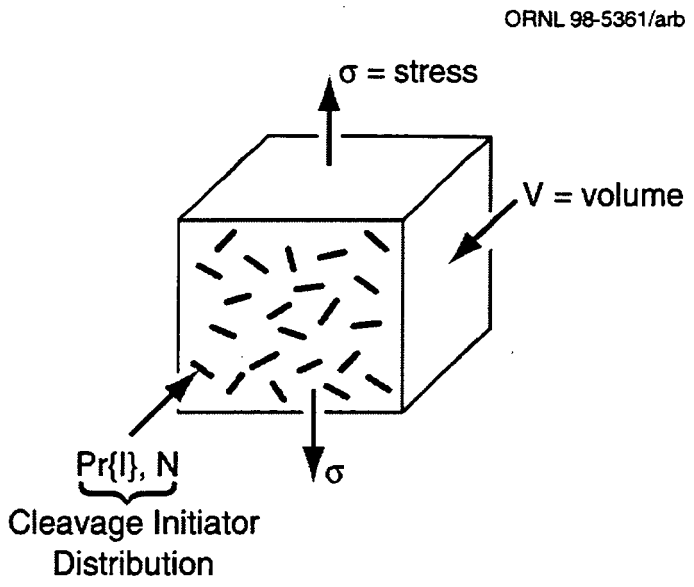

Fig. 1.3. Basis of the general statistical model.

If a particle (or grain boundary) fails, but the broken particle is not capable of initiating cleavage fracture in the matrix, the particle-sized microcrack will blunt under additional load and a void eventually forms. Such a void is not considered able to initiate cleavage fracture. Thus the cleavage fracture initiator distribution is affected by the void formation, leading to a conditional probability for cleavage initiation (Pr{I/O}), the condition being that the cleavage initiator must not become a void. The cleavage fracture process also contains another conditional event (i.e., that of propagation). An initiated cleavage crack must be able to propagate through the matrix in order to produce failure. Thus the conditional probability will be that of propagation after initiation (Pr{P/I}).

The cleavage fracture initiation process can be expressed in the form of the probability tree in Fig. 1.4.

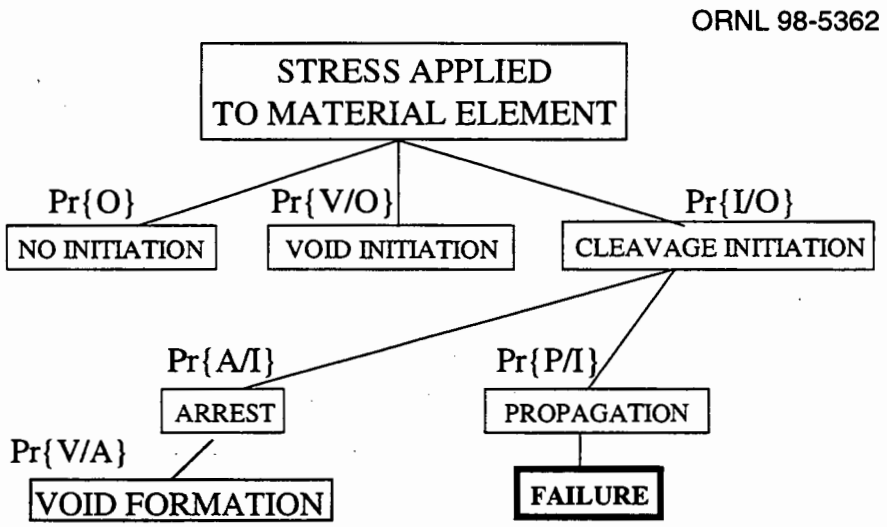

Fig. 1.4. Probability tree for a single potential cleavage initiator in a reference volume element.

The probabilities of the different events are defined as follows:

Pr{I} = probability of cleavage initiation

Pr{V} = probability of void initiation

Pr{O} = probability of "no event"

Pr{I/O} = conditional probability of cleavage initiation (no prior void initiation)

Pr{V/O} = conditional probability of void initiation (no prior cleavage initiation)

Pr{P/I} = conditional probability of propagation (in the event of cleavage initiation)

Pr{A/I} = conditional probability of arrest (in the event of cleavage initiation)

The following relations are clear from the probability tree:

$$Pr\{O\} + Pr\{V/O\} + Pr\{I/O\} = 1 \text{ (the sum of probabilities is unity)}$$

and

$Pr\{A/I\} + Pr\{P/I\} = Pr\{I/O\}$ (the sum of propagation and arrest equals the conditional initiation probability).

1.1.1 Unconditional Probability of Cleavage Initiation

To simplify the derivations, it is first advisable to assume that no microcracks arrest, and to evaluate the cumulative failure probability as that of cleavage initiation, leaving consideration of propagation to a later stage when initiation is controlled by a single local initiator being critical, weakest link statistics are applicable for the process.

Weakest link statistics indicate that at least one initiation is required for failure, and the cumulative probability of this initiation is equal to $P_f = 1 - S_r$, where S_r is the survival probability (i.e., the probability of no initiation). The cumulative failure probability for a volume element, with a uniform stress state, can thus be expressed as

$$P_f = 1 - [1 - Pr\{I/O\}]^N , \tag{1.1}$$

where N is the number of potential cleavage initiators in the volume element.

The relation between the unconditional cleavage initiation probability $Pr\{I\}$ and the conditional cleavage initiation probability $Pr\{I/O\}$can be determined directly from Fig. 1.4. Since one of three outcomes must occur,

$$Pr\{0\} + Pr\{V/0\} + Pr\{I/0\} = 1 . \tag{1.2a}$$

In Eq. (1.2a), the first term is an unconditional probability because no prior condition is specified, and the latter two terms are conditional probabilities because a previous condition is specified. It follows that

$$1 - Pr\{V/0\} = Pr\{0\} + Pr\{I/0\} . \tag{1.2b}$$

Then the fraction of all the defects that do not form voids but that undergo cleavage initiation, P{I}, is given by

$$\frac{Pr\{I/O\}}{Pr\{O\} + Pr\{I/O\}} = \frac{Pr\{I/O\}}{1 - Pr\{V/O\}} \equiv Pr\{I\} \ . \tag{1.2c}$$

Thus,

$$Pr\{I/O\} = Pr\{I\} \cdot (1 - Pr\{V/O\}) \ , \tag{1.2d}$$

which is the unconditional probability of cleavage initiation times the probability of <u>not</u> having void initiation. Eq. (1.2d) apparently makes a reliable estimation of the overall cleavage initiation probability more difficult. However, it will subsequently be shown that the problem is resolved for a sharp crack in small-scale yielding (SSY).

Normally, the number of initiators in an individual volume element is not known exactly. However, since the initiators are assumed to be randomly distributed in the material, the numbers of initiators in a large collection of volume elements can be shown to follow a Poisson distribution. Accordingly, the probability P_N of having N initiators in a volume element is

$$P_N = \frac{\overline{N}^N \cdot e^{-\overline{N}}}{N!} \ , \tag{1.3}$$

where $\overline{N}$ is the mean number of initiators in a volume element, related to the mean number of initiators per unit volume ($\overline{N}_V$) by $\overline{N} = \overline{N}_V \cdot V$.

The cumulative cleavage initiation probability for a single volume element, in terms of the mean number of initiators, by means of substituting Eq. (1.2d) into Eq. (1.1), becomes

$$P_f = 1 - \sum_{N=0}^{\infty} \left[1 - Pr\{I\} \cdot \left(1 - Pr\{V/O\}\right)\right]^N \cdot P_N \ . \tag{1.4a}$$

Then, by using Eq (1.3),

$$P_f = 1 - \sum_{N=0}^{\infty} \frac{\left\{\overline{N} \cdot \left[1 - Pr\{I\} \cdot \left(1 - Pr\{V/O\}\right)\right]\right\}^N \cdot e^{-\overline{N}}}{N!} . \tag{1.4b}$$

Eq. (1.4b) looks complicated, but it can be simplified by making use of the exponential equation. By definition, the exponential equation can be expressed as

$$e^x = \sum_{N=0}^{\infty} \frac{x^N}{N!} . \tag{1.5}$$

Inserting Eq. (1.5) into Eq. (1.4b) by setting x in Eq. (1.5) equal to the largest expression in brackets in Eq. (1.4b) yields the simple form

$$P_f = 1 - \exp\left\{-\overline{N} \cdot Pr\{I\} \cdot \left(1 - Pr\{V/O\}\right)\right\} \tag{1.6a}$$

or

$$P_f = 1 - \exp\left\{-\overline{N}_V \cdot V \cdot Pr\{I\} \cdot \left(1 - Pr\{V/O\}\right)\right\} . \tag{1.6b}$$

The previous derivation was for one volume element, but in the case of several (n) independent volume elements with varying sizes and stresses (Fig. 1.5), the cumulative cleavage initiation probability is obtained by summing

ORNL 98-5363

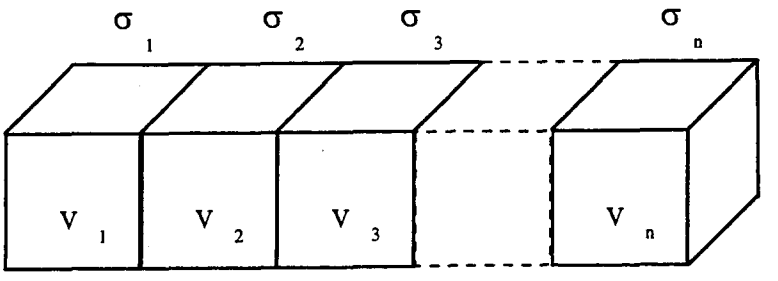

Fig. 1.5. Several independent volume elements.

the effects of the potential initiators in all the volume elements, giving

$$P_f = 1 - \exp \sum_{i=1}^{n} \left\{ -\overline{N}_V \cdot V_i \cdot Pr_i\{I\} \cdot \left(1 - Pr_i\{V/O\}\right) \right\} . \tag{1.7}$$

For a "sharp" crack in SSY, the stresses and strains are described by the HRR field.[18,19,20] One property of the HRR field is that the stress distribution retains proportionality (is self-similar) and another that the stresses have an angular dependence. The term "small-scale yielding (SSY)" is in this derivation used to describe the loading situation where the self-similarity of the stress field remains unaffected by loading. Thus the stress field can be divided into small fan-like elements, each with an angle increment $\Delta\theta$ (Fig. 1.6). In this case the cumulative cleavage initiation probability is written as

$$P_f = 1 - \exp \sum_{\theta=0}^{2\pi} \left[\sum_{x=0}^{x_p} \left\{ -\overline{N}_V \cdot B \cdot \Delta x \cdot x \cdot \sin(\Delta\theta) \cdot Pr_{x,\theta}\{I\} \cdot \left(1 - Pr_{x,\theta}\{V/O\}\right) \right\} \right] , \tag{1.8}$$

ORNL 98-5364/arb

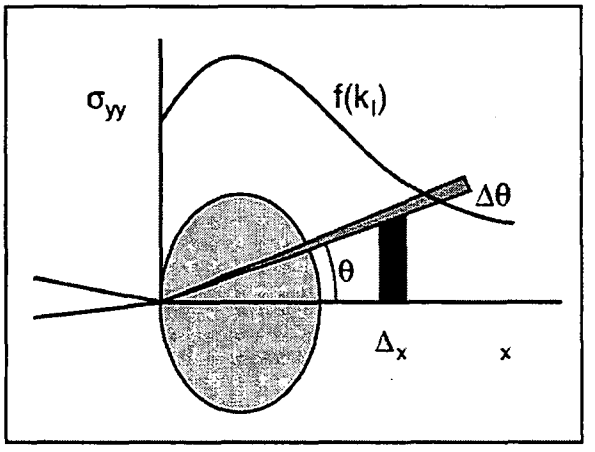

Fig. 1.6. Stress distribution in front of a crack showing definitions of $\Delta\theta$, θ, x and Δx.

where the dimension of the volume element in the x-direction, described by Δx, must clearly be larger than the initiator size ($\Delta x > 1 \ldots 10$ μm). The double summation indicates that the summation is performed over the whole cleavage fracture process zone, the radial limit of which is denoted by x_p. The cleavage fracture process zone is essentially restricted to the region of high tensile stresses and plastic strains. For simplicity, the stress distribution is assumed to be uniform over the specimen thickness, B, (crack front length). Accounting for the thickness dependence of the stress distribution would only lead to the addition of a third summation over the thickness, in

slices, ΔB. As long as the thickness dependence of the stress distribution is independent of K_I (SSY), the overall effect of the third summation does not affect the outcome of the derivation.

Due to the self-similar properties of the sharp crack stress field, it is possible to normalize the distance with the stress intensity factor to produce a dimensionless description of the stress distribution

$$U = \frac{x}{(K_I/\sigma_y)^2} . \tag{1.9}$$

When Eq. (1.9) is substituted into Eq. (1.8), the probability of cleavage initiation can be expressed in terms of K_I and U:

$$P_f = 1 - \exp\left\{B \cdot \frac{K_I^4}{\sigma_y^4} \cdot \sum_{\theta=0}^{2\pi} \left[\sum_{U=0}^{U_R} \left\{-\overline{N}_V \cdot \Delta U \cdot U \cdot \sin(\Delta\theta) \cdot Pr_{U,\theta}\{I\} \cdot \left(1 - Pr_{U,\theta}\{V/O\}\right)\right\}\right]\right\} . \tag{1.10}$$

The value of the double summation in Eq. (1.10) is always negative and independent of K_I. Thus the expression can be simply written as

$$P_f = 1 - \exp\left\{-B \cdot K_I^4 \cdot \text{constant}\right\} \tag{1.11a}$$

or

$$P_f = 1 - \exp\left\{-\frac{B}{B_0} \cdot \left(\frac{K_I}{K_0}\right)^4\right\} , \tag{1.11b}$$

where B_0 is a freely definable normalizing crack front length, K_0 is the scale parameter that corresponds to a cumulative initiation probability of $P_f = (1 - e^{-1}) = 0.6320$.

The remarkable feature of the cumulative cleavage initiation probability distribution is that it is really independent of the local cleavage initiator distribution. This result contains no approximations. The only assumption is that the initiators are independent on a global scale. In other words, it is assumed that the volume elements act independently for a constant K_I. Only if it is assumed that a certain fraction of the crack front must

experience critical initiations to cause macroscopic failure will the result differ from that of Eqs. (1.11a) and (1.11b). The result is valid only when the stresses inside the process zone are self-similar in nature, so that they can be described by a single parameter (e.g., K_I). The result is also applicable for other than SSY conditions, provided it is possible to transform the stress distribution to correspond to the SSY situation ($K_{ISSY} = f\{K_J\}$). Such an SSY correction is usually possible for cracks with a strong local tensile stress component. If the stress distributions inside the process zone are not self similar, Eqs. (1.11a) and (1.11b) will not be correct. For such cases, Eq. (1.8) must be used, and subsequently some quite far-reaching assumptions regarding the local cleavage initiation probability must be made.

1.1.2 Conditional Cleavage Propagation

Equations. (1.11a) and (1.11b) imply that an infinitesimally small K_I value leads to a finite failure probability. This is not true in reality. For very small K_I values, the stress gradient becomes so steep that even if cleavage fracture can initiate, it cannot propagate into the surrounding and other adjacent grains, thus causing a zone of arrested microcracks in front of the main crack.[21] If propagation following initiation is very difficult, a stable type of fracture may evolve. This is an effect often seen with ceramics. The need for propagation leads to a conditional crack propagation criterion, causing a limiting K_{min} value below which cleavage fracture is impossible. For structural steels in the lower shelf temperature range, the fracture toughness is controlled by the difficulty of propagation.

Hence, on the lower shelf, initiation is not the only requirement for cleavage fracture, but additionally a conditional propagation requirement must be fulfilled.

Figure 1.4 indicates that the probability of failure is governed by the probability of propagation following initiation at the same load. Thus the incremental probability of failure by propagation is the joint probability of initiation, between K_I and K_I+d K_I, and the probability of propagation following initiation. In order to both take advantage of and preserve the exponential form of the cumulative probability equation, it is convenient to express the incremental probability of initiation as the fraction of all the surviving specimens in which initiation will occur between K_I and K_I + d K_I. The resulting derivative is known as the hazard function, and is defined as

$$h(K_I) = \frac{1}{1 - P_f} \cdot \frac{d(P_f)}{dK_I} . \qquad (1.12)$$

For the cumulative cleavage initiation probability, Eq. (1.11b), the hazard function is simply

$$h_i(K_I) = \frac{4 \cdot K_I^3}{K_0^4} \cdot \frac{B}{B_0} \text{ (initiation)} . \tag{1.13}$$

When the hazard function for initiation is multiplied by the conditional probability of propagation (Pr{P/I}), the hazard function for failure is obtained as

$$h_f(K_I) = \Pr\{P/I\} \cdot \frac{4 \cdot K_I^3}{K_0^4} \cdot \frac{B}{B_0} \text{ (failure)} . \tag{1.14}$$

Referring to Eq. (1.12), it can be seen that

$$h(K_I) = - \frac{d\ln(1 - P_f)}{dK_I} , \tag{1.14a}$$

so that, assuming a value of K_{min} below which propagation cannot occur,

$$P_f = 1 - \exp - \int_{K_{min}}^{K_I} h(K_I)\,dK_I . \tag{1.14b}$$

Substituting Eq. (1.14) into Eq. (1.14b), the cumulative failure probability including propagation becomes[21]

$$P_f = 1 - \exp - \int_{K_{min}}^{K_I} \Pr\{P/I\} \cdot \frac{B}{B_0} \cdot \frac{4 \cdot K_I^3}{K_0^4} \cdot dK_I , \tag{1.15}$$

which still has the desired exponential form.

In order to apply Eq. (1.15), the conditional probability of propagation (Pr{P/I}) must be known in a functional form. Presently it is not possible to define a single specific function for Pr{P/I}, but some possible forms can be deduced from the stress distribution. If the probability of propagation is controlled by the steepness of the stress distribution, it will essentially be a function of the derivative of the HRR field (see Fig. 1.7).[22]

ORNL 98-5365/arb

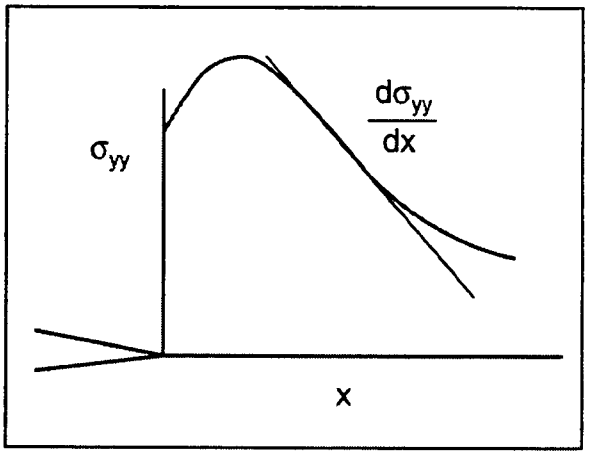

Fig. 1.7. Steepness of stress distribution in front of crack.

The stress distribution can be expressed as

$$\sigma_{yy} = \left(\frac{K_I^2}{x}\right)^{\frac{1}{N+1}} \cdot f(\theta) \ , \tag{1.16}$$

where N is the strain hardening exponent in the equation

$$\frac{\epsilon}{\epsilon_o} = \frac{\sigma}{\sigma_o} + \left(\frac{\sigma}{\sigma_o}\right)^N .$$

After eliminating x by substitution from Eq. (1.16), the derivative of the stress distribution becomes thus

$$\frac{\partial\sigma_{yy}}{\partial x} = -\left(\frac{1}{N+1}\right) \cdot \frac{\sigma_{yy}^{N+2}}{K_I^2 \cdot f(\theta)^{N+1}} \ . \tag{1.17}$$

It is seen from Eq. (1.17) that the steepness of the stress distribution is a combined function of the stress, angular location, and the stress intensity factor. The stress and angular dependence can be selected independently of K_I, thus leaving the probability of propagation to be a function of K_I. If Pr{P/I} is only controlled by the steepness of the stress distribution, then it should be possible to formulate trial functions of (K_I/K_{min}) that are likely to either overestimate or underestimate the true value of Pr(P/I). A high estimate can be obtained by choosing a cumulative probability function (cpf) for which the first derivative, which is the probability density function (pdf), has its peak at the left extreme of the curve. Using the same exponent as the exponent of K_I in Eq. (1.17), one such expression for the cpf is

$$Pr_1\{P/I\} = A_1 \cdot \left[1 - \left(\frac{K_{min1}}{K_I}\right)^2\right]. \tag{1.18a}$$

A lower estimate can be obtained by choosing a cpf for which the pdf is the product of two factors, one increasing with K_I, and the other decreasing with K_I, thus producing an intermediate peak in the pdf curve. Formulating this function is simplified by making the second factor the first derivative of the argument of the first factor. Again, using the exponent of K_I from Eq. (1.17), one such expression for the cpf is

$$Pr_2\{P/I\} = A_2 \cdot \left(1 - \frac{K_{min2}}{K_I}\right)^2. \tag{1.18b}$$

Consideration of another hypothesis is also worthwhile. Since Pr{P/I} is a measure of an instantaneous propagation rate with loading, it is possible that it is controlled by the changed steepness of the stress distribution:[23]

$$\frac{\partial}{\partial K_I}\left(\frac{\partial \sigma_{yy}}{\partial x}\right) = \left(\frac{2}{N+1}\right) \cdot \frac{\sigma_{yy}^{N+2}}{K_I^3 \cdot f(\theta)^{N+1}}. \tag{1.19}$$

Eq. (1.19) implies two additional possible forms for Pr{P/I} [Eqs. (1.20a) and (1.20b)]. Using the same logic as for Eqs. (1.18a) and (1.18b),

$$Pr_3\{P/I\} = A_3 \cdot \left[1 - \left(\frac{K_{min3}}{K_I}\right)^3\right] \tag{1.20a}$$

and

$$Pr_4\{P/I\} = A_4 \cdot \left(1 - \frac{K_{min4}}{K_I}\right)^3 . \tag{1.20b}$$

The possible forms of Pr(P/I) are presented graphically in Fig. 1.8. All the equations are functions growing from 0 to A, where A is a number smaller than 1. The constant A reflects the finite probability of crack arrest even in a uniform stress field, due possibly to misorientation between the microcrack and the possible cleavage crack planes in the first microcracked grain, and the need for the microcrack to cross a grain boundary.

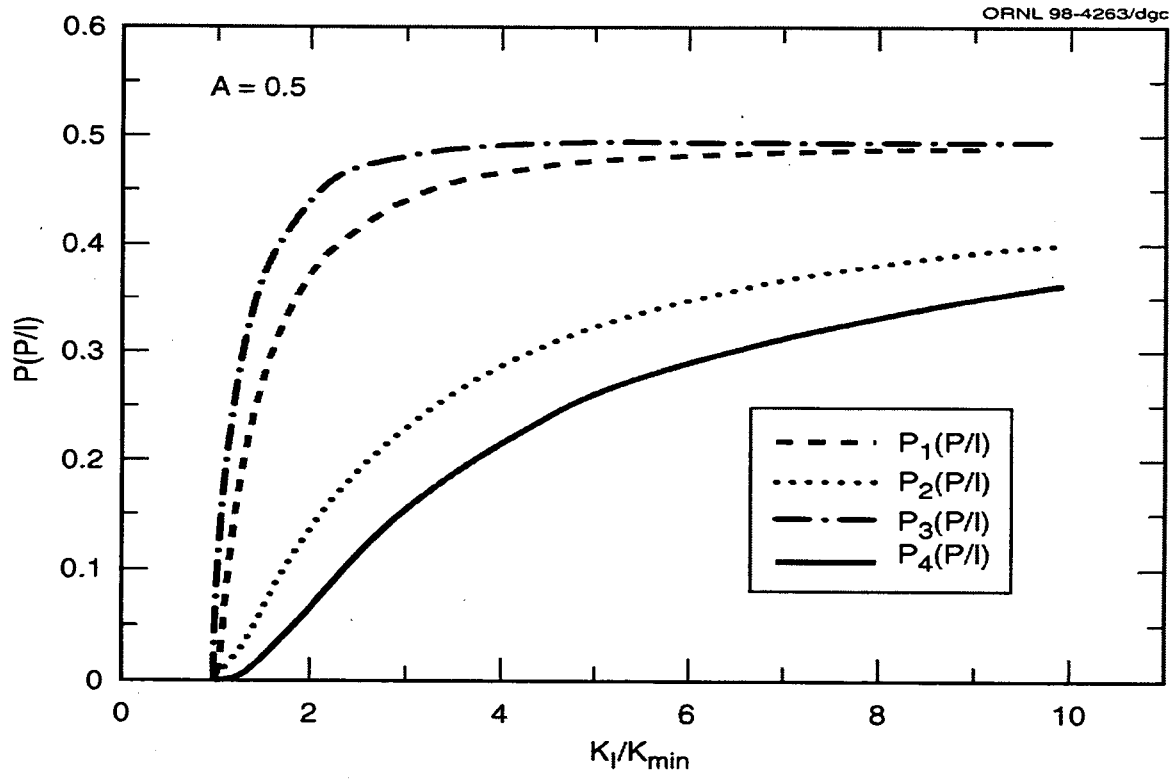

Fig. 1.8. Comparison of the different possible conditional propagation probability functions [Eqs. (1.18) and (1.20)] using A = 0.5 as the limiting propagation probability.

When Eqs. (1.18) and (1.20) are inserted into Eq. (1.15), the following possible forms for the total cumulative failure probability are obtained:

$$P_{f1} = 1 - \exp\left\{-\frac{B}{B_0} \cdot \frac{A_1}{K_0^4} \cdot \left(K_I^2 - K_{min1}^2\right)^2\right\} \tag{1.21a}$$

$$P_{f2} = 1 - \exp\left\{-\frac{B}{B_0} \cdot \frac{A_2}{K_0^4} \cdot \left(K_I - K_{min2}\right)^3 \cdot \left(K_I + K_{min2}/3\right)\right\} \tag{1.21b}$$

$$P_{f3} = 1 - \exp\left\{-\frac{B}{B_0} \cdot \frac{A_3}{K_0^4} \cdot \left(K_I^4 - 4 \cdot K_{min3}^3 \cdot K_I + 3 \cdot K_{min3}^4\right)\right\} \tag{1.21c}$$

$$P_{f4} = 1 - \exp\left\{-\frac{B}{B_0} \cdot \frac{A_4}{K_0^4} \cdot \left(K_I - K_{min4}\right)^4\right\}. \tag{1.21d}$$

The equations are compared graphically in Fig. 1.9, where K_{min} refers to K_{min4}, by means of plotting numerically normalized curves for each equation, with all four normalized curves required to pass through the point at which $K_I / K_{min4} = 5$ with the same ordinate and the same slope. Experimentally it is virtually impossible (it would require more than 1000 tests) to measure differences in the four expressions. They start clearly to deviate from each other only at very low cumulative probability values. The expression producing the most conservative (i.e., the lowest) estimate for the minimum fracture toughness is P_{f4}. The expression for P_{f4} is also the expression already in general use as a modification of Eq. (1.11b).

The individual parameter values used in Fig. 1.9 are presented in Table 1.1. The table essentially confirms the trends seen in Fig. 1.9. The expression P_{f1} is essentially identical with P_{f3}, P_{f2} is essentially identical with P_{f4}, and P_{f4} yields the most conservative estimate of K_{min}. For engineering safety assessment purposes it is clearly advisable to use P_{f4} to describe the cumulative failure probability.

Table 1.1. Relation between different possible cumulative failure probability parameters

P_{f1}	$A_1/A_4 = 0.66$	$K_{min1}/K_{min4} = 2.28$
P_{f2}	$A_2/A_4 = 0.90$	$K_{min2}/K_{min4} = 1.20$
P_{f3}	$A_3/A_4 = 0.60$	$K_{min3}/K_{min4} = 2.48$
P_{f4}	$A_4/A_4 = 1$	$K_{min4}/K_{min4} = 1$

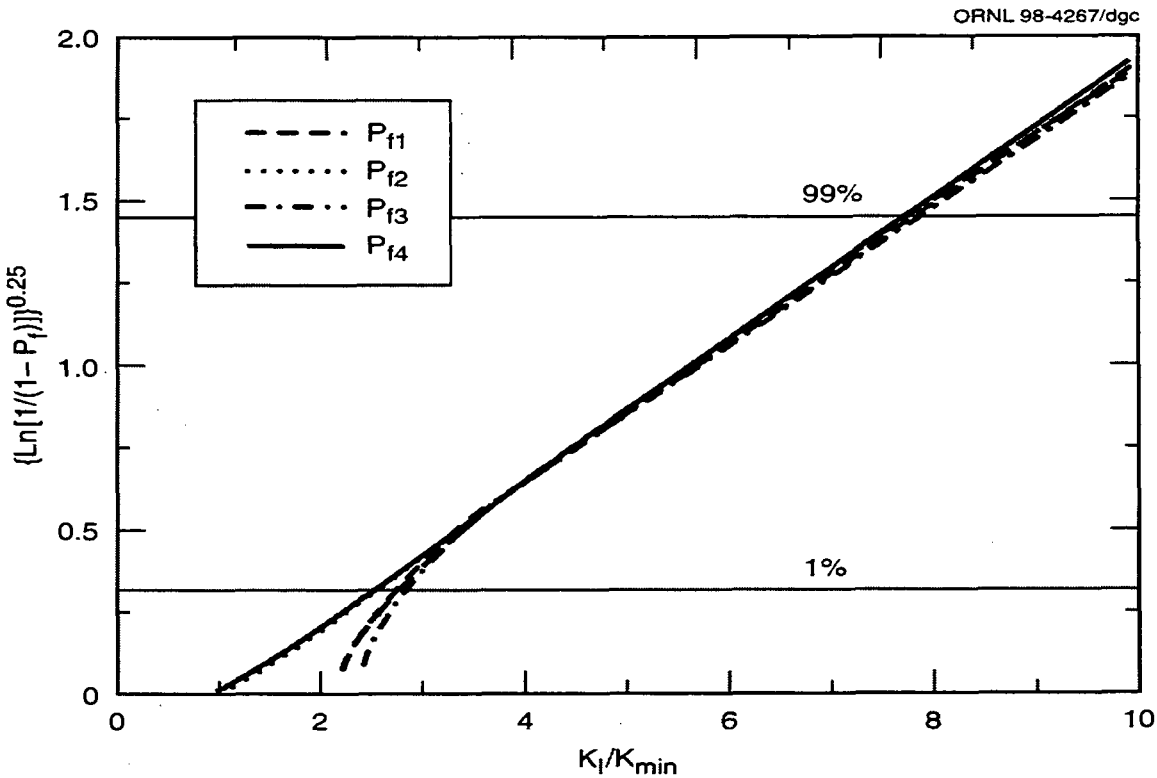

Fig. 1.9. Comparison of different possible cumulative failure probability expressions, Eqs. (1.21a) through (1.21d). The expressions are plotted against a normalized form of P_{f4}, using $K_0/K_{min4} = 5$ and $A_4 = 1$.

1.1.3 Lower Shelf Toughness

The above derivations are based on the assumption that the probability of cleavage initiation is less than unity.[22] This is normal for configurations like plain and notched specimens and cracked specimens in cases where initiation is sufficiently difficult. For material conditions where initiation is simple, the probability of cleavage initiation in the case of a crack may become unity. This can occur on the so called "lower shelf" of the material. Essentially it means that all possible initiation sites are activated and initiation occurs as soon as the crack is loaded, making the initiation event independent of the load level (and subsequently independent of specimen thickness). Thus, for cracked configurations, the lower shelf toughness may be controlled entirely by the probability of propagation. For plain and notched configurations, however, the probability of initiation will still be a function of load level even on the lower shelf. Therefore, a simple correlation between notched and cracked configurations may not be possible for the lower shelf material conditions.

As previously stated, in the discussion of Eqs. (1.14), (1.14a), and (1.14b), the conditional probability of propagation (Pr{P/I}) is related to the hazard function for failure. However, Pr{P/I} does not as such constitute a

hazard function because the hazard function (like the incremental distribution) must have the units of $1/K_I$. Let it be assumed that the probability of initiation with no prior event is given by

$$P_i = 1 - \exp\left(-\frac{K_i}{K_e}\right) . \tag{1.21e}$$

Then, by using the definition of the hazard function given by Eq. (1.14a), the hazard function for initiation is given by

$$h_i(K_I) = \frac{1}{K_e} . \tag{1.21f}$$

Multiplying the hazard function for initiation by the conditional probability of propagation, Pr{P/I}, the hazard function for failure is

$$h_f(K_I) = \frac{1}{K_e} \cdot \Pr\{P/I\} . \tag{1.21g}$$

Therefore, substitution of the normalization parameter $1/K_e$ in the place of the constant A, and using the same trial functions used in Eqs. (1.18 and 1.20), logical forms for the hazard function of propagation alone become

$$h_{P1}(K_I) = \frac{1}{K_{e1}} \cdot \left[1 - \left(\frac{K_{min1}}{K_I}\right)^2\right] \tag{1.22a}$$

$$h_{P2}(K_I) = \frac{1}{K_{e2}} \cdot \left(1 - \frac{K_{min2}}{K_I}\right)^2 \tag{1.22b}$$

$$h_{P3}(K_I) = \frac{1}{K_{e3}} \cdot \left[1 - \left(\frac{K_{min3}}{K_I}\right)^3\right] \tag{1.22c}$$

$$h_{P4}(K_I) = \frac{1}{K_{e4}} \cdot \left(1 - \frac{K_{min4}}{K_I}\right)^3 . \tag{1.22d}$$

The corresponding cumulative failure probabilities are

$$P_{f1LS} = 1 - \exp\left\{-\frac{K_{min1}}{K_{e1}} \cdot \left[\frac{K_I}{K_{min1}} + \frac{K_{min1}}{K_I} - 2\right]\right\} \tag{1.23a}$$

$$P_{f2LS} = 1 - \exp\left\{-\frac{K_{min2}}{K_{e2}} \cdot \left[2 \cdot \ln\left(\frac{K_{min2}}{K_I}\right) + \frac{K_I}{K_{min2}} - \frac{K_{min2}}{K_I}\right]\right\} \tag{1.23b}$$

$$P_{f3LS} = 1 - \exp\left\{-\frac{K_{min3}}{K_{e3}} \cdot \left[\frac{K_I}{K_{min3}} + \frac{1}{2} \cdot \left(\frac{K_{min3}}{K_I}\right)^2 - \frac{3}{2}\right]\right\} \tag{1.23c}$$

$$P_{f4LS} = 1 - \exp\left\{-\frac{K_{min4}}{K_{e4}} \cdot \left[\frac{K_I}{K_{min4}} - 3 \cdot \ln\left(\frac{K_I}{K_{min4}}\right) - 3 \cdot \frac{K_{min4}}{K_I} + \frac{1}{2}\left(\frac{K_{min4}}{K_I}\right)^2 + \frac{3}{2}\right]\right\} . \tag{1.23d}$$

Eqs. (1.23a) through (1.23d) are compared in graphic form in Fig. 1.10 for an imaginary lower shelf data set with a median fracture toughness of approximately 40 (units not specified). The same trend as before for the initiation + propagation case is seen. The expression P_{f1LS} is essentially identical with P_{f3LS}, P_{f2LS} is essentially identical with P_{f4LS}, and P_{f4LS} yields the most conservative estimate of K_{min}, which is about 20. The expressions P_{f1LS} and

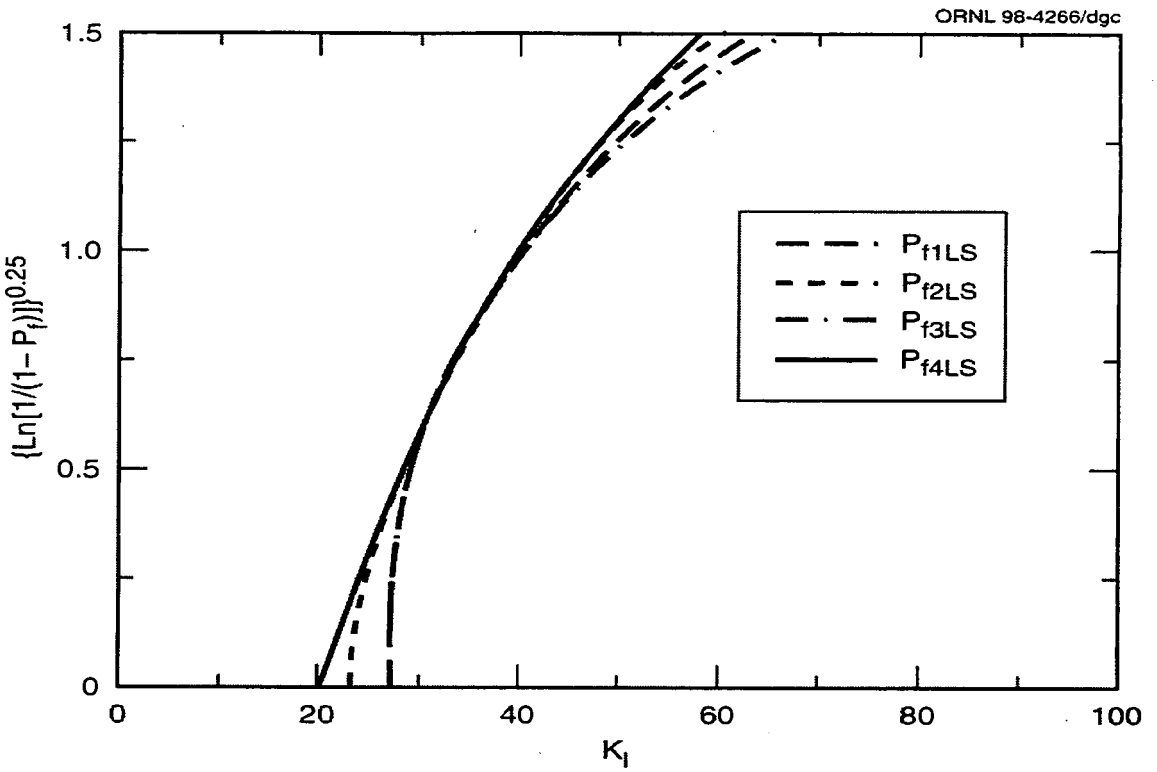

Fig. 1.10. Comparison of different possible cumulative failure probability expressions for lower shelf behavior, Eqs. (1.23a) through (1.23d).

P_{f3LS} appear unrealistic in shape compared to existing lower shelf data. Expression P_{f2LS} appears, intuitively, from the stress distribution point of view to be most likely the correct one, but the expression P_{f4LS} is almost identical in shape and slightly more conservative. Additionally, the form of P_{f4} (for initiation + propagation) is very suitable for statistical estimation because it is identical to a simple three-parameter Weibull distribution with a fixed shape (exponent = 4). Thus, P_{f4} and P_{f4LS} are selected as the basis for the master curve scatter and size effect.

1.1.4 Conclusions

The master curve scatter in the case of initiation + propagation is described best by Eq. (1.21d), which can be reformulated in the form of a three-parameter Weibull expression with the exponent fixed to 4:

$$P_f = 1 - \exp\left\{-\frac{B}{B_0}\cdot\left(\frac{K_I - K_{min}}{K_0 - K_{min}}\right)^4\right\}. \tag{1.24}$$

K_0 equals the load level corresponding to a 63.2 % cumulative failure probability, B_0 is a freely selected normalizing thickness, e.g., 25 mm and K_{min} is the lower limiting fracture toughness corresponding to zero probability of failure.

By writing Eq. (1.24) for two different specimen sizes and equating the values of P_f, the size effect, implied by Eq. (1.24), takes the form

$$K_{IC_2} = K_{min} + (K_{IC_1} - K_{min}) \cdot \left(\frac{B_2}{B_1}\right)^{1/4} . \tag{1.25}$$

The theory implicit in Eq. (1.22) predicts that the size effect described by Eq. (1.25) disappears in the lower shelf toughness range, and also that the scatter changes (compare Figs. 1.9 and 1.10) somewhat. On the lower shelf, the cumulative failure probability is described by Eq. (1.23d), which is of a somewhat more complex form than Eq. (1.24). Unfortunately, the derivation is incapable of predicting when the lower shelf prevails, thus making it difficult to decide when to use Eq. (1.24) and when to use Eq. (1.23d). Experimentally the problem can be addressed by performing tests in both regions. From an engineering assessment point of view, however, a conservative estimate is obtained with Eq. (1.24) also on the lower shelf.

When cleavage fracture is governed by initiation rather than propagation, the resulting equations contain no mathematical approximations, although their derivations employ several assumed mathematical representations of physical behavior that are deemed to be reasonable in the absence of adequate experimental data. The main assumption is that the initiators are independent on a global scale. In other words, it is assumed that the volume elements that represent the material ahead of the crack tip are independent for a constant K_I. Only if it is assumed that a certain fraction of the crack front must experience critical initiations to cause macroscopic failure will the result differ from what is presented here. The only other restriction comes from the demand that the volume elements in the x-direction must be clearly larger than the initiator size, but this demand is valid only for the transition region where it is easily fulfilled. On the lower shelf, initiation is automatic and does not depend on the volume element size.

In the case of crack propagation, the mathematical models contain more uncertainty, but in this case, a conservative result has been chosen.

In the derivation, the cleavage fracture process zone was assumed to be equal to the region of high stresses and plastic strain. However, the result is not sensitive to the definition of the process zone as long as it is assumed

that the stress and strain distributions inside the process zone scale with K_I, CTOD or J. This aspect becomes important when examining the effect of large-scale yielding and ductile tearing.

1.2 Background of the Master Curve Temperature Dependence

The foregoing modeling of data scatter and size adjustment do not as such lead to a prediction of the temperature dependence of cleavage fracture toughness. This would require a more detailed mechanistic description of the initiation and propagation mechanisms, and so far, such a detailed description does not exist. Thus the temperature dependence associated with the master curve approach is empirical in nature and should therefore be regarded as an approximative description.[23,24]

1.2.1 Background

Two models claiming to predict the temperature dependence of cleavage fracture toughness are the RKR-model (Ritchie, Knott & Rice)[25] and the Beremin model (known as the local approach).[26,27] Both models essentially assume a constant cleavage fracture stress (σ_c, σ_w) and the temperature dependence arises solely from the temperature dependence of the yield strength. Both models thus predict an inverse dependence between fracture toughness and yield strength:

$$K_{IC} \sim \sigma_y^{-c} \ . \tag{1.25}$$

For a moderately strain-hardening material (n = 10) with a cumulative probability curve of the fracture stress parameter (σ_c, σ_w) characterized by a Weibull slope of 22, both models yield c = 4.5.

The models were originally developed for materials with the ductile-to-brittle transition occurring at low temperatures, where the change in yield strength with temperature was considerable. However, for more brittle materials, where the ductile-to-brittle transition occurs at or above room temperature, the models are unable to predict the temperature dependence correctly. This can well be seen with the following examples. Fig. 1.11 shows fracture toughness results for an A533B Cl.1 steel (JRQ)[28] in both unirradiated and irradiated conditions. The unirradiated data are seen to follow approximately an inverse relationship with the yield strength ($c \approx 5.5$), but the irradiated data are seen to have a much steeper slope, something not predicted by the models. The picture becomes even more interesting, when the fracture data are plotted against temperature (Fig. 1.12).

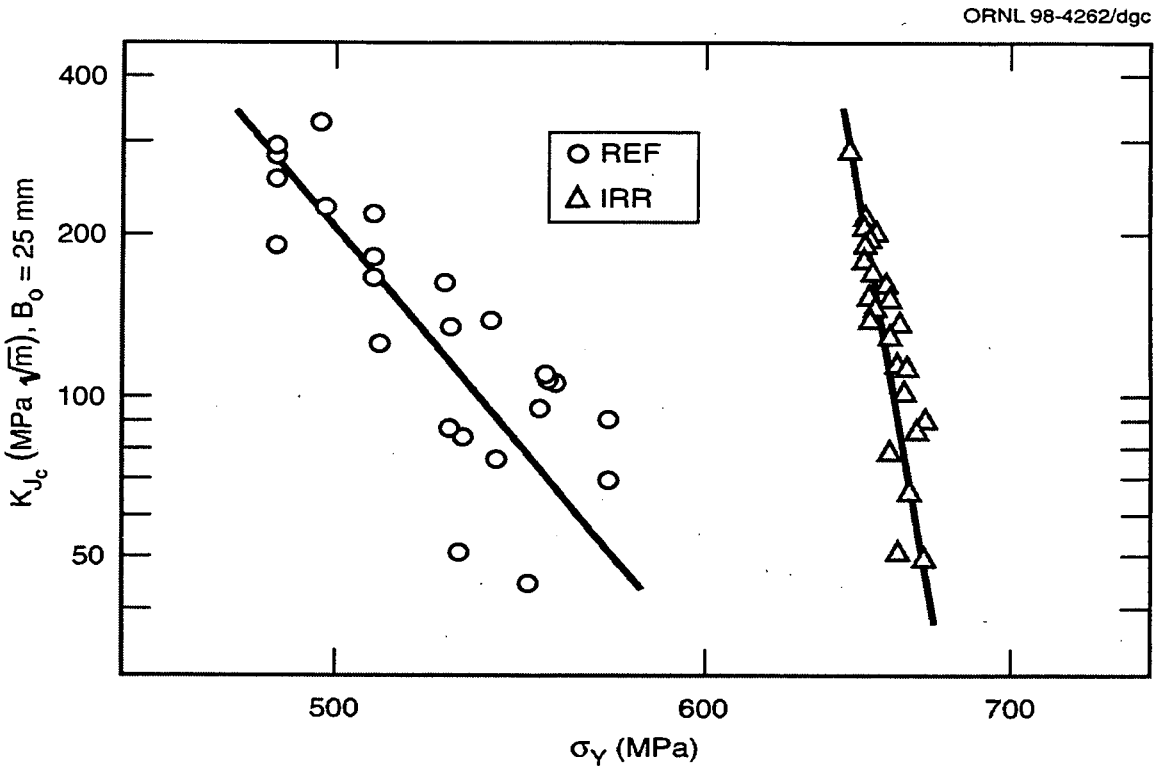

Fig. 1.11. Relation between fracture toughness and yield strength for unirradiated and irradiated material. A533B CI1 (JRQ) 12.5 mm RCT.

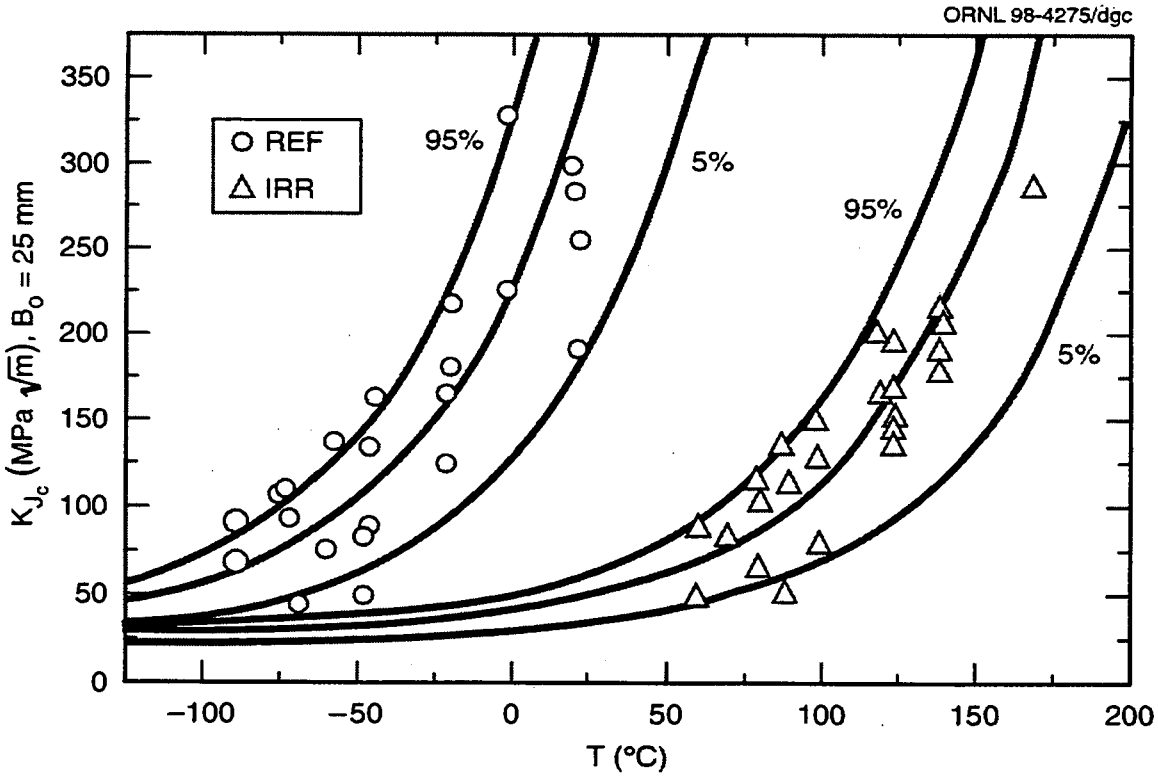

Fig. 1.12. Relation between fracture toughness and temperature for unirradiated and irradiated material. A533B CI1 (JRQ) 12.5 mm RCT.

Figure 1.12 shows that for both material states the temperature dependence of fracture toughness is essentially the same. A possible explanation for the behavior shown in Figs. 1.11 and 1.12 can be deduced from a further analysis of the yield strength. Normally, the yield strength is divided into a thermal and an athermal part. The athermal part is connected to the strengthening effect of grain boundaries and precipitates, whereas the thermal part is more connected to the dislocation mobility in the matrix. The thermal part of the yield strength appears to be quite insensitive to material composition or irradiation, as shown in Fig. 1.13, where data for three materials[28] are fitted to a decaying exponential expression. The constant inside the exponent is connected to the activation energy of dislocation mobility. It appears, that for materials with a ferritic matrix, the dislocation mobility in the matrix controls the temperature dependence of yield strength.

If the fracture toughness data in Fig. 1.11 are replotted against only the thermal part of yield strength, a dramatic change is seen (Fig. 1.14). Both material states are described by straight lines of identical slope, even though the locations of the lines are different.

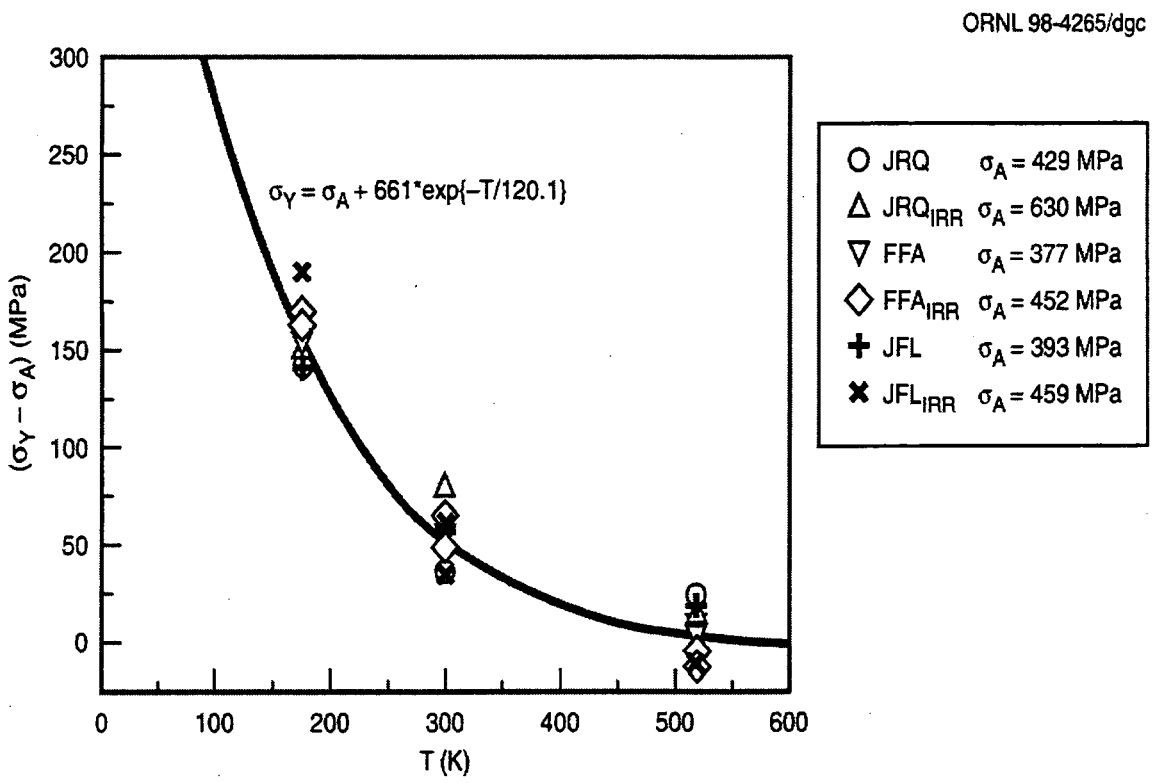

Fig. 1.13. Temperature dependence of yield strength for ferritic steels. Thermal part of yield strength is given for three pressure vessel steels in both unirradiated and irradiated conditions.

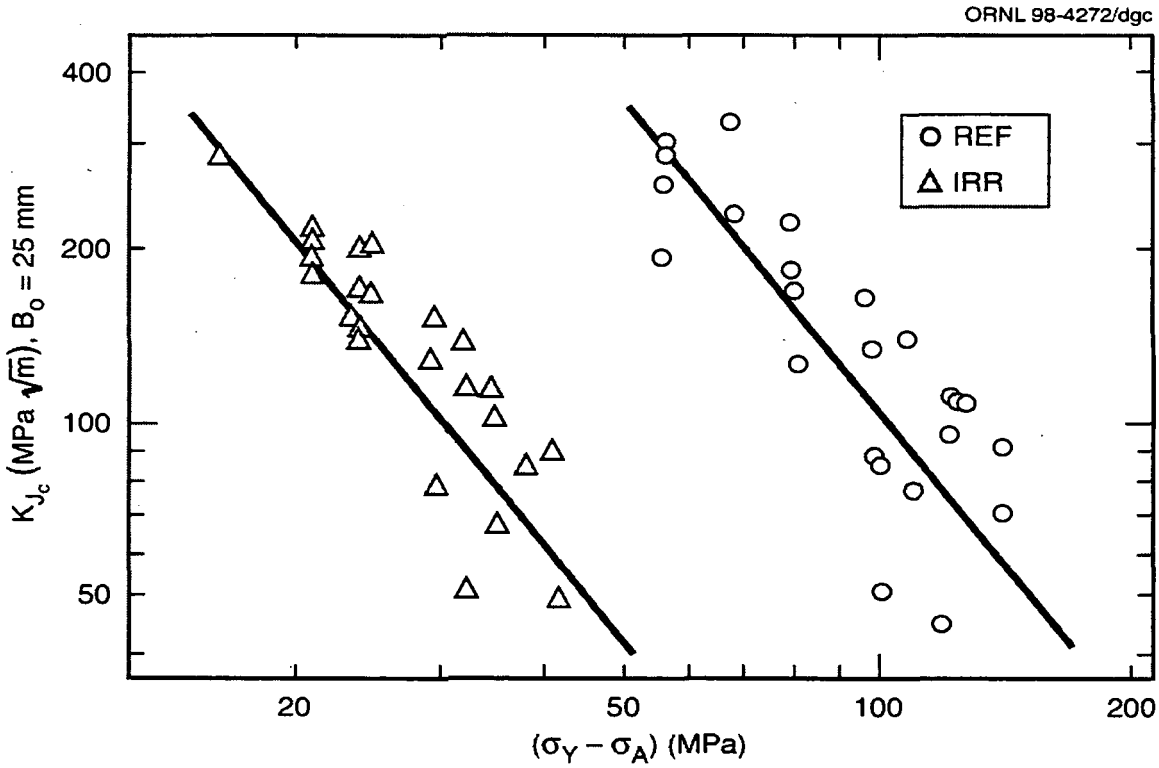

Fig. 1.14. Relation between fracture toughness and thermal part of yield strength for unirradiated and irradiated material.

The above result leads to the following postulate: The temperature dependence of cleavage fracture toughness is mainly controlled by the thermal part of the material's yield strength, whereas the position on the temperature scale is more controlled by the a thermal part of the yield strength.

The above postulate provides the basic theory for a unified description of the fracture toughness temperature dependence for ferritic steels, and the master curve was developed.

1.2.2 The Master Curve

To develop the empirical master curve, a large number of data sets were selected. Since fracture toughness testing of nuclear-grade pressure vessel steels is most common, understandably most of the data sets used corresponded to nuclear-grade pressure vessel steels and welds. The data were analyzed with the master curve size adjustment and scatter expressions, applying a maximum-likelihood estimate algorithm. For each temperature, where more than three test results were available, the fracture toughness corresponding to a 63.2 % cumulative failure probability (K_0) was determined (adjusted to correspond to 25-mm crack front length). It was decided to describe the temperature dependence with an exponential equation, normalized with the temperature at which the median

(practically the same as the mean) fracture toughness for a 25-mm crack front length is 100 MPa√m. This corresponds to a K_0 of 108 MPa√m at T_0. The equation thus had the following form:

$$K_0 = a + (108 - a) \cdot \exp\{c \cdot (T - T_0)\} \ . \tag{1.26}$$

The parameters a and c are fitted so as to yield the best fit for all the different materials. The thus-obtained, "original" master curve is presented in Fig. 1.15.[28]

The materials consisted of two weld metals (72W & 73W) in both the unirradiated and irradiated conditions, four sets of A533B Cl.1 steel (including the original "million dollar" K_{IC} data set (HSST02) used to develop the original ASME K_{IC} reference fracture toughness curve), an Eastern European pressure vessel steel (10MnNi2Mo), and a modified A508 Cl.2 steel (PTSE-2) with a low CVN upper shelf energy (60 J) and a low yield strength (280 MPa).

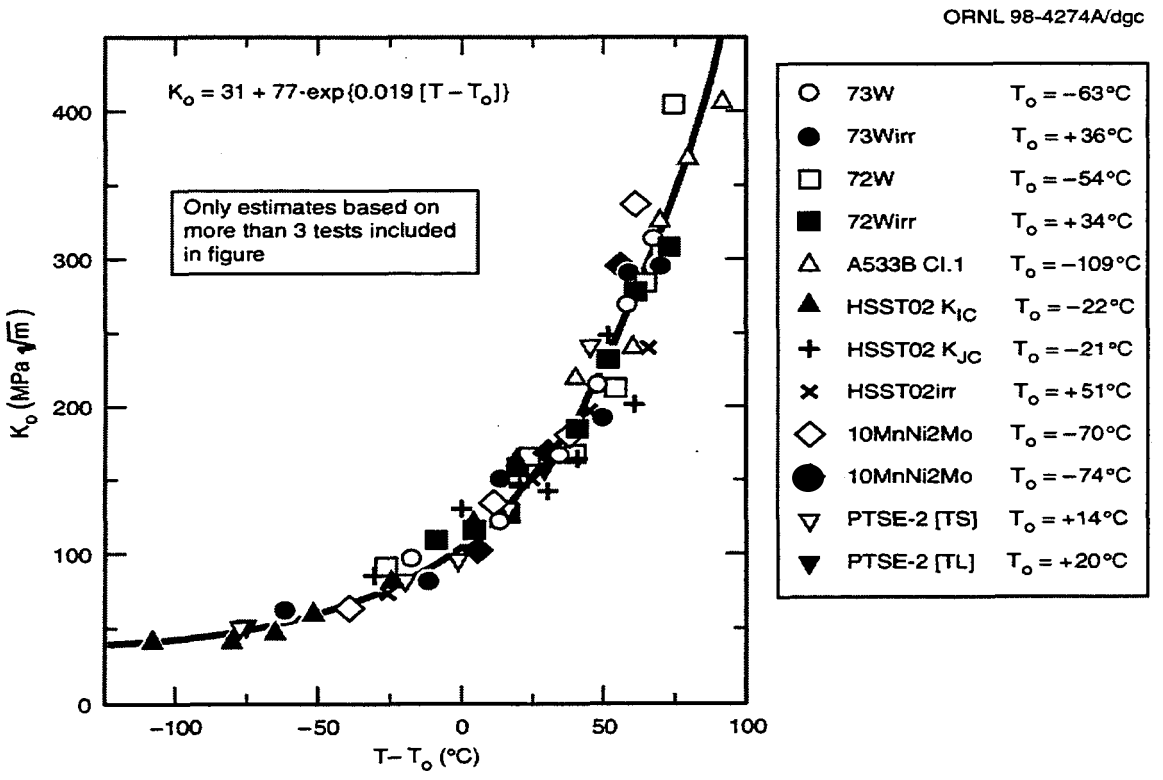

Fig. 1.15. Fracture toughness "Master Curve" for ferritic steels and welds. Original data used to develop the master curve.

The obtained expression has subsequently been verified to give an adequate description of the cleavage fracture toughness temperature dependence for a large variety of both pressure vessel steels and normal structural steels (and weldments) with yield strengths ranging from 280 to 1100 MPa.[29–32] It seems (based on experimental evidence) valid even for ferritic stainless steel.[33,34] Deviations from the master curve temperature dependence are usually found to be caused by loss of constraint and ductile crack growth effects. It is, however, recognized that the master curve temperature dependence is empirical in nature and that small deviations from it can be expected in isolated cases. As an additional detail, it can be noted that the temperature dependence curves in Fig. 1.12 are based on the master curve. In principle, it is possible to develop material specific temperature dependencies, but this would require testing on the order of 100 identical specimens.

Since the postulate behind the master curve temperature dependence is related to thermal behavior, it is not expected to be accurate on the lower shelf, where the fracture toughness is unaffected by thermal aspects. Thus extrapolation of the master curve toward lower shelf temperatures should be avoided unless experimental data related to these temperatures is available.

1.3 References

1. C. J. McMahon, Jr., and M. Cohen, *Acta Metall.* **13**, 591–604 (1965).

2. J. F. Knott, *J.I.S.I.* **205**, 288–91 (1967).

3. J. F. Knott, *J.I.S.I.* **204**, 1014–21 (1966).

4. G. T. Hahn, B. L. Averbach, W. S. Owen, and M. Cohen, p. 91 in *Fracture*, ed. B. L. Averbach et al., John Wiley and Sons, New York, 1959.

5. D. A. Curry, *Metal Sci.* **14**, 319–26 (1980).

6. M. G. Vassilaros, "Fracture Behavior of Modern Low Carbon Steels," Doctoral Dissertation, University of Cambridge, June 1991, Advisor–Dr. John Knott.

7. J. J. Lewandowski and A. W. Thompson, *Metall. Trans. A* **17A**, 1769–86 (1986).

8. D. J. Alexander and O. M. Bernstein, *Metall. Trans. A* **20A**, 2321–35 (1989).

9. J. J. Lewandowski and A. W. Thompson, *Acta Metall.* **35**, 1453–62 (1987).

10. A. V. Samant and J. J. Lewandowski, *Metall. Mater. Trans. A* **28A**, 389–99 (1997).

11. A. V. Samant and J. J. Lewandowski, *Metall. Mater. Trans. A* **28A**, 2297–2307 (1997).

12. F. R. Stonesifer and R. W. Armstrong, pp. 1–6 in *Advances in Research on the Strength and Fracture of Materials*, ed. D. M. R. Taplin, Pergamon Press, New York, 1978.

13. D. A. Curry and J. F. Knott, *Met. Sci.* **12**, 511–14 (1978).

14. D. A. Curry and J. F. Knott, *Met. Sci.* **13**, 341–45 (1979).

15. K. Wallin, T. Saario, and K. Törrönen, *Met. Sci.* **18**, 13–16 (1984).

16. T. Lin, A. G. Evans, and R. O. Ritchie, *J. Mech. Phys. Solids* **34**, 477–96 (1986).

17. K. Wallin, "Statistical Modelling of Fracture in the Ductile to Brittle Region," pp. 415–45 in *Defect Assessment of Components, Fundamentals, and Applications*, ESIS/EGF publication 9, 1991.

18. J. W. Hutchenson, *J. Mech. Phys. Solids* 13–31 (1968).

19. J. W. Hutchenson, *J. Mech. Phys. Solids* 333–47 (1968).

20. J. R. Rice and Rosengren, *J. Mech. Phys. Solids* 1–12 (1968).

21. D. Stenstra, "Stochastic Micromodeling of Fracture in the Ductile to Brittle Transition Region," Ph.D. dissertation, MM-6013-90-11, Texas A&M University, College Station, Tex., 1990.

22. K. Wallin, "Microscopic Nature of Brittle Fracture," *Journal de Physique* **3**(IV), 575–84 (1993).

23. K. Wallin, "Irradiation Damage Effects on the Fracture Toughness Transition Curve Shape for Reactor Pressure Vessel Steels," *The International Journal of Pressure Vessels and Piping* **55**(1), 61–79 (1993).

24. K. Wallin, "Fracture Toughness Transition Curve Shape for Ferritic Structural Steels," pp. 83–88 in *Proc. of the Joint FEFG/ICF Int. Conf. on Fracture Engineering Materials and Structures*, ed. S. H. Teoh and K. H. Lee, 1991.

25. R. O. Ritchie, J. F. Knott, and J. R. Rice, "On the Relationship Between Critical Tensile Stress and Fracture Toughness in Mild Steel," *J. Mech. Phys. Solids* **21**, 395–410 (1973).

26. A. Pineau, "Review of Fracture Micromechanisms and a Local Approach to Predicting Crack Resistance in Low Strength Steels," pp. 553–77 in *Advances in Fracture Research, 5th Int. Conf. on Fracture, Vol. 2*, ed. D. Francois, Pergamon Press, Oxford, 1981.

27. F. Mudry, "A Local Approach to Cleavage Fracture," pp. 165–86 in *Seminaire international sur L'Approch Locale de la Rupture*, Moret-sur-Loing, 1986.

28. K. Wallin, M. Valo, R. Rintamaa, K. Törrönen, and R. Ahlstrand, "Conclusions Regarding Fracture Mechanics Testing and Evaluation of Small Specimens as Evidenced by the Finnish Contribution to the IAEA/CRP-3 Programme," pp. 495–509 in *IAEA/NEA Specialists' Meeting on Irradiation Embrittlement and Optimization of Annealing, Paris, France, Sept. 20–23, 1993*, Paris, IAEA/NEA, IWG-LMNPP 93/03, 1993.

29. K. Wallin, "Effect of Strain Rate on the Fracture Toughness Reference Temperature T_0 for Ferritic Steels," pp. 171–82 in *Recent Advances in Fracture*, The Minerals Metals and Materials Society, 1997.

30. K. Wallin, "A Simple Theoretical Charpy-V-K-Correlation for Irradiation Embrittlement," ASME Pressure Vessel and Piping Conference, Honolulu, Hawaii, July 23–27, 1989, pp. 93–100 in *Innovative Approaches to Irradiation Damage and Fracture Analysis*, ed. D. L. Marriot, T. R. Mager, and W. H. Bamford, PVP-vol. 170, New York, American Society of Mechanical Engineers (ASME).

31. K. Wallin, K. Törrönen, R. Ahlstrand, B. Timofeev, V. Rybin, V. Nikolaev, and A. Morozov, "Theory Based Statistical Interpretation of Brittle Fracture Toughness of Reactor Pressure Vessel Steel 15ХМФА and its Welds," *Nuclear Engineering and Design* **135**, 239–46 (1992).

32. K. Wallin, "Validity of Small Specimen Fracture Toughness Estimates Neglecting Constraint Corrections," p. 19 in *Constraint Effects in Fracture: Theory and Applications*, ed. Kirk and Bakker, ASTM STP 1244, 1994.

33. K. Wallin, "New Improved Methodology for Selecting Charpy Toughness Criteria for Thin High Strength Steels," p. 41 in *IIW '94 Annual Assembly, Beijing, China, September 5–9, 1994*, Beijing, IIW, Commission X, 1994.

34. K. Wallin, "Small Specimen Fracture Toughness Characterization—State of the Art and Beyond," pp. 2333–44 in *Advances in Fracture Research*, ICF9, ed. B. L. Karihaloo, Y.-W Mai, M. I. Ripley, and R. O. Ritchie, Pergamon, Amsterdam, 1997.

2. EXPERIMENTAL CONFIRMATION OF THE MASTER CURVE APPROACH

The test method for the determination of T_o, ASTM method E1921-97, is designed to provide a suitable compromise between the fewest number of specimens required while at the same time having acceptable accuracy of the reference temperature determination. The recommended method has been tested on fracture toughness data obtained from a number of sources, and a list of T_o values accumulated is given in Table 2.1. The data sources are partially identified in the table. It is prudent to point out that most of the fracture toughness data had been developed without access to a standardized test practice, so there is some measure of uncertainty in comparing results between laboratories. The criterion applied for acceptance of data in the present case was evidence of appropriate elastic-plastic analyses and sufficient data replication to reasonably conform to the requirements of the standard method. Most of the steels evaluated were commercially produced. In a few cases, there had been supplemental heat treatments or irradiation conditions applied.

As an exercise, when Charpy V-notch (CVN) transition curves were reported, the temperatures of 28-J energy were used to make estimates of a test temperature that yields a median K_{Jc} of 100 MPa√m for 1T compact specimens.[1] The test temperature estimate is thus for T_o. This estimation scheme is discussed in Section 3.

Another potential relationship to consider is that between T_o and the drop-weight, DW_{NDT}, reference temperature used in the American Society of Mechanical Engineers (ASME) *Boiler and Pressure Vessel Code*.[2] Figure 2.1 displays the result of this attempted correlation. The evidence to claim a correlation is weak at best and the reason for this, in all probability, resides with the DW_{NDT} temperature. Drop weight specimens have a brittle weld crack starter bead, and this, coupled with the impact loading effect, creates an uncertain result. Interlaboratory welding practices can alter heat-affected zone properties that in turn disrupt the reproducibility of the method. Despite the serious deficiencies of the two empirical methods (CVN and DW_{NDT}), both tend to show conservative bias in transition temperature compared to the more accurate T_o temperature.

2.1 Master Curve for Engineering Applications

Although the stated purpose of the standard method has been defined as the determination of temperature T_o, the last few paragraphs in the standard method introduce the master curve concept as an engineering application for temperature T_o. The master curve can be used to more accurately establish the fracture mechanics-based transition temperature toughness of materials.[3] Note specifically in E1921-97, Paragraphs 10.3 (establishment of a transition temperature curve; master curve) and 10.4 (uses for master curve). The procedure for setting up the

Table 2.1. Examples of reference temperatures, T_o, and predictions of T_o from nonfracture mechanics test methods

Material	Strength		Reference	T_o	CVN T_{28J} - 18°C	Drop-weight NDT
	σ_{ys}	σ_{UTS}				
Normalized A302B	534	689	ORNL unpublished data	69	68.4	65
Modified A302B (Z7)	476	638	NUREG/CR-6426	–87	–67	–26
SNUPPS weld	528	652	ORNL HSST	–62	–67	–59
A533B Plate 14A	650	820	ORNL heat-treated plate	–44	–20	40
A533B Plate 02	476	628	NUREG/CR-4092	–23	–28	–18
A553B Weld 72W	498	606	STP 1046, Vol. 2	–59	–62	–23
A533B Weld 73W	490	599	STP 1046, Vol. 2	–62	–69	–34
A533B welds, irradiated	630	730	NUREG/CR-5913	37	6	46
A508 class 2 weld (beltline)	512	613	NUREG/CR-6249	–58	–44	–55
A508 class 2 weld (nozzle)	545	655	NUREG/CR-6249	–32	–44	–50
A508 class 2 weld, irradiated (beltline)	646	747	ORNL/NRC/LTR-95/18	27	47	—
A508 class 2 weld, irradiated (nozzle)	701	791	ORNL/NRC/LTR-95/18	62	40	—
A533B HSST Plate 13A	444	600	NUREG/CR-5788	–70	–56	–23
A533B Morland	470	620	NRL-Risley 1006(R)	–92	–87	–15
20MnMoNi55	450	610	GKSS 93/E/81	–123	–89	—
20MnMoNi55 irradiated	586	—	GKSS 93/E/81	–68	–38	—
CrMoV	660	802	GKSS 93/E/81	60	—	—
A36	250	455	Sorem et al., WRC Bulletin 351	–38	–10	—
A508 class 3	480	635	Iwadate et al., STP 803, Vol. II	–45	–49	—
A470 class 6[a]	767	870	Iwadate et al., STP 803, Vol. II	–63	–63	—
A508 class 3	456	599	MPC/JSPS-RR, STP 1207	–106	—	–30
A508 class 2	441	—	Macdonald, STP 1114	–46	—	—
A553B heat treated	538	607	Link, STP 1244	–55	–28	4
SM41C	304	461	Ando, Fatigue & Fracture Eng. Mat. Str.	–123	—	—
NiCrMo	745	812	Ando, Fatigue & Fracture Eng. Mat. Str.	–54	—	—
A508 class 2 heat treated	670	800	NUREG/CR-4249, TSP-3	–20	0	30

[a]No specimen size adjustment.

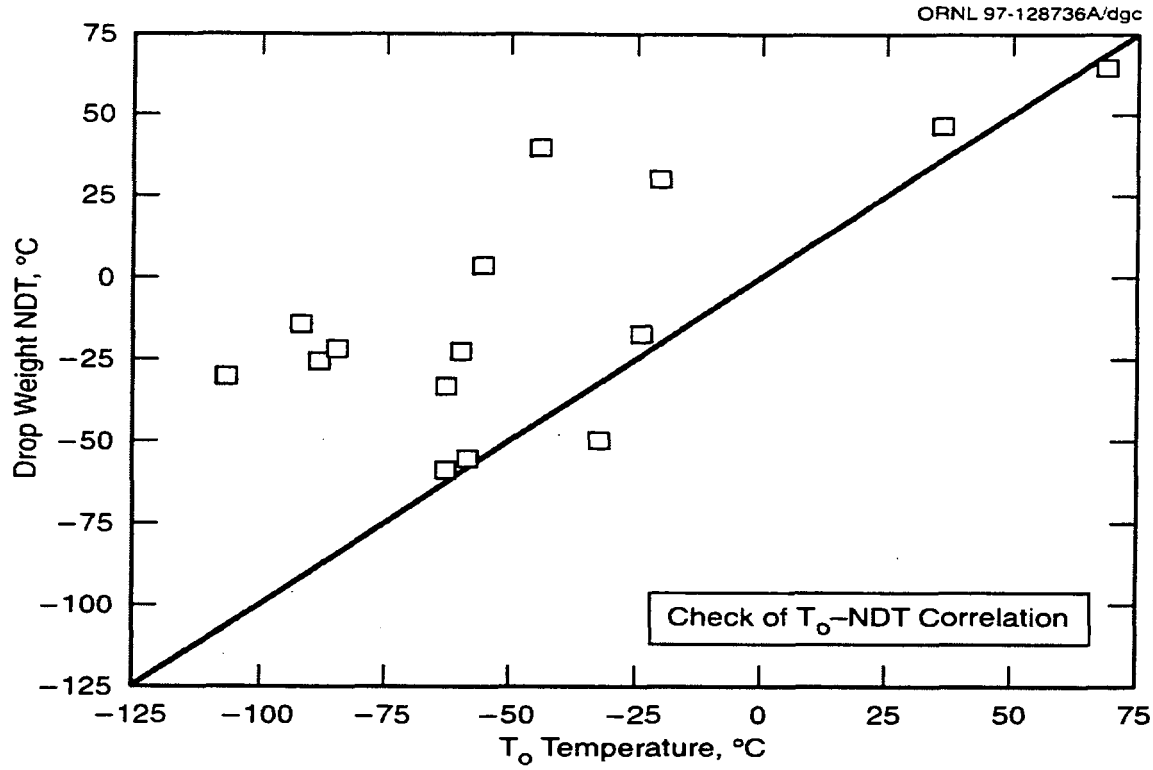

Fig. 2.1. Correlation between T_o temperature and drop-weight NDT.

master curve is explicit and as such it can be justified for inclusion in the mandatory steps part of the standard. The postulate applied is that one (to temperature normalized) universal transition range curve exists that applies to all ferritic and pearlitic type structural steels.

The concept that there is a single transition range curve shape is not new. The ASME Code has used the concept of a universal curve for more than 25 years in the form of the lower-bound K_{Ic} curve (Section XI) and lower-bound K_{Ia} (K_{IR}) curve (Sections III and XI).[4,5] The master curve represents a significant technological improvement to both of the presently used ASME lower-bound curves from several standpoints: (1) the specimen size requirements for data validity are modest in comparison to the size requirements established for validity of K_{Ic} and K_{Ia}, (2) data scatter in K_{Jc} is accepted as a natural outcome of material variability at the microstructural level that can be quantified using weakest-link type statistics, and (3) the data scatter distributions are modeled enabling greater accuracy in positioning of the transition range and enabling the setting of tolerance bounds on data scatter with appropriately established statistical significance. The reference temperature, T_o, is established by fracture mechanics-based testing of materials, not through inference using indirectly related empirical test methods.

The master curve applies to K_{Jc} data obtained from 1T size specimens or alternatively K_{Jc} data from specimens of other sizes where the values are size corrected to 1T equivalence. The following equation mathematically defines the master curve, corresponding to 50% cumulative failure probability, $K_{Jc(med)}$:

$$K_{Jc(med)} = 30 + 70 \exp[0.019 (T - T_o)] \quad \text{MPa}\sqrt{\text{m}} . \tag{2.1}$$

The test temperature is T (°C), and T_o (°C), is used as the material-specific reference temperature. Master curves for about 16 of the cases listed in Table 2.1 are presented in Appendix A. Each curve is positioned by the tabulated T_o values. The data points that appear along with the master curve are median values, $K_{Jc(med)}$, obtained from multiple tests that were made at the various temperatures, all normalized to T_o. Data points that do not lie on the master curve visually indicate the offset of T_o that would be calculated from that data set. Excessive deviations from the master curve trend would be a matter for concern, calling for evaluation modifications as deemed necessary.

2.2 Appendices Attached to the Method

There are three appendices attached to the standard method that are added as nonmandatory supplemental information. These represent instructional material provided for special applications in research and design matters. As an example, Appendix X3.0 of the standard instructs on setting tolerance bounds and making adjustments to tolerance bounds. Appendix B of this report demonstrates how the standard deviation on data scatter had been derived and on how the coefficients used in the tolerance bound equations had been developed. Margins are attached with considerable latitude allowed in the form of confidence level selection. Use of margin adjustment is advisable in engineering applications since lower tolerance bounds are set using only a few data. Margin takes care of the uncertainty in the temperature T_o when only the minimum recommended six specimens are used. The following standard deviation on T_o has been determined semiempirically:[1]

$$\sigma_{To} = \beta / \sqrt{N} \quad (°C) . \tag{2.2}$$

When the test temperature is nominally within 15°C of temperature T_o, the coefficient, β, is 18°C. When tests are made at temperatures more than 15° below T_o, then β is adjusted to sustain margin adjustment equivalence as the lower bound of the transition range is approached. The alternate values of β are listed in Appendix X3.0 of the standard as a function of $K_{Jc(med)}$.

An example of the use of the master curve to establish a lower-bound curve on data scatter using only a few precracked Charpy specimens is shown in Fig. 2.2.[6] Seven precracked Charpy specimens of Heavy-Section Steel Technology (HSST) Program Plate 02 were tested at –50°C; about 25°C below the T_o temperature. The Charpy data shown had been converted to 1T equivalence. The dashed curve shown is the 2% tolerance bound curve on the master curve after a margin adjustment of 10°C for the seven specimens tested and for a selected 85% confidence level on the T_o uncertainty estimate. The data for the large compact specimens were HSST Plate 02 data obtained from Ref. 7. This particular data bank is the one that had been used to establish the ASME lower-bound K_{Ic} curve. The Plate 02 portion of these data had virtually dictated the shape and position of the ASME lower-bound K_{Ic} curve. However, the ASME data plotted in Fig. 2.2 were not size-adjusted to 1T equivalence and it is notable that even with specimens up to 10T size, there are no fracture toughness data below the master curve 2% tolerance bound for 1T specimens. Evidently, the implication from this observation is that the weakest-link model must have only a moderate size effect on lower tolerance bound curves[8] (see Fig. 2.3). Even though the master curve median fracture toughness trend shows obvious sensitivity to specimen size effect, the three lower the tolerance bound curves at 5, 3, and 1 percent cumulative probability show very little size dependence. Note that this plot is specific to tests made at T_o temperature.

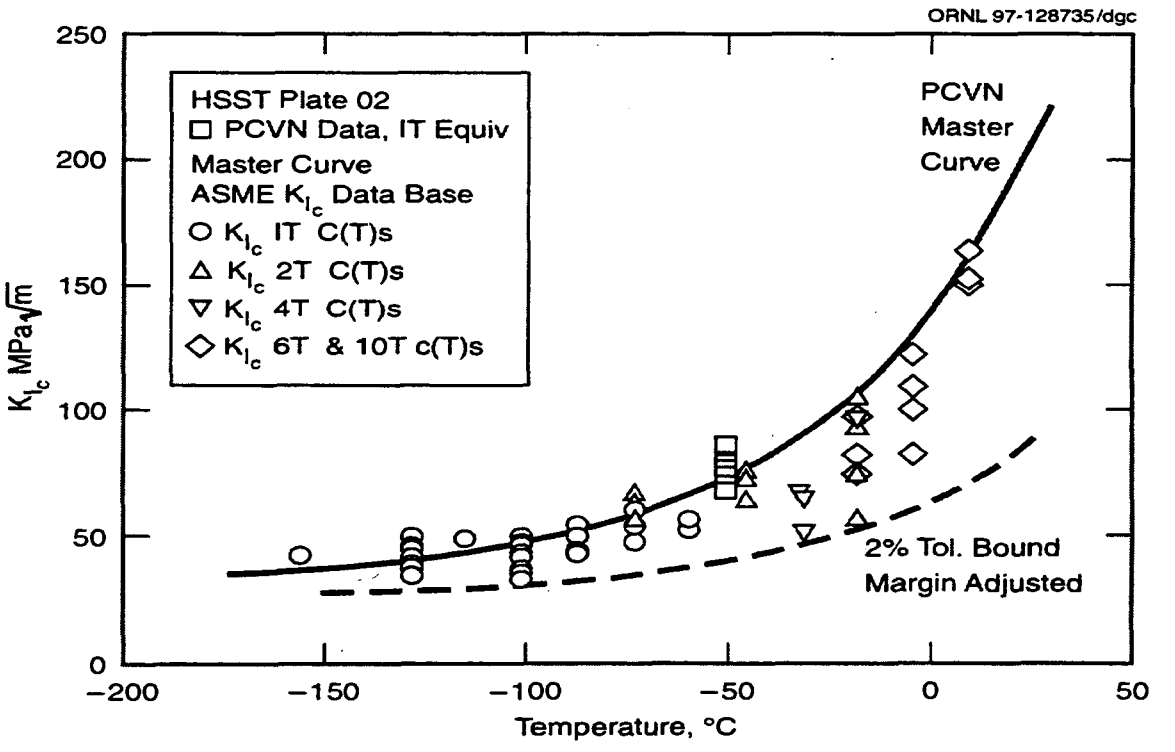

Fig. 2.2. Master curve positioned by T_o determined from precracked Charpy specimens.

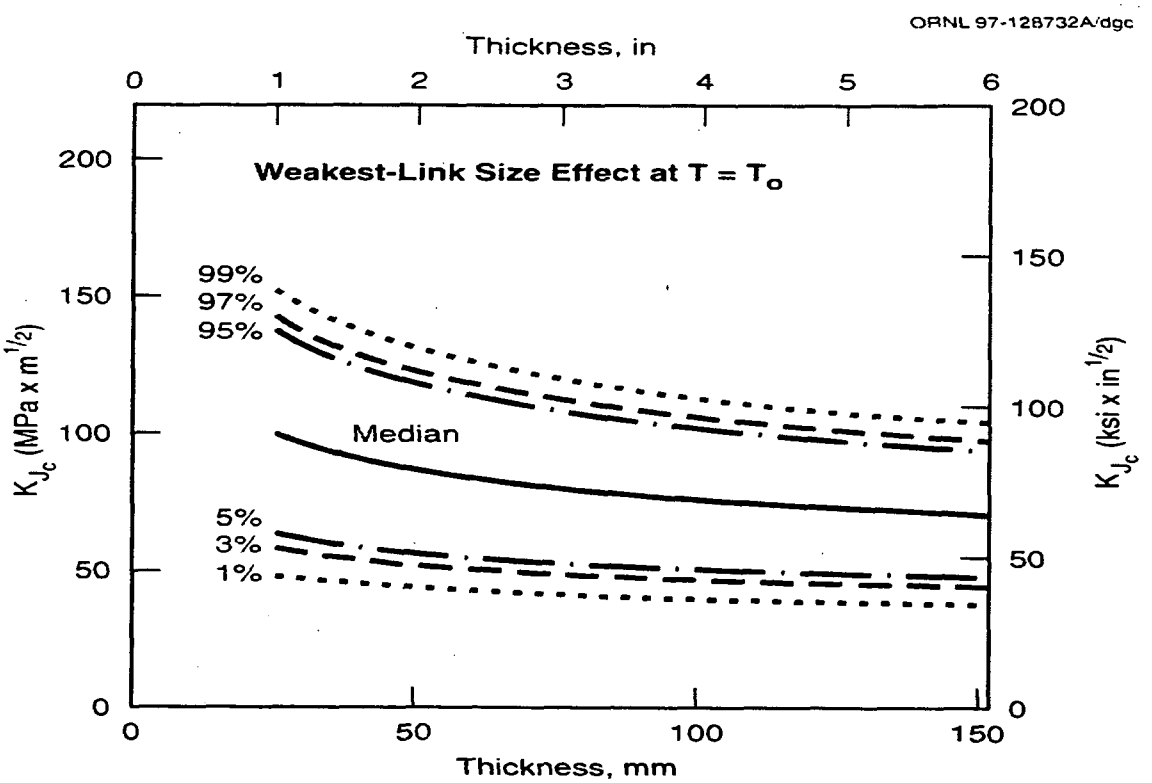

Fig. 2.3. Fracture toughness trends for size effect as predicted by weakest-link theory.

2.3 Problems Associated with Low Upper-Shelf Materials

The master curve concept has been developed by observing the characteristics of typical commercial steels that have reasonably suitable upper-shelf fracture toughness. In addition, the evidence gathered regarding specimen side grooving showed no particular effect on K_{Jc}, at least through most of the transition range.[9] However, it is now known that certain materials of low upper-shelf toughness (as indexed by Charpy transition curve), can generate deceptive master curve information. Low upper-shelf CVN toughness automatically implies low ductile tearing resistance as measured by the K_R curve. Hence, the well-known influence of side grooving practice on K_R curve toughness development will tend to show up in K_{Jc} data even before upper-shelf temperatures are reached. K_{Jc} distributions developed at temperatures between T_o and the upper shelf can be top-end truncated by ductile instabilities.

Figure 2.4 shows K_{Jc} data developed on a brittle low upper-shelf plate of A 302 grade B steel. The CVN 41-J temperature is 105°C and upper-shelf CVN energy is 79 J. Drop-weight NDT temperature is about 75°C. The K_R curve developed on this material along with a crack drive curve for a 1T compact specimen is shown in Fig. 2.5. Tangency between the two curves indicates that the maximum K_{Jc} value for the material when tested as a 1T specimen is about 125 MPa√m. Hence, it is impossible for this low upper-shelf material to have a typical Weibull

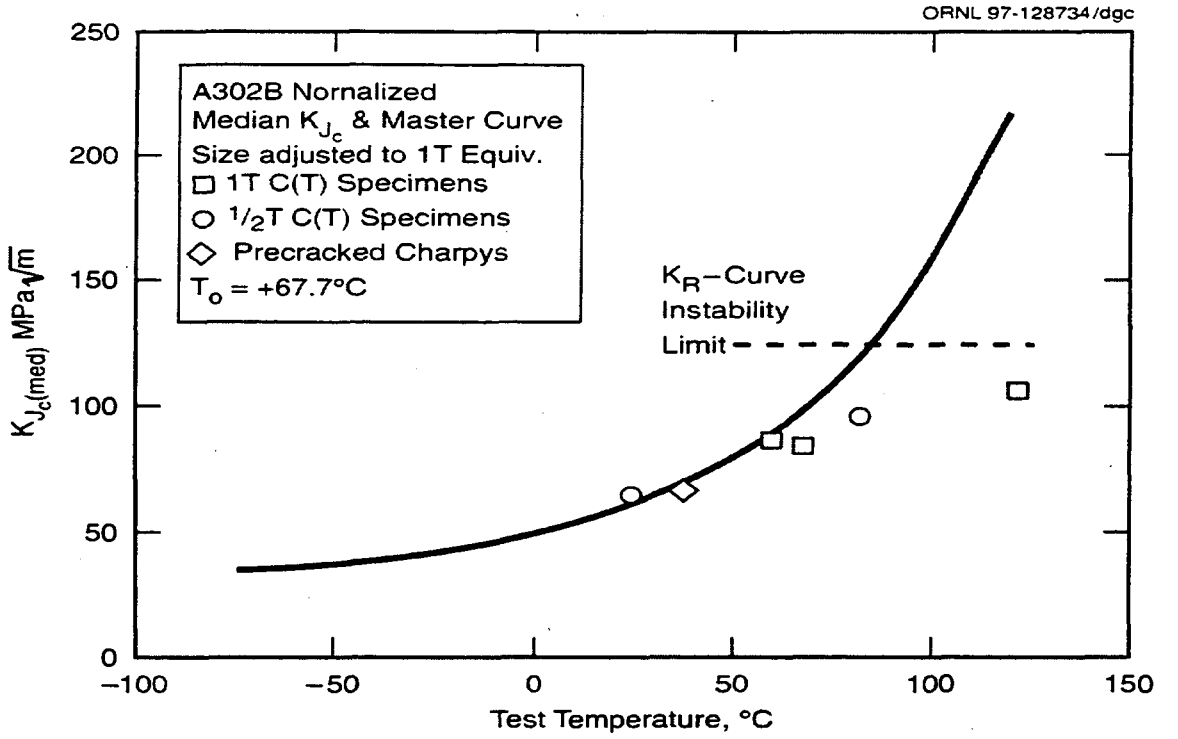

Fig. 2.4. Illustration of the difficulties of proving the master curve with low upper-shelf steels.

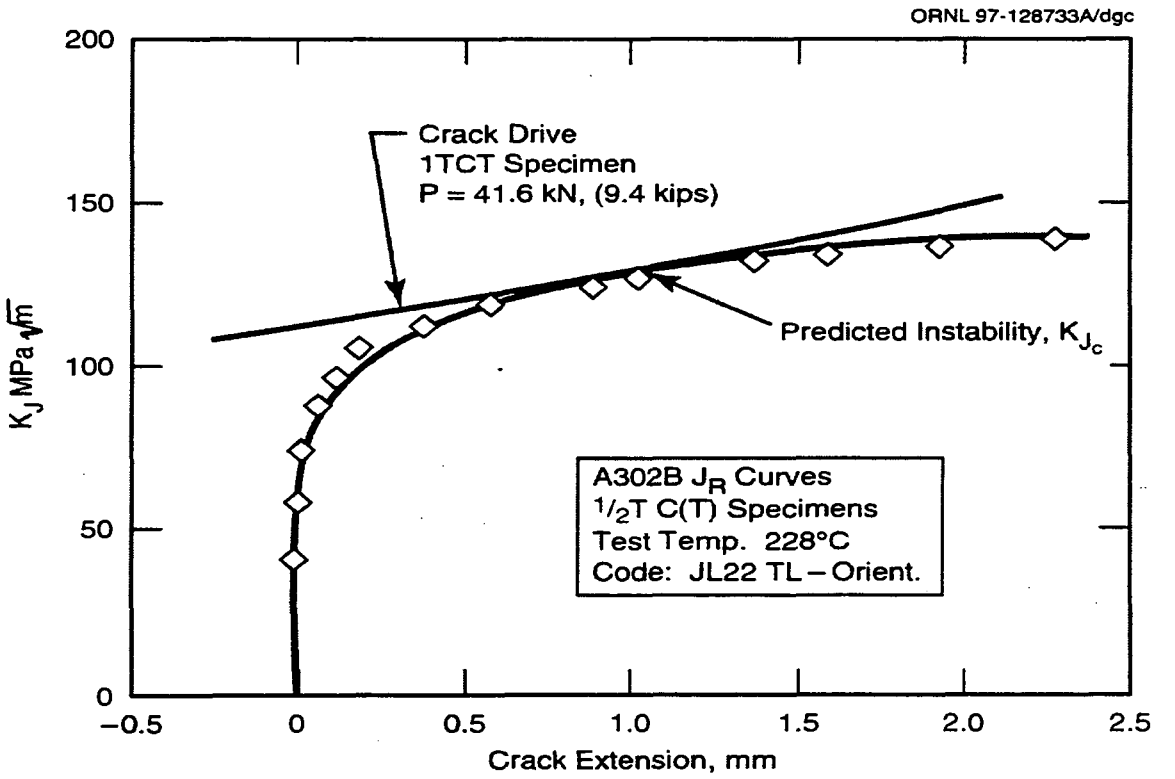

Fig. 2.5. Prediction of ductile instability K_{J_c} for a 1T C(T) specimen of a low upper-shelf steel.

data distribution at temperatures that are only moderately above T_o. As a consequence, median K_{Jc} values cannot track the master curve fracture toughness at temperatures slightly above T_o.

2.4 References

1. K. Wallin, "A Simple Theoretical Charpy V-K_{Ic} Correlation for Irradiation Embrittlement," in *Innovative Approaches to Irradiation Damage and Fracture Analysis*, PVP-Vol. 170, American Society of Mechanical Engineers, New York, July 1989.

2. "Conducting Drop-Weight Test to Determine Nil-Ductility Transition Temperature of Ferritic Steels," E 208-95a, in *Annual Book of ASTM Standards*, Vol. 03.01, American Society for Testing and Materials, 1996.

3. K. Wallin, "Recommendations for the Application of Fracture Toughness Data for Structural Integrity Assessments," in *Proceedings of the Joint IAEA/CSNI Specialists Meeting on Fracture Mechanics Verification by Large-Scale Testing*, USNRC Report NUREG/CP-0131 (ORNL/TM-12413), September 1993.

4. "Rules for Construction of Nuclear Power Plant Components," *ASME Boiler and Pressure Vessel Code. An American National Standard*, Sect. III, Div. 1, American Society of Mechanical Engineers, New York, 1992.

5. "Rules for Inservice Inspection of Nuclear Power Plant Components," *ASME Boiler and Pressure Vessel Code. An American National Standard*, Sect. XI, American Society of Mechanical Engineers, New York, 1992.

6. M. A. Sokolov, D. E. McCabe, Y. A. Davidov, and R. K. Nanstad, "Use of Precracked Charpy and Smaller Specimens to Establish the Master Curve," in *Small Specimen Test Techniques*, ASTM STP 1329, ed. W. R. Corwin, S. T. Rosinski, and E. van Walle, American Society for Testing and Materials, 1998.

7. ASME Section XI Task Group on Flaw Evaluation, *Flaw Evaluation Procedures: ASME Section XI*, EPRI NP 719-SR, Electric Power Research Institute, Palo Alto, Calif., August 1978.

8. M. A. Sokolov, "Statistical Analysis of the ASME K_{Ic} Database," *Journal of Pressure Vessel Technology, Transactions of the ASME* **120**, 24–28 (February 1998).

9. E. Morland, *The Effect of Side-Grooving on the Fracture Toughness of A533B-1 Steel in the Transition Regime*, NRL Risley Report, NRL-R-1006(R), Naval Research Laboratory, November 1988.

3. TEST METHOD

3.1 Specimen Designs

The three specimen designs recommended are (1) the standard compact specimen, including all variations described in other American Society for Testing and Materials (ASTM) standards, (2) the three-point bend bar with two cross-section options, and (3) the disk-shaped compact specimen. For all compact specimen designs, the half-height-to-width ratio, H/W, is maintained fixed at 0.6, and the thickness-to-width ratio, B/W, is fixed at 0.5. Two alternative thickness-to-width ratios are allowed for bend bars: B/W = 0.5 and B/W = 1.0. The span-to-width ratio for all bend bars is fixed at S/W = 4.

Despite the fact that several recent ASTM test methods have been modified to allow an expanded range of usable crack aspect ratios, a/W, the present standard retains the traditional $0.45 \leq a/W \leq 0.55$ for specific reasons. In this case, setting the aspect ratio at nominally 0.5 satisfies two needs. First, it maximizes the initial remaining ligament size to maximize the toughness measuring capacity of the specimen prior to constraint loss. Second, it provides a square initial remaining ligament for maximized constraint control. In addition, the basic specimen designs all have dominant bending stress fields, which also benefit constraint control. Specimens that have dominant tension stress fields such as double-edge-notched tension panels, center-cracked tension panels, and surface-cracked tension panels, lack efficiency of constraint control and, as a consequence, such specimens are not recommended for use in transition range fracture toughness evaluations.

3.2 Specimen Preparation

The procedures for specimen preparation are not different from a machining tolerance standpoint than those used in other ASTM fracture mechanics-based standards. However, the precracking practice is far more precisely specified in the present method because it is important to prevent warm prestressing in the specimen precracking process. This is a special concern because tests, for the most part, are performed at temperatures much lower than the precracking temperature. Also taken into account is that $K_{min} = 20$ MPa$\sqrt{m}$ is an experimentally proven lower-bound value of K_{Jc}, obtainable in tests made at extremely low temperatures. Finish sharpening of the fatigue precrack must be conducted sufficiently below K_{min}.

3.3 Alternate Measurement Locations

Because the J-integral is a fracture toughness value inferred from work done on specimens, it is preferable to measure load versus load point displacement in tests. However, in some cases, load point displacement measurements are not conveniently obtained and displacement measured at other locations can be substituted, provided the computational practices are appropriately modified. In the case of three-point loaded bend bars where the crack mouth opening displacement is measured, finite-element (FE) solutions can be used to develop measurement location-specific η_p values. A comparison is made between three independent FE determinations in Appendix C. These solutions have indicated that there is very limited sensitivity of η_p values to material work hardening property, n. However, crack aspect ratio introduces variability into crack mouth η_p. On the other hand, when load point displacement is used, the η_p is essentially constant for both n and crack size variations. An alternative to the FE approach is to develop an expression that can convert crack mouth displacement into load point displacement.[1] FE solutions are used to establish plastic hinge locations as a function of material work hardening and crack aspect ratio. Direct conversion of mouth displacement to load point displacement eliminates the need for development of crack aspect ratio dependent η_p values.

3.4 Test Temperature Estimation

For situations in which the investigator has no prior fracture mechanics data to work with for test temperature selection, the transition curve from standard Charpy V-notch (CVN) specimens can be used to provide some help. The test practice suggests that the 28-J CVN temperature has an approximate correlation to the T_o temperature for 1T size specimens, given by the following equation:[2]

$$T_{1T} = T_{28J} - 18°C \ . \tag{3.1}$$

The median K_{Jc} at $T_{(1T)}$ is predicted to be near 100 MPa√m. There, of course, is significant uncertainty attached to the Eq. (3.1) correlation, due principally to CVN data scatter, but even with this, the range of uncertainty is not sufficient to result in unsuitable test temperature selection. The constant term on the right side of Eq. (3.1) is adjusted in the test method to account for specimen size effects. The objective is to aim for $K_{Jc(med)}$ equal to 100 MPa√m, for all specimen sizes. A special offset of 50°C from T_{28J} has been specified for precracked Charpy specimens that are slow loaded in three-point bend. Here the aim is for $K_{Jc(med)}$ to be below 100 MPa√m. The precracked CVN specimen size will not permit testing to a $K_{Jc(med)}$ of 100 MPa√m, since the result would be an excessive percentage of invalid K_{Jc} values.

A statistical evaluation of the Eq. (3.1) correlation had indicated a standard deviation on the estimate for $T_{o(1T)}$ of 15°C.[2] Given that a one-tail standard normal deviate at 0.15 cumulative probability is only 1.04, one should expect about an 85% probability of finding the estimated test temperature to be no more than 15°C below the temperature of $K_{Jc(med)}$ equal to 100 MPa√m. If the estimated test temperature should happen to be more than 15°C low, the likely penalty is that more than six replicate specimens may be required as stipulated in the standard. The potential for error in test temperature estimated from Eq. (3.1) can also be reduced by testing more than the usual number of CVN specimens sufficient to obtain a good CVN transition temperature curve. Despite a probable appearance of good CVN curve accuracy, there can be significant accuracy improvement to T_{28J} determination by using perhaps double or triple the usual number of standard CVN specimens in the transition range.

3.5 Replicate Specimen Requirements

As previously mentioned, an objective in the establishment of specimen replication requirements is to have acceptable accuracy in T_o determination while at the same time using the fewest number of specimens possible. A study to establish an appropriate number was conducted by Monte Carlo sampling from large data populations. In this study, two large experimentally generated data populations were obtained from a Materials Properties Council/Japanese Society for Promotion of Science round-robin activity.[3] Two test temperatures gave two data populations of about 50 replicate K_{Jc} values. The sample sizes (simulated replication number) selected varied from 3 to 10, taken in increments of one. Each sample size level was repeated 100 times. Hence, for each sample size there would be 100 K_{Jc} median values determined, and the grand average values plus the standard deviation on these $K_{Jc(med)}$ data were determined. The round-robin material was A 508 class 3 plate, and the specimens were 1T compacts sampled at the quarter and three-quarter through-thickness locations. About 18 laboratories were involved, and the entire round-robin activity had been completed well before any ASTM committee development work had been started on test standard E 1921. The two data populations used for the Monte Carlo simulations were for test temperatures of −100 and −75°C.

Table 3.1 shows the results generated at the −100°C test temperature, which also happens to be close to the T_o temperature of the material, namely −109°C. The standard deviation on $K_{Jc(med)}$ determinations was used as the basis for deciding sufficient data replication for the test standard. Note that the standard deviation versus sample size diminishes rapidly at first, then slowing between sample sizes of 5 to 8. A required sample size of 6 seems to be a defensible selection. The data population at −75°C represents a decent magnitude of shift away from the optimum test temperature selection. Those results are shown in Table 3.2. The standard deviation on $K_{Jc(med)}$ has

Table 3.1. Monte Carlo simulation
(100 trials; population, 50 1T C(T) A 508 class 1, three specimens; −100°C test temperature)

Sample size	Population size	Number of trials	$K_{Jc(med)}$ (MPa√m)	Standard deviation (MPa√m)	Total population, −100°C
3	50	100	113.8	12.9	$K_{Jc(med)}$ = 113.0 MPa√m
4	50	100	113.0	10.2	T_o = −109°C
5	50	100	112.5	8.8	
6	50	100	113.8	9.0	
7	50	100	112.5	8.0	
8	50	100	112.5	7.4	
9	50	100	111.9	6.7	
10	50	100	113.3	6.9	

Table 3.2. Monte Carlo simulation
(100 trials; population, 50 1T C(T) A 508 class 1, three specimens; −75°C test temperature)

Sample size	Population size	Number of trials	$K_{Jc(med)}$ (MPa√m)	Standard deviation (MPa√m)	Total population
3	50	100	154.2	16.5	$K_{Jc(med)}$ = 153 MPa√m
4	50	100	154.4	15.0	T_o = −104°C
5	50	100	154.5	12.5	
6	50	100	153.4	11.8	
7	50	100	151.9	11.6	
8	50	100	152.2	11.1	
9	50	100	153.7	9.1	
10	50	100	153.4	8.5	
20	50	100	153.1	6.1	

increased slightly, as might have been expected due to the higher test temperature, but, nevertheless, the recommended sample size of 6 develops a plateau for a consistent compromise level of uncertainty.

3.6 K_{Jc} Calculation

Specimens tested at an appropriate temperature for the determination of T_o will have test records that vary from linear elastic at instability to others that will contain substantial plastic deformation prior to cleavage instability. For consistency of computational practice, all toughness determinations start with computation of J-integral. Because many tests are made at cryogenic temperatures where the experience base on instrumented crack growth measurement techniques is incomplete, the method seeks to de-emphasize the need for accurate measurement of stable crack growth. Consequently, the J-integral calculation is not corrected for slow-stable crack growth.

However, crack growth to the point of crack instability is posttest measurable, and if the visual evidence of growth indicates more than 5% of the initial remaining ligament dimension, then the K_{Jc} value is declared to be invalid and the results are used as censored data in the analysis. A 5% ligament size change will result in about a 2% error in J that in turn corresponds to about 1% error in K_{Jc}. Such an error is insignificant within the perspective of typical transition range data scatter.

For convenience in application, the J-integral at the point of cleavage fracture, J_c, is converted into its equivalent in units of stress intensity factor as follows:

$$K_{Jc} = \sqrt{J_c E} \ . \tag{3.2}$$

The plane stress elastic modulus, E, is used in Eq. (3.2) specifically to avoid the possible overestimate of K_{Jc}. This is because there is no experimental nor analytical basis to show that crack front conditions will always be pure plane strain. It is easy to demonstrate that the use of a plane strain modulus would alter the plastic component of K_{Jc} such that it could increase K_{Jc} up to 5% in some cases. In this method the selection of elastic modulus to be used on experimental work has some importance and the plane strain elastic modulus option is explicity not offered.[4,5]

3.7 Side Groove Effects

Specimen side grooving after fatigue precracking is an option allowed by the standard. Presumably the principal advantage of side grooving is to reduce crack front curvature. Initial information that has been developed on side grooving effects indicate that K_{Jc} values are not significantly altered. Table 3.3 lists some examples from the Heavy-Section Steel Irradiation (HSSI) Program Tenth Irradiation Series.[6] Although these data are few, the evidence is reasonably convincing. Morland (NRL, Risley, United Kingdom) has conducted a more extensive evaluation, testing about 160 compact specimens of A 533 grade B steel.[7] The experiment covered two specimen sizes (1/2T and 1T), three levels of side grooving (0, 20, and 50%), and five test temperatures (−90, −70, −50, −30, and −10°C). Figure 3.1 presents only the data that were of relevance to the present transition range standard. All data points shown are either $K_{Jc(med)}$ or average K_{Jc} when replication was not sufficient for median determinations. Additionally, all median/average K_{Jc} values have been adjusted to 1T equivalence. Here a pattern develops where the potential impact of side grooving is unambiguously displayed. Side grooving has no significant effect on $K_{Jc(med)}$ for values less than 200 MPa√m. Above 200 MPa√m, side grooving begins to make some difference. Tabulations of crack growth in Reference 6 indicated that many of the specimens tested at

Table 3.3. Comparison of K_{Jc} (MPa√m) for 1T compact specimens with and without side grooves

Test temperature (°C)	Beltline		Nozzle	
	With side grooves	Without side grooves	With side grooves	Without side grooves
0	197	140	220	145
	274	256	229	168
	317	296		300
		a		
		a		
–25	119	120	87	84
	133	139	147	96
	193	139		97
	267	143		114
		151		120
				121

[a]R curve.

temperatures of −30 and −10°C where $K_{Jc(med)}$ > 200 MPa√m, had significant slow-stable crack growth prior to fracture. Hence, it appears that intrinsic K_R curve effects via side grooving had influenced the dK_J/da development rate and consequently the K_{Jc} values. In particular, the influence of side grooving can show strong impact on low upper-shelf materials. Figure 3.2 gives an example. Low upper-shelf materials develop onset of slow-stable growth at low K_J values and the dJ/da fracture toughness development rate is highly influenced by the side grooving. Hence, it follows that low upper-shelf materials are more likely to present difficulties when testing to obtain T_0 temperatures. The A 533 grade B steel used by Morland (Fig. 3.1) had the more typical upper-shelf fracture toughness; consequently, the impact of the side grooving was delayed to high toughness values. Examples for low toughness steels are presented in Sections 2 and 4.

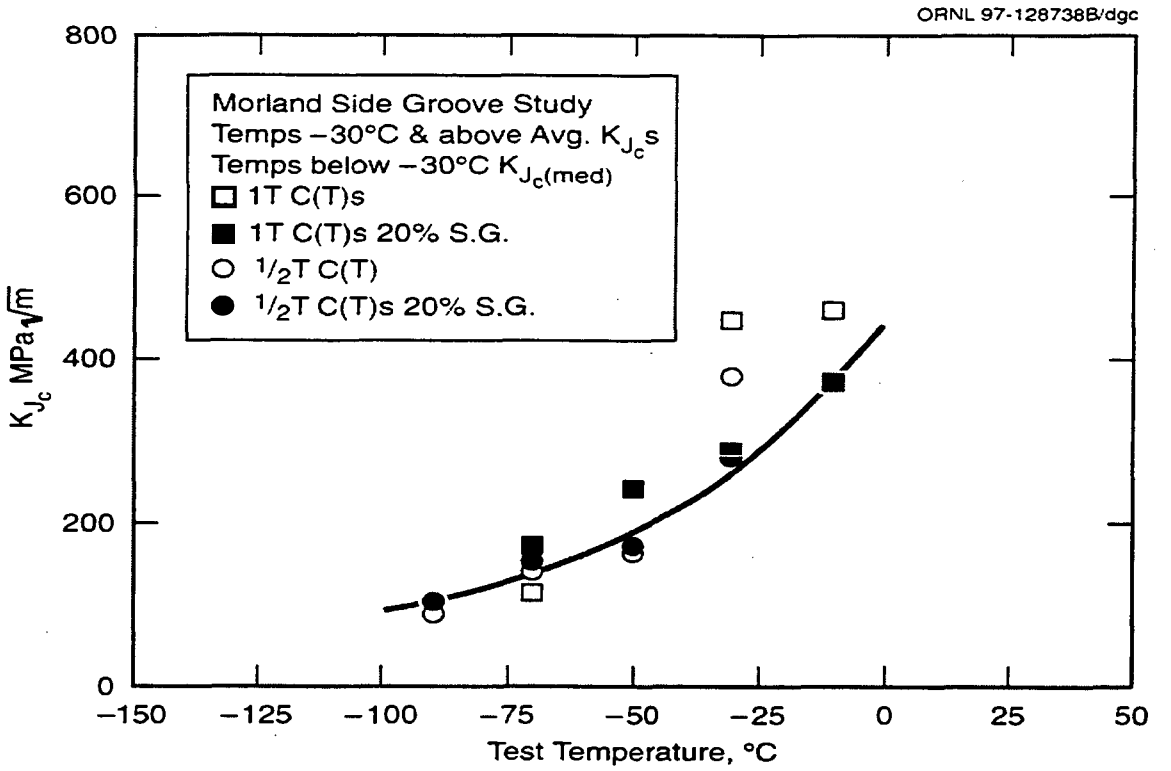

Fig. 3.1. Data from side-groove study of Morland. Median K_{Jc} from data after normalization to 1T equivalence.

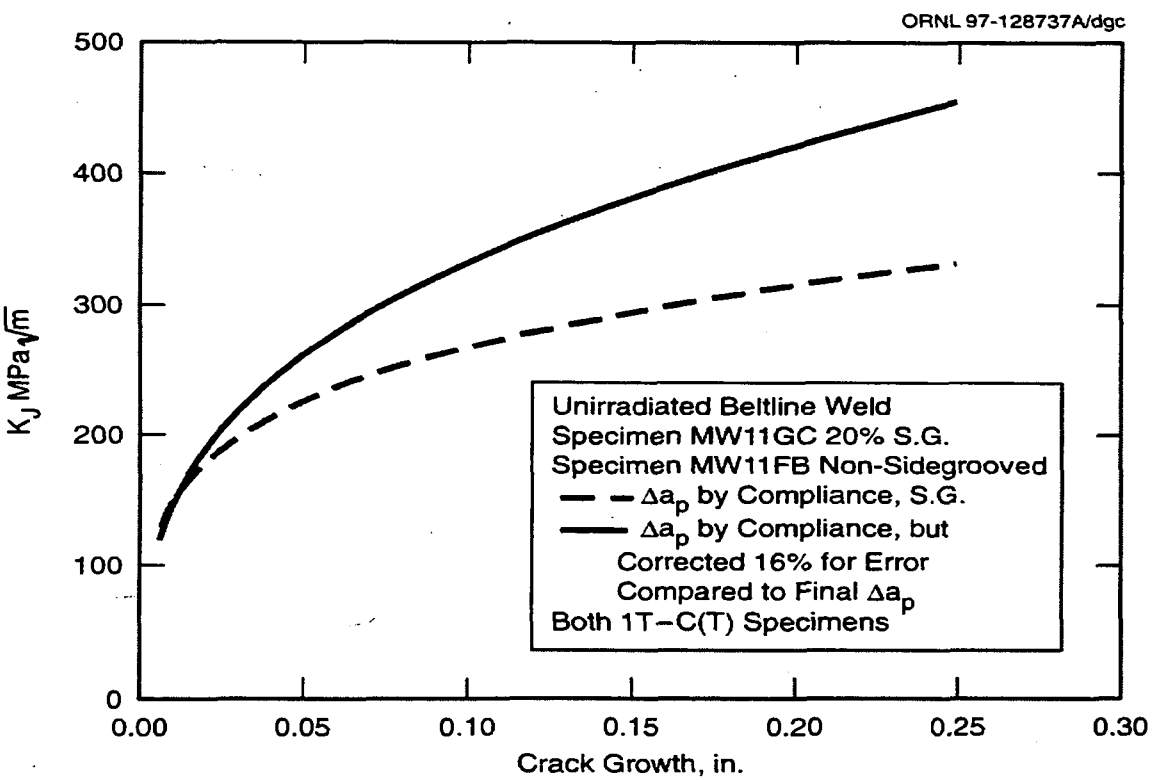

Fig. 3.2. R-curves of a low upper-shelf weld metal, comparing straight-side and side-grooved specimens.

3.8 References

1. J. H. Underwood, E. J. Troiano, and R. T. Abbott, "Simpler J_{Ic} and Data Analysis Procedures for High-Strength Steels," pp. 410–21 in *Fracture Mechanics: Twenty-Fourth Volume, ASTM STP 1207*, ed. J. D. Landes, D. E. McCabe, and J. A. M. Boulet, American Society for Testing and Materials, 1994.

2. K. Wallin, "A Simple Theoretical Charpy V-K_{Ic} Correlation for Irradiation Embrittlement," in *Innovative Approaches to Irradiation Damage and Fracture Analysis*, PVP-Vol. 170, American Society of Mechanical Engineers, New York, July 1989.

3. W. A. Van Der Sluys and M. T. Miglin, "Results of MPC/JSPS Cooperative Testing Program in the Brittle-to-Ductile Transition Region," pp. 308–24 in *Fracture Mechanics: Twenty-Fourth Volume, ASTM STP 1207*, ed. J. D. Landes, D. E. McCabe, and J. A. M. Boulet, American Society for Testing and Materials, 1994.

4. ASTM Standard E 813-89, "J_{Ic}, A Measure of Fracture Toughness," in *Annual Book of ASTM Standards*, Vol. 03.01, American Society for Testing and Materials, 1996.

5. ASTM Standard E 1737-96, "J-Integral Characterization of Fracture Toughness," in *Annual Book of ASTM Standards*, Vol. 03.01, American Society for Testing and Materials, 1996.

6. D. E. McCabe, R. K. Nanstad, S. K. Iskander, and R. L. Swain, *Unirradiated Material Properties of Midland Weld WF-70*, USNRC Report NUREG/CR-6249 (ORNL/TM-12777), January 1994.

7. E. Morland, *The Effect of Side-Grooving on the Fracture Toughness of A533B-1 Steel in the Transition Regime*, NRL Risley Report, NRL-R-1006(R), Naval Research Laboratory, November 1988.

4. VALIDITY REQUIREMENTS

4.1 Selection of a Numerical Value, M, for Controlling Constraint

Test conditions among replicate specimens must be reasonably identical before the data can be analyzed by a Weibull model. For fracture mechanics data, the crack tip constraint must be reasonably controlled over the full range of the data. In most fracture mechanics test methods, constraint is controlled by limiting the crack tip opening displacement (CTOD) relative to the initial remaining ligament dimension, b_o. The CTOD is not always measured directly, since it is often more convenient to deal with its analytical equivalent, the J-integral. These two fracture toughness parameters are viewed as being interchangeable, according to the following linear relationship:

$$J = m\,\sigma_{ys}\,(\mathrm{CTOD})\ , \tag{4.1}$$

where σ_{ys} is material yield strength and the coefficient m in Eq. (4.1) is used to scale the linear relationship. Values of m can be calculated by finite-element analysis or otherwise can be determined experimentally. When J is substituted for CTOD, then specimen size requirements are set by the following inequality:

$$B,\ b_o \geq M\left(J/\sigma_{ys}\right)\ , \tag{4.2}$$

where dimension B is specimen thickness and b_o is the initial remaining ligament size. The non-dimensional coefficient M is again a factor established either by experiment or by finite-element analysis. This coefficient is used to establish specimen size requirements and is applied in several ASTM standard methods.[1-3] Different M values are used, depending on the primary objective of the standard, and the physical significance attached to the toughness parameter. For example, E 1737-96 and E 1152-95 use M = 20 for J-R curve development, and E 1737-96 and E 813-89 use M = 25 for plane strain J_{Ic} determination. In the case of cleavage fracture, E 1737-96 uses M = 200 to qualify individual specimen J_Q values as J_c.

For the present ductile-brittle transition range standard, the relationship given by Eq. (4.2) is applied in a rearranged form by combining it with Eq. (3.2), giving:

$$K_{Jc(limit)} = (E b_o \sigma_{ys}/M)^{1/2} . \tag{4.3}$$

In this case, specimen size is assumed to be predetermined by the investigator, and the objective is to calculate a fracture toughness limitation for the specimen size being used. To arrive at an appropriate M value for the transition range standard, the results from both numerical analyses and from experimental data were considered. In the first case, the three-dimensional finite-element results of Nevalainen and Dodds[4] were considered. Both the compact, C(T), and three-point bend, SE(B), geometries had been analyzed. Work hardening, n, was modeled using the Ramberg-Osgood power law, selecting three n value levels. The practical range for engineering materials covered was n = 5, 10, and 20. For the analyses, material strength had been assumed to be constant over the range of n values, using the nondimensional ratio of $E/\sigma_o = 500$. The denominator, σ_o, is material proportional limit, which is known to have a nonlinear relationship to material yield strength. Values of J are calculated for a modified boundary layer model of a crack tip region for three-dimensional specimens. The near crack tip volume is subjected to a maximum principal tensile stress that is not to exceed a specified value. When the two values of J differ by more than 20%, constraint is assumed to have diminished sufficiently to cause elevation of the measurable toughness with respect to a full constraint value. In Reference 4 it was determined that SE(B) specimens require higher values of M than the C(T) specimens. Table 4.1 lists the critical M values, M_{ND}, declared for SE(B) specimens. This table lists the Nevalainen-Dodds M_{ND} values based on fixed material strength at $E/\sigma_o = 500$. These M_{ND} values are adjusted to account for different material yield strengths that better match up with the strain-hardening n values.

Table 4.1. Adjustments to Nevalainen-Dodds M_{ND} values for single-edge-notched bend specimens (a/W = 0.5)

R-O (n values)	σ_{ys} (ksi)	σ_{ys}/σ_o	E/σ_o adjusted	M_{ND}	M_{adj}
5	54	1.20	667	25	40
10	64	1.08	506	55	60
20	131	1.01	231	115	53

Recognizing that n values and material strength properties have significant interactive characteristics, and that M_{ND} values tend to scale linearly in proportion to strength, leads to the following adjustment formula:

$$M_{adj} = (\sigma_{ys}/\sigma_o) \frac{(E/\sigma_o)\,adj}{500} (M_{ND}) \ . \tag{4.4}$$

The adjusted M values listed in the last column of Table 4.1 tend to suggest a compromise M value from 3D analysis of about 50.

It is also possible to rationalize an alternative M_{adj} equation. If the relationship between material yield strength and n values that had been reported by Rosenfield and Hahn[5] are used, the outcome is slightly changed. Their experiments were made on steels ranging in yield strength from 25 to 400 ksi. Table 4.2 reports median correlation values taken from a graph in this paper.

Table 4.2. Examples of material yield strength and median n values[a]

n	Yield strength (ksi)	Yield strength (MPa)	Equation (4.5) M_{adj}
5	51	350	29.4
10	101	700	29.7
20	197	1289	32.1

[a]A. R. Rosenfield and G. T. Hahn, "Numerical Description of the Ambient Low-Temperature and High Strain Rate Flow and Fracture Behavior of Plain Carbon Steel," pp. 962–80 in *Transactions of the ASM* vol. 59, 1996.

Noting in Table 4.1 that the following equality is a reasonable approximation, namely $M_{ND}/500 \cong n/100$, Eq. (4.4) can be simplified:

$$M_{adj} \cong \frac{E}{\sigma_{ys}} \left(\frac{n}{100} \right) \ . \tag{4.5}$$

Data scatter shown in Reference 5 on the n value versus the material yield strength correlation is quite broad so that details such as assuming a σ_{ys}/σ_o ratio contribution to the adjustment is rendered pointless. Hence the M_{ND} to M_{adj} relationship in Eq. (4.5) appears to be sufficiently precise (see the alternate solutions in Table 4.2). M_{adj} of 30 can also be argued on the basis of interpretive judgment.

The experimental alternative to numerical analysis uses a visually based postulate that a change in constraint will create a separate family of K_{Jc} data perceptibly different than the constraint-controlled data distribution. Oftentimes, Constraint loss becomes apparent when data depart from the linear relationship of normal Weibull plots. Two examples are shown in Figs. 4.1 and 4.2. Both data sets had been developed using precracked Charpy specimens that had approximately 4.6-mm (0.18-in.) nominal initial remaining ligament size. Additionally, both materials are low upper-shelf steels. The dashed square data points are cases where K_{Jc} exceeded $K_{Jc(limit)}$ based on the M values of 30. A third example is shown in Fig. 4.3, where the data were developed using 1/2T SE(B) specimens that had B × 2B cross section; thus the initial remaining ligament dimensions were more than twice that of the precracked Charpy specimens.[6] In addition, the A 36 steel tested was not a low upper-shelf material. In the Fig. 4.3 case, the point of departure from the Weibull slope of 4 was at M = 35.

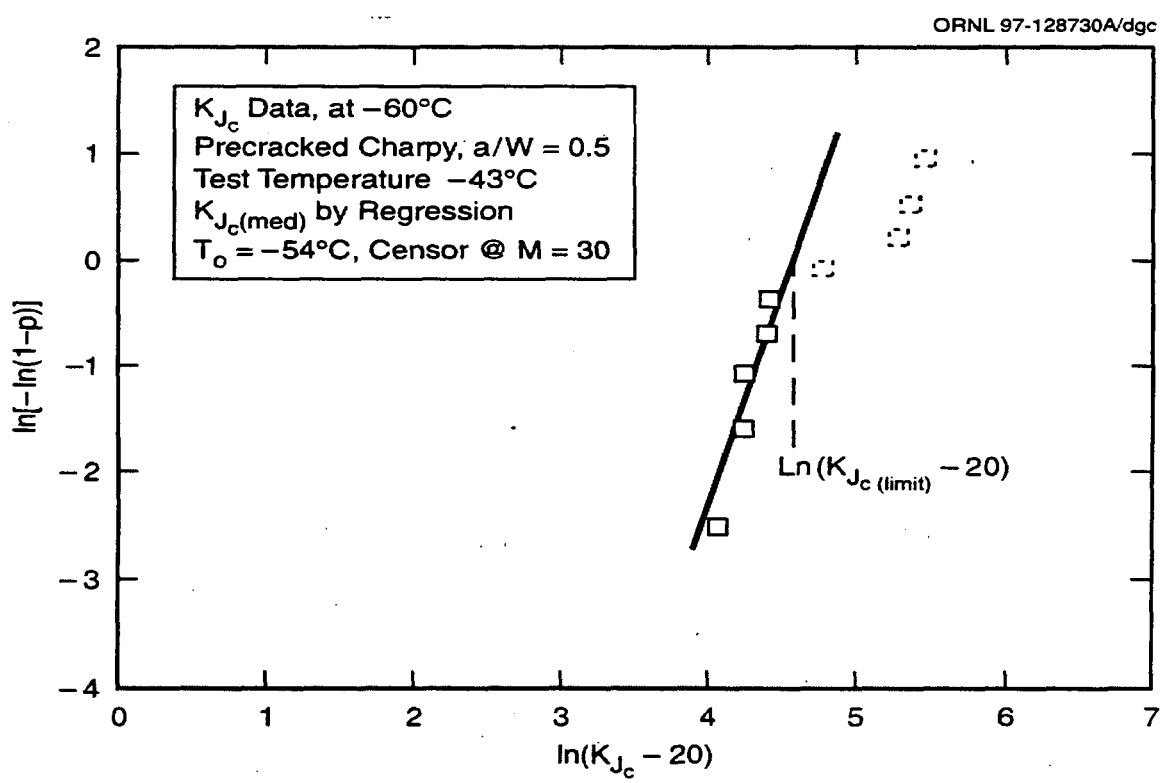

Fig. 4.1. Weibull plot of K_{Jc} data obtained from precracked Charpy specimens of irradiated WF-70 weld metal.

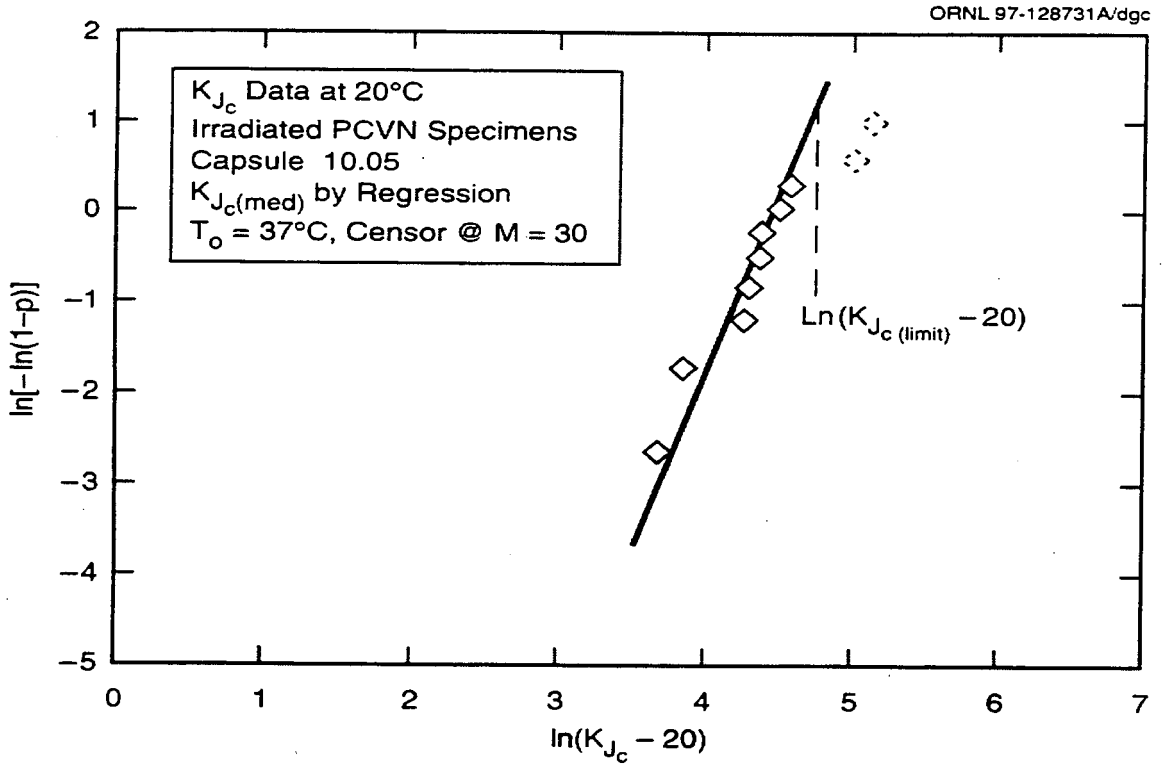

Fig. 4.2. Weibull plot of K_{Jc} data obtained from precracked Charpy specimens of as-received WF-70 weld metal.

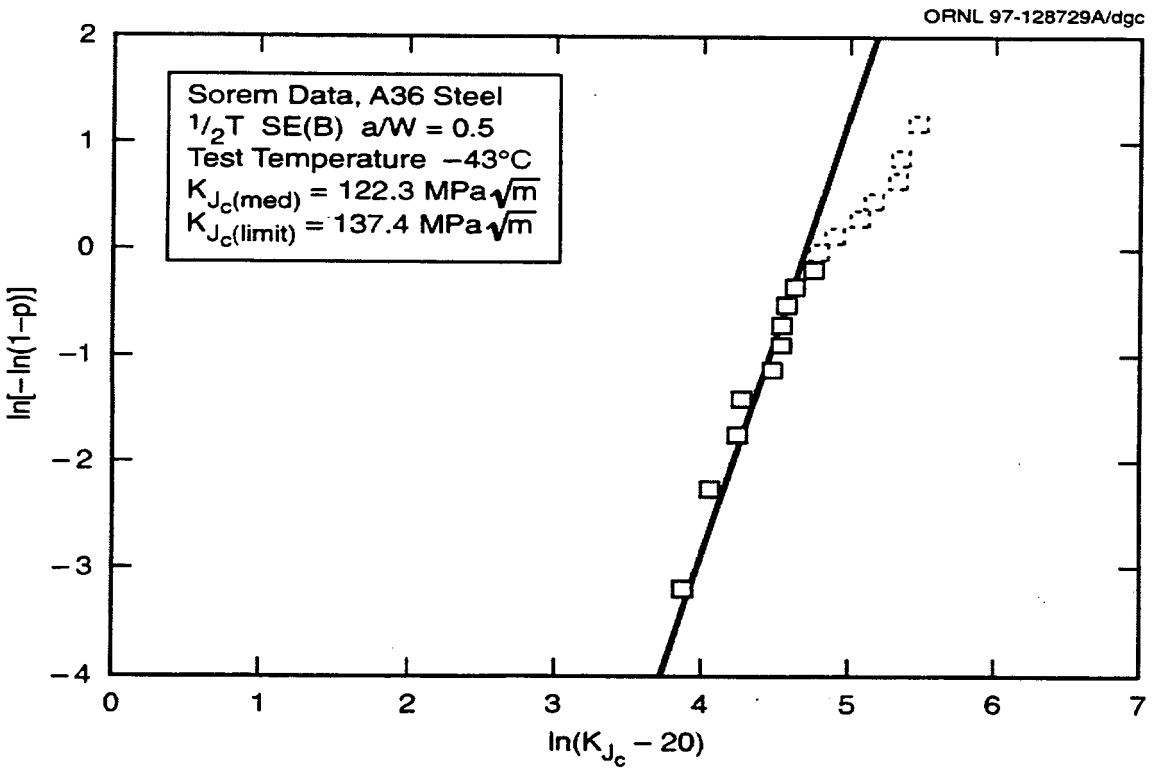

Fig. 4.3. Weibull plot of K_{Jc} data on A 36 steel. (*Source:* W. A. Sorem, R. H. Dodds, Jr., and S. T. Rolfe, "An Analytical Comparison of Short Crack and Deep Crack CTOD Fracture Specimens of an A 36 Steel," *WRC Bulletin 351*, February 1990.

From the experimental evidence developed to date, the M value of 30 appears to be sufficient for control of data input into Weibull analyses. One can argue for the M value of 50 as being theoretically more accurate from a constraint control point of view, but a $K_{Jc(limit)}$ set by such an argument impacts statistical analyses when data censoring is used and consequently the T_o temperature that is determined.

4.2 Rationale for Setting Crack Growth Limits

A second validity requirement on K_{Jc} values imposed is that there shall be no more than 5% of crack growth, relative to initial remaining ligament, prior to cleavage instability. There are two reasons for setting this limitation, one being that J-integral determinations without crack growth adjustment begin to show significant error at about this point, and the second being that the impact of R-curve effects on K_{Jc} values, even in low upper-shelf materials, is acceptable up to this point. This crack growth limitation allows the side-grooving practice to be optional in the present practice.

Having imposed this second validity requirement, it was of value to determine if the utility of the standard method might be crippled by a combined interaction between the two criteria. Four example materials were selected for evaluation on the basis of their differences in K_R-curve toughness. The materials ranked from best to worst K_R-curve toughness are A 533 grade B base metal,[7] submerged-arc weld in A 533 grade B base plate,[8] 2.25Cr-1Mo base metal,[9] and a low upper-shelf weld metal in A 508 class 2 base plate. Figure 4.4 shows by bar graph comparison the range of valid K_{Jc} values set by the constraint limit (cross-hatched) and by the stable crack growth limit (open). For constraint control, the top of the bar is dictated by $K_{Jc(limit)}$ and it is assumed to be a 98% cumulative probability K_{Jc} value. The bottom of the bar was calculated for the corresponding 2% cumulative probability. For the crack growth limit, the K_R-curve toughness after 5% of stable crack growth was used for the top K_{Jc}value of the bar. All such limit values are specimen size dependent so that each material was evaluated for a 1/2T specimen and a 4T specimen. This covers the range of specimen sizes typically used in laboratory experiments.

Except for one material, the bottom line conclusion from Fig. 4.4 is that the two validity requirements on K_{Jc} data do not have detrimental interfering characteristics; that is, except for all but low upper-shelf steels. Here, R-curve development dominates data validity, and, as such, the interference voids any advantage from increasing specimen size to improve K_{Jc} capacity. Hence, the master curve toughness trend is not followed at higher test temperatures. Low upper-shelf materials present a special challenge in T_o determination and master curve establishment. This issue is the next topic covered.

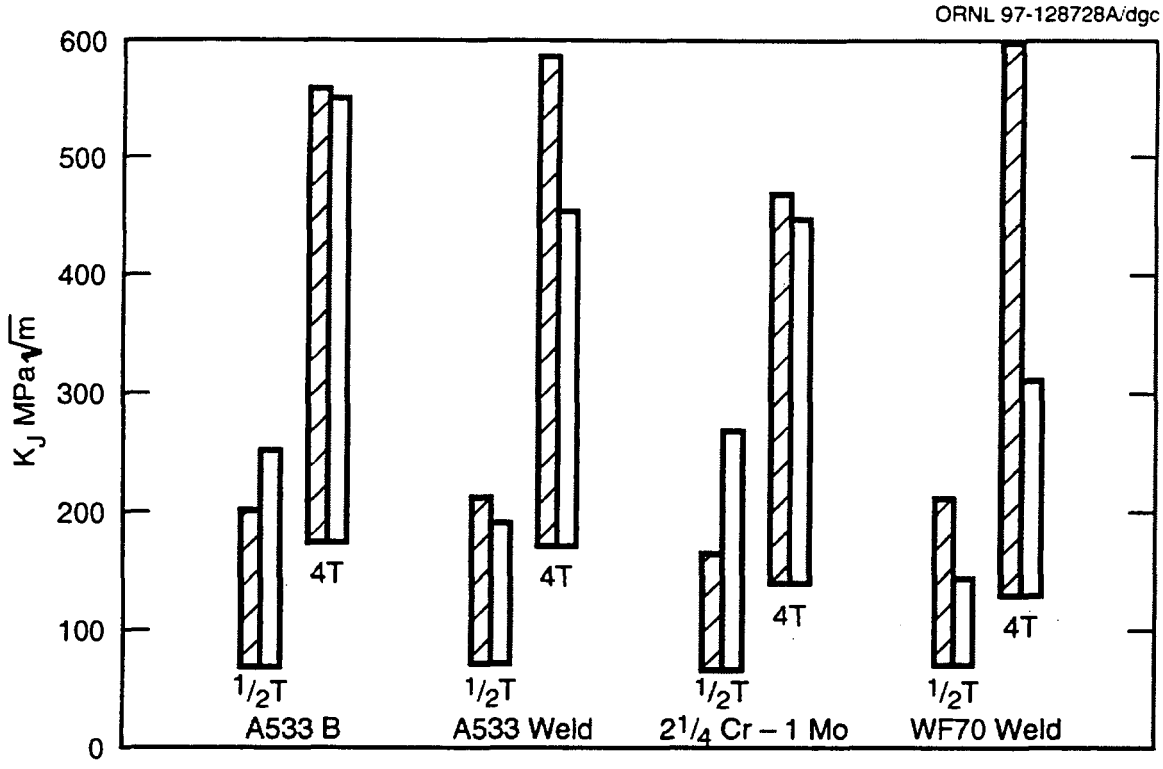

Fig. 4.4. Range of valid data for two test specimen sizes, 1/2T and 4T. Two K_{Jc} data validity criteria; constraint (cross-hatched) and 5% crack growth limitation (open) applied to four materials.

4.3 Impact of Low Upper-Shelf Materials on Establishment of Master Curve

As mentioned previously, easy slow-stable crack growth at low K_J values can create several problems in master curve development. Some low upper-shelf materials display K_R-curve upper plateau just marginally above the preferred 100 MPa$\sqrt{m}$ toughness level at which T_o temperature is most accurately determined. Side grooving versus not side grooving also becomes an important consideration. Data distributions can become distorted if part of a data sampling fails by ductile instabilities, as opposed to onset of cleavage fracture. Testing at temperatures near to upper shelf will also show diminished weakest-link behavior and specimen size effects will tend to vanish. All of these difficulties had developed to certain degrees in the plot shown in Fig. 4.5.

The weld metal tested is WF-70, a Babcock and Wilcox designation that identifies the heat of weld wire and flux lot used in fabrication.[10] It is known as a low upper-shelf metal. K_{Jc} values were determined in large numbers and were spread over a sufficiently wide temperature range extending into the upper-shelf region. K_J-R curves were made from side-grooved 1T compact specimens at 0, 150, and 288°C. Figure 4.6 points out the difference in fracture toughness level that is likely to develop after 5% of slow-stable crack growth in a 1T compact specimen.

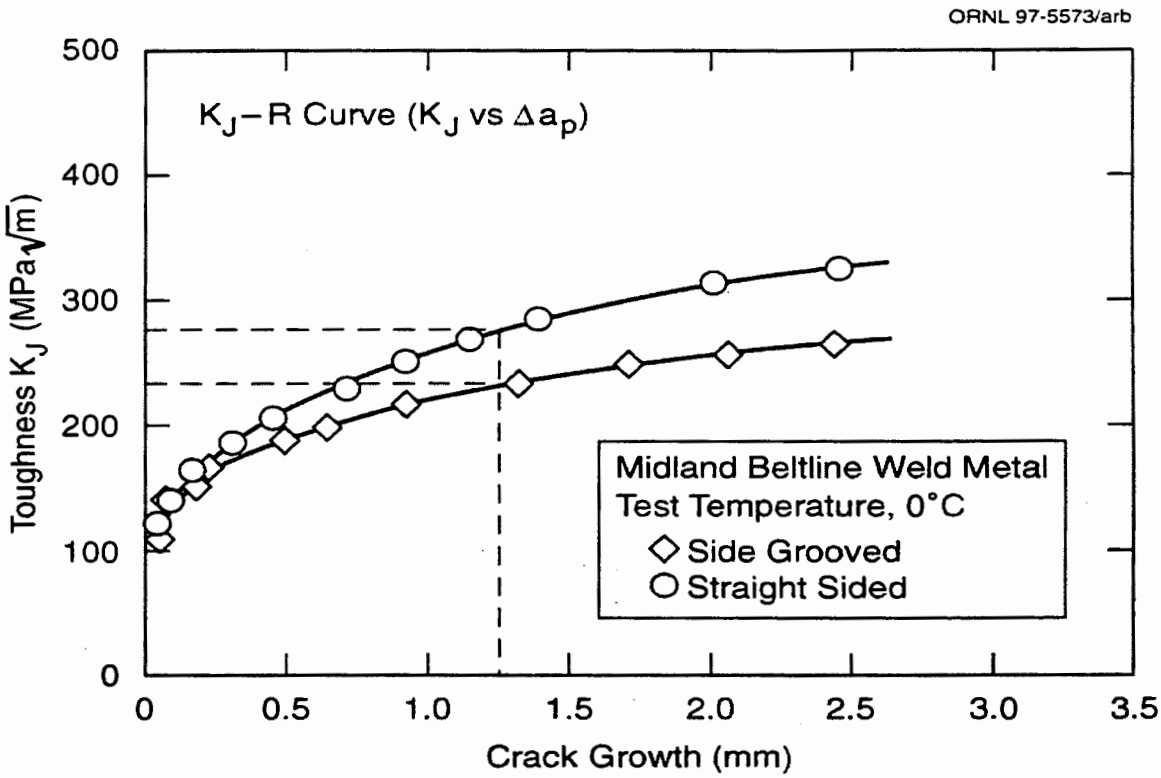

Fig. 4.5. Theoretical limitations on K_{Jc} data based on K_J ductile instability behavior of low upper-shelf steels.

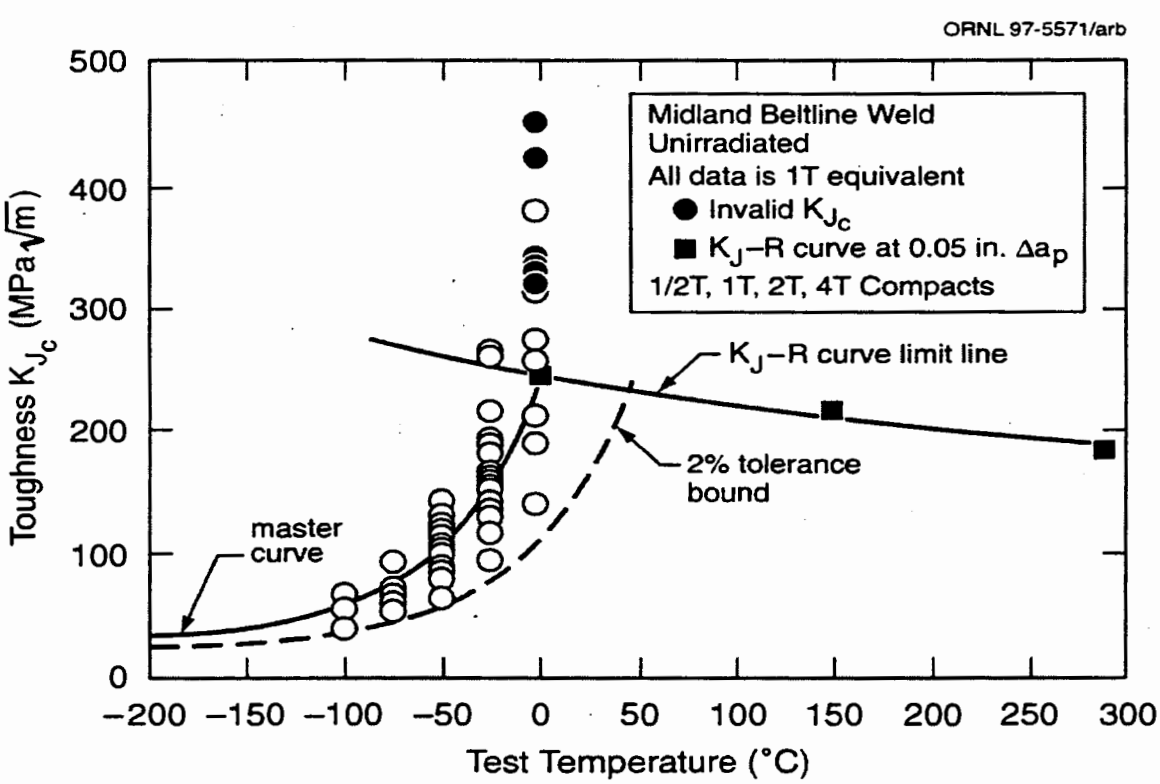

Fig. 4.6. Effect of side grooving practice on the ductile tearing resistance of a low upper-shelf weld metal.

Ductile instabilities are possible at that point in side-grooved specimens because the K_R-curve slope is substantially reduced. On the other hand, specimens of the same material that have not been side grooved would probably have no ductile instabilities at or above 300 MPa√m. The filled square data points in Fig. 4.5 are for K_J at 5% of crack growth on the R-curve for side-grooved specimens. The curve connecting these points crosses the master curve at a toughness level where interpretation difficulties begin. Focusing on the data at 0°C, there were nine 1T compact specimens, six of which were not side grooved and the data from three of these excessively exceeded the K_J-R curve limit line. The three highest K_{Jc} values shown at 0°C came from non-side-grooved 2T compact specimens and these K_{Jc} values had been size adjusted upward to 1T equivalence. Hence, most of the data generated at 0°C were affected by the previously mentioned special problems, namely, K_R curve differences and size effect adjustments in a temperature range where size effects tend to vanish. Once again, low upper-shelf materials have interjected difficulties into the test practice that will require some future considerations and adjustments that have not been addressed at the present time.

4.4 Pop-ins

Crack pop-in is a phenomenon that is most often observed in tests made in the lower half of the transition range. Pop-in crack initiation occurs due to a cleavage instability, and crack arrest develops when the built-up elastic strain energy in a specimen cannot sustain the running cleavage crack propagation. The evidence for this assertion can be found in data sets that contain a fair mixture of pop-ins and unarrested cracks among unambiguous K_{Jc} determinations. The irradiated specimens of the ORNL HSSI Fifth Irradiation Series provide a good example.[11] About 110 C(T) specimens had been tested after irradiation to a fluence of 1.5×10^{19} n/cm^2. Four test temperatures indicated in Fig. 4.7 were used. About 28 specimens had shown crack pop-in. This figure represents only one of the two materials that contributed to this observation. The pop-in data appear to be part of the data scatter band, favoring the lower end because of the previously mentioned stored elastic energy situation. This evidence suggests that pop-ins cannot be excluded from consideration as a part of data populations. The difficulty in incorporating pop-in values is to distinguish a genuine pop-in from test record artifacts that develop from other sources. Common artifact sources are slight fixture misalignments or ice buildup at points in the loading linkage. Generally, test record discontinuities from such artifact events are small, usually corresponding to less than 1% equivalent crack advance. Hence, the following compliance/crack increment relationship was adopted for evaluations:

$$\Delta a_i = \frac{b_o}{\eta}\left(\frac{C_i - C_o}{C_i}\right), \tag{4.6}$$

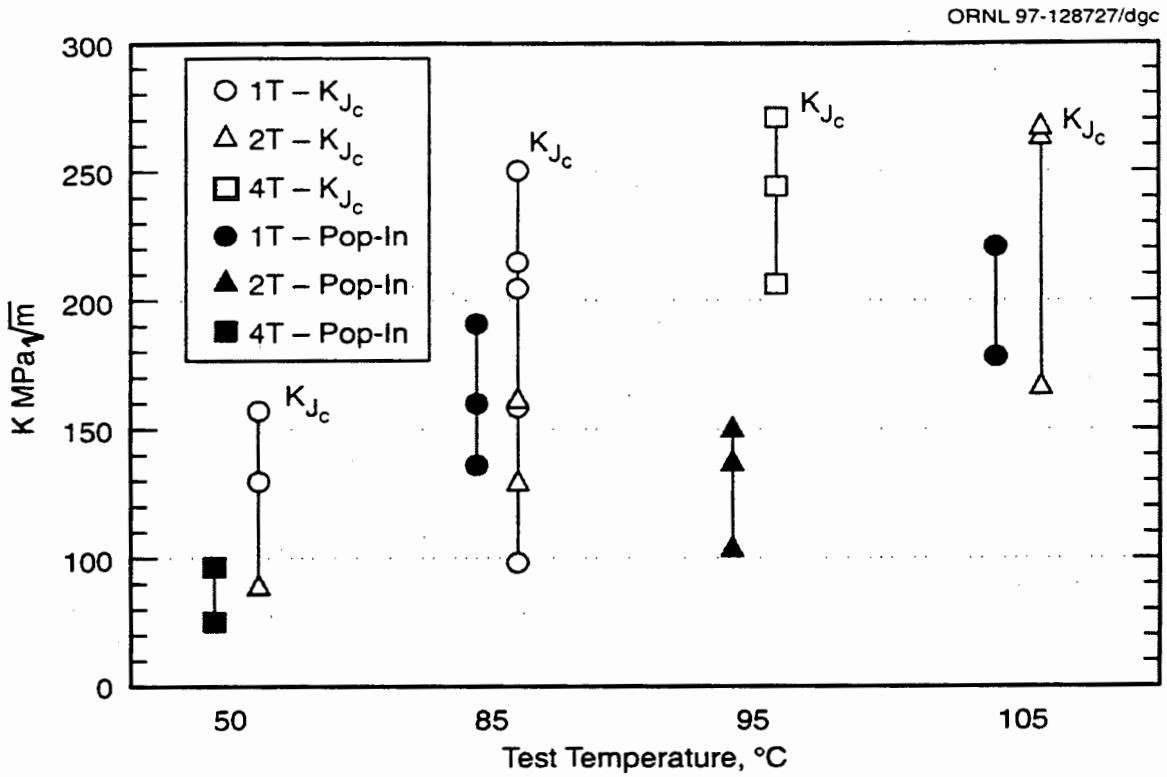

Fig. 4.7. K_{Jc} at pop-in versus K_{Jc} at full cleavage for irradiated compact specimens from the ORNL HSSI Fifth Irradiation Series.

where C_o and C_i represent before and after pop-in compliance values ($\Delta\upsilon/\Delta P$), η is the dimensionless coefficient used to calculate J-integral from plastic work done on specimens, and b_o is the initial remaining ligament of the specimen. Apparent pop-ins can be ignored when $\Delta a_i < 0.01\ b_o$. Substituting this into Eq. (4.6) gives:

$$\frac{C_i}{C_o} = 1 + 0.01\eta\left[\frac{W}{a_o} - 1\right]^{-1} . \tag{4.7}$$

Most anomalous pop-in events will occur in the initial linear elastic part of the load-displacement test record where the evaluation of C_i/C_o ratio can be determined by load ratios, as illustrated in Fig. 4.8. When load-displacement records develop nonlinear plastic deformation, the likelihood of events being real pop-ins increases. At the same time, the establishment of the C_i/C_o ratio also becomes a little more complex than the example shown in Fig. 4.8.

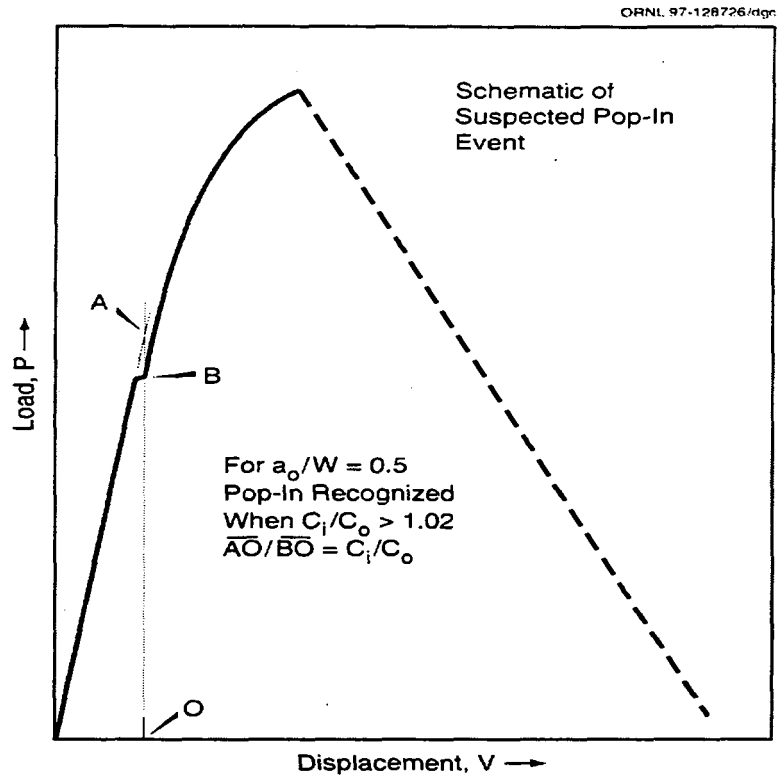

Fig. 4.8. Schematic of pop-in magnitude. Construction lines $\overline{AO}$ and $\overline{BO}$ are used to calculate crack advance.

4.5 References

1. ASTM Standard E 813-89, "J_{Ic}, A Measure of Fracture Toughness," in *Annual Book of ASTM Standards*, Vol. 03.01, American Society for Testing and Materials, 1996.

2. ASTM Standard E 1737-96, "J-Integral Characterization of Fracture Toughness," in *Annual Book of ASTM Standards*, Vol. 03.01, American Society for Testing and Materials, 1996.

3. ASTM Standard E 1152-95, "Determining J-R Curves," in *Annual Book of ASTM Standards*, Vol. 03.01, American Society for Testing and Materials, 1996.

4. M. Nevalainen and R. H. Dodds, *Numerical Investigation of 3-D Constraint Effects on Brittle Fracture in SE(B) and C(T) Specimens*, UIUL Eng-95-2001, University of Illinois, Champaign-Urbana, 1995.

5. A. R. Rosenfield and G. T. Hahn, "Numerical Descriptions of the Ambient Low-Temperature and High Strain Rate Flow and Fracture Behavior of Plain Carbon Steel," pp. 962–80 in *Transactions of the ASM*, Vol. 59, 1966.

6. W. A. Sorem, R. H. Dodds, Jr., and S. T. Rolfe, "An Analytical Comparison of Short Crack and Deep Crack CTOD Fracture Specimens of an A 36 Steel," *WRC Bulletin 351*, February 1990.

7. D. E. McCabe, *A Comparison of Weibull and β_{Ic} Analysis of Transition Range Fracture Toughness Data*, USNRC Report NUREG/CR-5788 (ORNL/TM-11959), January 1992.

8. R. K. Nanstad, F. M. Haggag, D. E. McCabe, S. K. Iskander, K. O. Bowman, and B. H. Menke, *Irradiation Effects on Fracture Toughness of Two High-Copper Submerged-Arc Welds, HSSI Series 5*, USNRC Report NUREG/CR-5913, Vol. 1 (ORNL/TM-12156/V1), October 1992.

9. K. Wallin, "Statistical Aspects of Constraint with Emphasis on Testing and Analysis of Laboratory Specimens in the Transition Region," pp. 264–88 in *Constraint Effects in Fracture, ASTM STP 1171*, ed. E. M. Hackett, K. H. Schwalbe, and R. H. Dodds, American Society for Testing and Materials, 1993.

10. D. E. McCabe, R. K. Nanstad, S. K. Iskander, and R. L. Swain, *Unirradiated Material Properties of Midland Weld WF-70*, USNRC Report NUREG/CR-6249 (ORNL/TM-12777), January 1994.

11. D. E. McCabe, *Evaluation of Crack Pop-Ins and the Determination of Their Relevance to Design Considerations*, USNRC Report NUREG/CR-5952 (ORNL/TM-12247), February 1993.

5. MASTER CURVE PARAMETER ESTIMATION

5.1 Applied Statistical Methods

This section contains the background information on statistical methodologies that have been applied to the establishment of the standard. Topics covered are the determination of standard deviation, selection of the maximum likelihood method for fitting a scale parameter, K_o, and determination of an optimum test temperature range.

5.2 Standard Deviation

The scatter model associated with the master curve is essentially a three-parameter Weibull distribution with two of the parameters fixed. As such, it has certain statistical characteristics represented by gamma functions, Γ, as presented in Eq. (5.1):[1]

$$\sigma_{K_I-K_{min}} = (K_o - K_{min}) \cdot \sqrt{\Gamma(1.5)-\Gamma(1.25)^2} = 0.254 \cdot (K_o - K_{min})$$

$$K_{0.5} - K_{min} = (\ln 2)^{1/4} (K_o - K_{min}) = 0.912 \cdot (K_o - K_{min})$$

$$\bar{K}_I - K_{min} = (K_o - K_{min}) \cdot \Gamma(1.25) = 0.906 \cdot (K_o - K_{min}) \tag{5.1}$$

$$\sigma_{K_I-K_{min}} = (\bar{K}_I - K_{min}) \cdot \sqrt{\frac{\Gamma(1.5)}{\Gamma(1.25)^2} - 1} = 0.28 \cdot (\bar{K}_I - K_{min}) ,$$

where $\bar{K}_I$ and $K_{0.5}$ are the mean and median values of fracture toughness, respectively, at the test temperature and Γ is a function that can be obtained in mathematical handbooks. The most important information in Eq. (5.1) is that the mean and median toughnesses are essentially the same ($\approx 0.91 \cdot [K_0-K_{min}]$) and that the characteristic scatter has a 28 % standard deviation with respect to both.

5.3 Small Sample Statistics

Usually, fracture toughness data sets correspond, at any single temperature, to less than 30 results. Thus the sets represent small samples from a statistical point of view. Small samples cannot describe the actual distribution accurately without the aid of additional information. One can state that, if the sample size is less than 30 and no additional information is available, no attempts to fit a specific distribution to the data should be made. Even if an apparently good description of the data is obtained without the aid of additional information, the fitted distribution can still be much in error. For small sample data sets, the only independent estimate with good accuracy is the estimate of the mean. This is the main reason why the master curve method, with the aid of additional information, fixes all but one parameter, the parameter related to the mean. As an example of the reliability of small sample data, Fig. 5.1 shows the reliability in terms of sample size, using failure probability coordinates.[2] For samples of four different sizes, n, all represented by the straight lines in Fig. 5.1, any results falling within the 5 and 95% confidence bands is reasonably possible. It is clear from the figure that any attempt to estimate the Weibull slope or minimum value from small data sets is precarious. Even with a sample of 100, the estimate of the minimum value will have a considerable uncertainty. The only sensible approach is to fix all but one parameter. The confidence limit curves in Fig. 5.1 are plotted by using a set of continuous empirical functions to approximate the solution to Eq. (5.2), discussed below, for P_{rank}, with i, n, and the confidence level z′

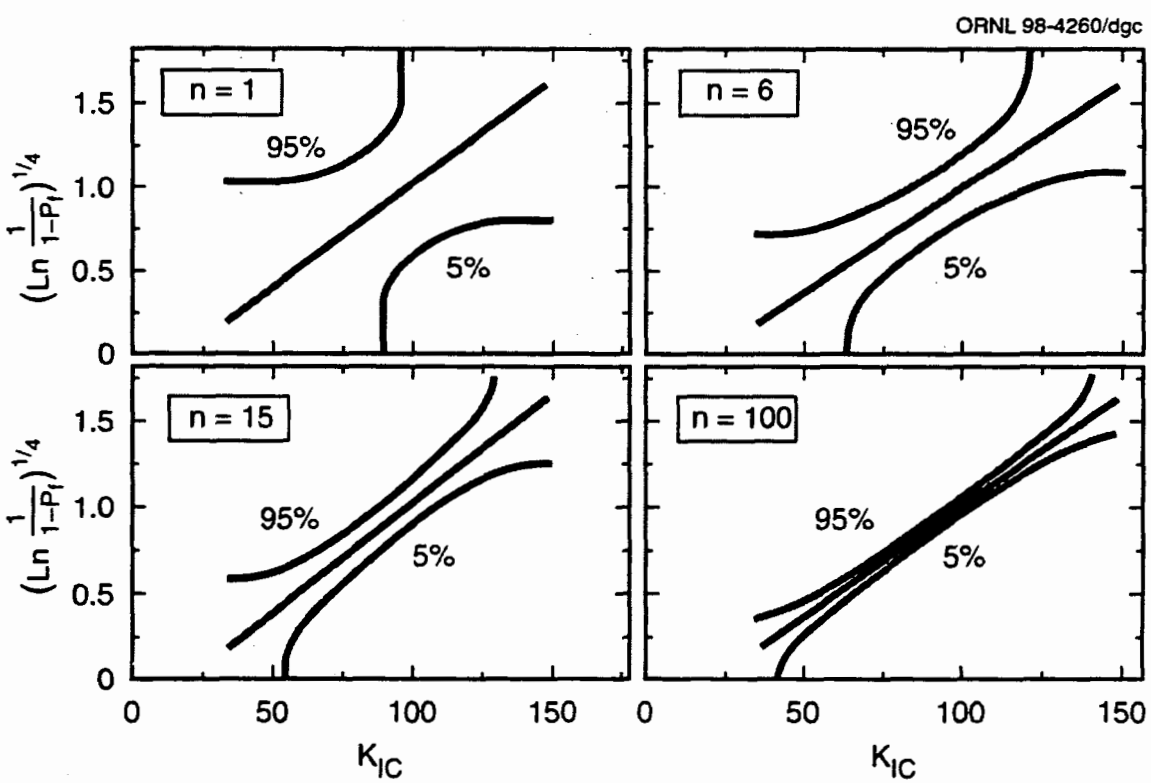

Fig. 5.1. Reliability of small sample data sets of size n, when expressed in cumulative probability coordinates.

specified. The limit curves in Fig. 5.1 represent both one-sided confidence limits on cumulative probability for given values of z′, i, and n, and one-sided confidence limits on toughness for given values of z′, n, and median cumulative probability.

5.4 Least Squares Estimation

There are several possible methods of estimation that can be applied to determine the scale parameter, K_0. The simplest way would be to just calculate the mean and then transform this to K_0 with Eq. (5.1). This does not, however, allow for any kind of censoring and is therefore not the best approach for analysis of fracture toughness data. Another obvious method is the one based on least squares estimation. However, even though this method allows for a simple form of upper-end censoring, it contains a weakness; i.e., it involves the use of rank probability estimates. These are estimates of the cumulative probabilities associated with the rank order numbers of each of the data points, the rank order numbers, i, being determined by listing the data in order of ascending value. The weakness with the rank probability estimates is that they are not measured values but estimates of cumulative probability based on order statistics. The least-squares method assumes randomly distributed errors, but the errors in the rank probabilities are not randomly distributed. Each data point corresponds to a certain cumulative failure probability with a certain confidence. This can be expressed in mathematical form, using the binomial expression, as[2]

$$z' = 1 - \sum_{j=1}^{i} \frac{n!}{(j-1)! \cdot (n-j+1)!} \cdot P_{rank}^{j-1} \cdot (1 - P_{rank})^{n-j+1} \tag{5.2}$$

where z′ is the probability that (i.e. the fraction of repeated trials with samples of size n for which) the true cumulative probability associated with at least the ith value in n values will be equal to or less than P_{rank}. Usually people prefer to use simple approximations of the median rank probability estimate (z′ = 0.5). Three common estimates of the median rank probability are[2]

$$P_{rank} = \frac{i - 0.5}{n} \tag{5.3}$$

$$P_{rank} = \frac{i}{n + 1} \tag{5.4}$$

$$P_{rank} = \frac{i - 0.3}{n + 0.4} . \tag{5.5}$$

All three estimates are of the form

$$P_{rank} = \frac{i - A}{n + B} \tag{5.6}$$

where

$$B = 1 + 2A . \tag{5.7}$$

Equations (5.6) and (5.7) can be combined and rearranged to read

$$i - nP_{rank} = -A + (1 + 2A)P_{rank} , \tag{5.8}$$

from which the constant A can be evaluated graphically. The three approximations given by Eqs. (5.3), (5.4), and (5.5) are compared with the outcome of Eq. (5.2) in Fig. 5.2. It can be seen that Eq. (5.5) is clearly the best estimate of the median rank probability.

The problem with the least-squares estimation procedure is that it is essentially intended to be used in connection with symmetric distributions with random errors. Since the master curve distribution function is nonsymmetrical and the error in the rank probability estimate is not random in nature, the least-squares estimation is not ideal for estimating K_0. Additionally, several possible fitting criteria exist, depending on how the three-parameter Weibull equation is linearized:

$$P_f = 1 - \exp - \left[\frac{K_i - K_{min}}{K_o - K_{min}}\right]^4 \tag{5.9}$$

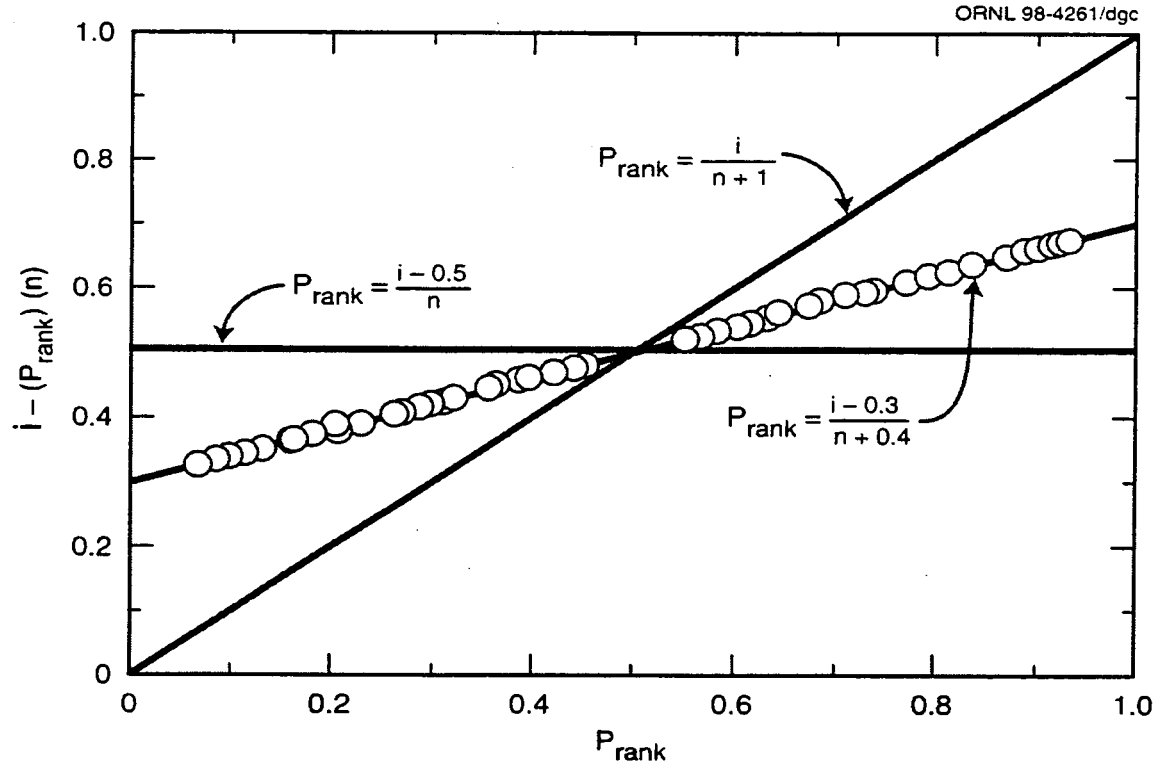

Fig. 5.2. Comparison of different estimates of median rank probability (lines) with binomial theory estimate (circles).

Writing Eq. (5.9) in the form

$$\left[\ln\left(\frac{1}{1 - P_f}\right)\right]^{1/4} = \frac{K_i - K_{min}}{K_o - K_{min}} \tag{5.10}$$

implies a linear equation with $x = (K_i - K_{min})$, zero intercept, and slope equal to the reciprocal of $(K_0 - K_{min})$. Minimizing the sum of the squares of the errors with respect to the slope leads to

$$K_0 = K_{min} + \frac{\sum_{i=1}^{r} (K_i - K_{min}) \cdot \left(\ln\frac{1}{1 - P_f}\right)^{1/4}}{\sum_{i=1}^{r} \left(\ln\frac{1}{1 - P_f}\right)^{1/2}}, \tag{5.11}$$

where r is the number of uncensored results. On the other hand, taking logarithms again in Eq. (5.10) leads to

$$\ln\left[\ln\left(\frac{1}{1-P_f}\right)\right] = 4\ln(K_i - K_{min}) - 4\ln(K_o - K_{min}) , \tag{5.12}$$

which implies a linear equation with $x = \ln(K_i - K_{min})$, slope = 4, and intercept equal to $-4\ln(K_0 - K_{min})$. Minimizing the sum of the squares of the errors with respect to the intercept leads to

$$K_0 = K_{min} + \exp\frac{\sum_{i=1}^{r}(K_i - K_{min}) - \sum_{i=1}^{r}\frac{1}{4}\ln\ln\frac{1}{1-P_f}}{r} , \tag{5.13}$$

where, again, r is the number of uncensored results. In the above equations, the use of rank probabilities limits the censoring to the upper end of the distribution; i.e., all censored values must be higher than any of the uncensored values.

In principle, both Eqs. (5.11) and (5.13) are correct. However, they produce different results because the fitted distribution is nonsymmetrical. Due to these and other deficiencies in the least-squares estimation procedure with respect to the master curve distribution, it has been decided to use the maximum likelihood estimate to determine K_0 or T_0.

5.5 Method of Maximum Likelihood (MML)

The method of maximum likelihood (MML) does not make use of the cumulative probability distribution directly. Instead, it uses the first derivative, namely, the probability density function. This way, the individual cumulative probabilities are not needed. The probability density function for the master curve distribution function is

$$f_c(K_c) = \frac{4(K_c - K_{min})^3}{(K_0 - K_{min})^4} \cdot \exp\left(-\left\{\frac{K_c - K_{min}}{K_0 - K_{min}}\right\}^4\right) . \tag{5.14}$$

The MML method examines the likelihood, expressed as a joint probability, that a certain probability density function is the product of all the discrete probability densities for the measured values. Thus the likelihood is defined as[3]

$$L = \Pi_{i=1}^{n} f_c(K_c) \Rightarrow$$

$$L = \Pi_{i=1}^{n} \frac{4(K_{ci} - K_{min})^3}{(K_0 - K_{min})^4} \cdot \exp\left(- \left\{ \frac{K_{ci} - K_{min}}{K_0 - K_{min}} \right\}^4 \right) . \tag{5.15}$$

Equation (5.15) gives the likelihood that a certain master curve distribution describes the data. K_0 is solved so as to produce a maximum in the likelihood L. This can be performed numerically using Eq. (5.15) directly, or analytically, taking the derivative of Eq. (5.15) with respect to K_0. The normal MML does not include censoring, but censoring is easily implemented by making use of the survival distribution function (S_c).

Any data in the set not corresponding to failure is not a part of the probability density function (pdf), but rather of the survival distribution function (sf). For computational purposes, it is convenient to utilize a single algebraic expression for the effective distribution function, written as the product of two factors. The first factor is the pdf, raised to the power δ_i, where δ is the Kronicker Delta, to which a value of 1 is assigned for fracture and 0 for survival. The second factor is the sf, which equals $(1 - P)$ raised to the power $1 - \delta_i$. In every case, one of the exponents will be 1 and the other zero, rendering one factor always equal to 1 and giving the product the appropriate value for fracture or nonfracture. Algebraically, the product has the appearance of an incremental joint, or conditional, probability of failure. Thus,[3]

$$\text{Conditional probability} = f_c(K_c)^{\delta_i} \cdot S_c(K_c)^{1-\delta_i} . \tag{5.16}$$

The master curve survival function is

$$S_c(K_c) = \exp\left(- \left\{ \frac{K_c - K_{min}}{K_0 - K_{min}} \right\}^4 \right) , \tag{5.17}$$

and the censored maximum likelihood expression thus becomes

$$L = \Pi_{i=1}^{n} f_c(K_c)^{\delta_i} \cdot S_c(K_c)^{1-\delta_i} \Rightarrow$$

$$L = \Pi_{i=1}^{n} \frac{4(K_{ci} - K_{min})^{3\delta_i}}{(K_0 - K_{min})^{4\delta_i}} \cdot \exp\left(- \left\{ \frac{K_{ci} - K_{min}}{K_0 - K_{min}} \right\}^4 \right) . \tag{5.18}$$

Equation (5.18) is solved similarly to Eq. (5.15). An interesting feature of Eq. (5.18) is that it does not restrict the censoring to any specific part of the data set, but each datum is treated individually. Thus random censoring is mathematically possible; i.e., the censoring rules in the ASTM master curve standard might be relaxed.

The analytical solution of Eq. (5.18) is simplified by taking the logarithm of L (maximum of L is equivalent to maximum of ln[L]).

$$\ln L = \sum_{i=1}^{n} \left(\ln 4 + 3\delta_i \cdot \ln(K_{ci} - K_{min}) - 4\delta_i \cdot \ln(K_0 - K_{min}) - \left\{ \frac{K_{ci} - K_{min}}{K_0 - K_{min}} \right\}^4 \right) . \tag{5.19}$$

By solving for $\partial \ln(L)/\partial K_0 = 0$, the randomly censored maximum likelihood estimate of K_0 is obtained as

$$K_0 = \left(\frac{\sum_{i=1}^{n} (K_i - K_{min})^4}{\sum_{i=1}^{n} \delta_i} \right)^{1/4} + K_{min} . \tag{5.20}$$

Equation (5.20) has one deficiency. For small numbers of valid data the estimate of K_0 will tend to be consistently a little low, and therefore slightly biased. For example, if there is only one valid test result, the value of K_0 calculated from Eq. (5.20) will be equal to the measured value, not K_0. Thus, because estimating errors in K_0 tend to consistently have the same algebraic sign, with magnitudes depending on sample size, a bias correction is required. Two different bias corrections for K_0 have been proposed, one based on the mean estimate of K_0 and another based on the median estimate of K_0. The basis of both bias corrections is the recognition, from mathematical considerations, that repeated estimates of K_0 from samples of size n drawn from the same true

Weibull population will be distributed according to a Gamma probability density function. The expression for a bias correction is derived by assuming that the uncorrected estimate obtained by the MML corresponds to a certain integral of the pdf (either the mean or the median). Since the true value is a parameter of the pdf, the resulting integral produces a ratio between the estimated value and the true value, the reciprocal of which is the bias correction, expressed as a multiplying factor. The bias correction factor based on the assumption that the MML is the expected (mean) of the theoretical distribution is analytical. The bias correction factor based on the assumption that the MML is the median of the theoretical distribution is numerically determined, but it is represented to a very close approximation by an analytical expression. Both solutions, as developed, do not consider censoring. The proposed bias corrections are compared graphically in Fig. 5.3. It is seen that the two bias corrections are effectively identical in numerical magnitude. For the master curve method the simpler and slightly more conservative bias correction (based on the median estimate of K_0) was chosen.

The bias correction could actually be omitted, since this would lead only to making estimates for small data sets slightly more conservative. For consistency, however, the master curve standard includes the bias correction, which, when combined with Eq. 5.20, yields the bias corrected K_0 estimate

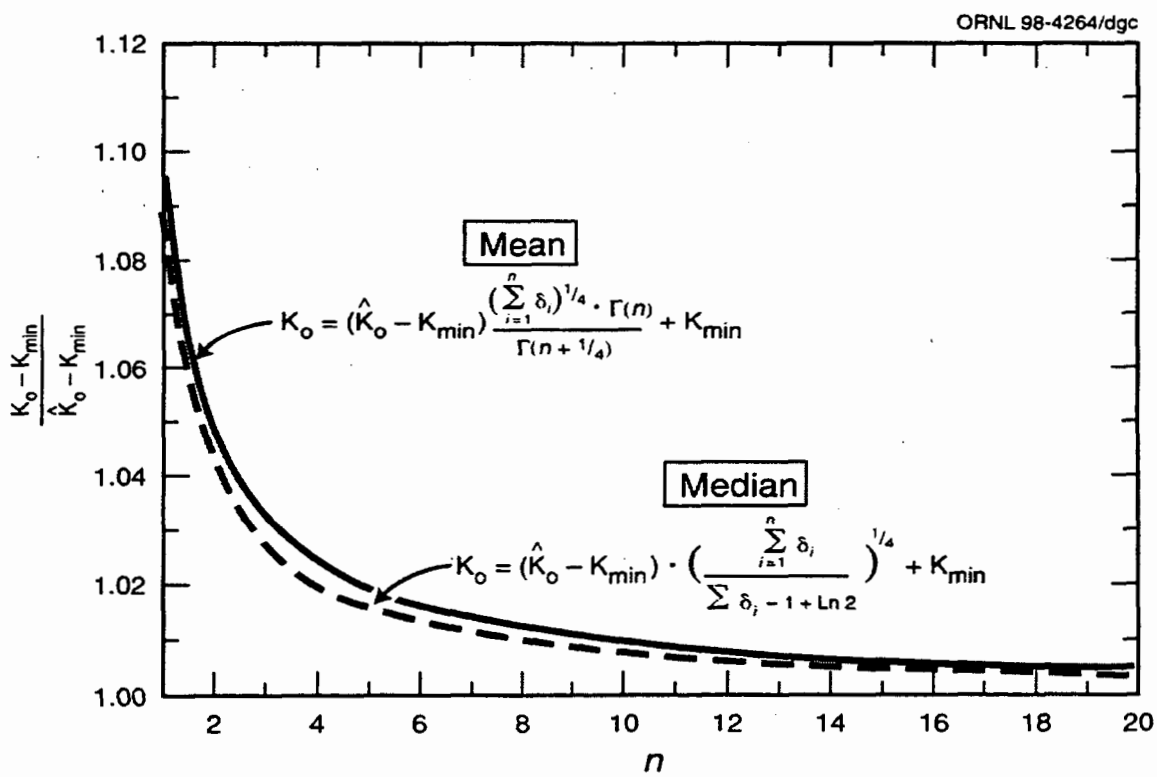

Fig. 5.3. Comparison of mean and median bias corrections for maximum likelihood estimate of K_0.

$$K_0 = \left(\frac{\sum_{i=1}^{n} (K_i - K_{min})^4}{\sum_{i=1}^{n} \delta_i - 1 + \ln 2} \right)^{1/4} + K_{min} \ . \tag{5.21}$$

The accuracy of the K_0 estimate will be a function of uncensored data $r = \sum_{i=1}^{n} \delta_i$.

The standard deviation of the bias corrected MML estimate is approximately[4]

$$\sigma_{\hat{K}_0 - K_{min}} \approx \frac{0.28 \cdot (K_o - K_{min})}{\sqrt{r}} \ . \tag{5.22}$$

An important feature of the MML estimate to note is that the accuracy of the estimate of K_0 is not affected by the degree of censoring, i.e. it is not affected by the n/r ratio. Nor is it affected by the nature of censoring (random, upper end, lower end, etc.) It is *only* a function of the number of uncensored data (r). This can easily be verified, e.g., by Monte Carlo simulations, using different censoring criteria and degrees of censoring. This property makes the MML procedure extremely valuable. In principle, not a single test result (fulfilling the requirements related to fatigue precracking, crack shape and test performance) needs to be omitted from the analysis. Any invalid data can be given the toughness value corresponding to the validity criterion and be treated as non-failures.

The confidence of the transition temperature T_0 will be affected also by the testing temperature because a fixed proportional error in K_0 will have different meanings for T_0, depending of the location on the master curve. Figures. 5.4 and 5.5 give the resulting 5 and 95% confidence bounds for T_0 when tests are performed at a single temperature. Figure 5.4 gives a general (normalized by r) view of the confidence bounds, and Fig. 5.5 gives them specifically for r = 6. Both figures show that testing at temperatures lower than T_0–50°C is not advisable, due to the poor confidence of the T_0 estimate. The confidence bounds in Figs. 5.4 and 5.5 were developed by Monte Carlo simulation using the theoretical distribution of estimates of K_0, which is a gamma distribution, and applying Eq. (5.21) and the master curve temperature dependence. Each simulation consisted of 10,000 trials from which the 5 and 95% confidence limits were derived by rank analysis.

The confidence bounds in Figs. 5.4 and 5.5 are presented essentially in an inverted form, i.e. as corrections, so as to produce a safety factor description for T_0. For example, when the 5% confidence bound ($\Delta T_{05\%}$) is added to the T_0 estimate, the probability that the true T_0 is still higher than the adjusted estimate ($T_{05\%}$) is 5 %. Basically, the

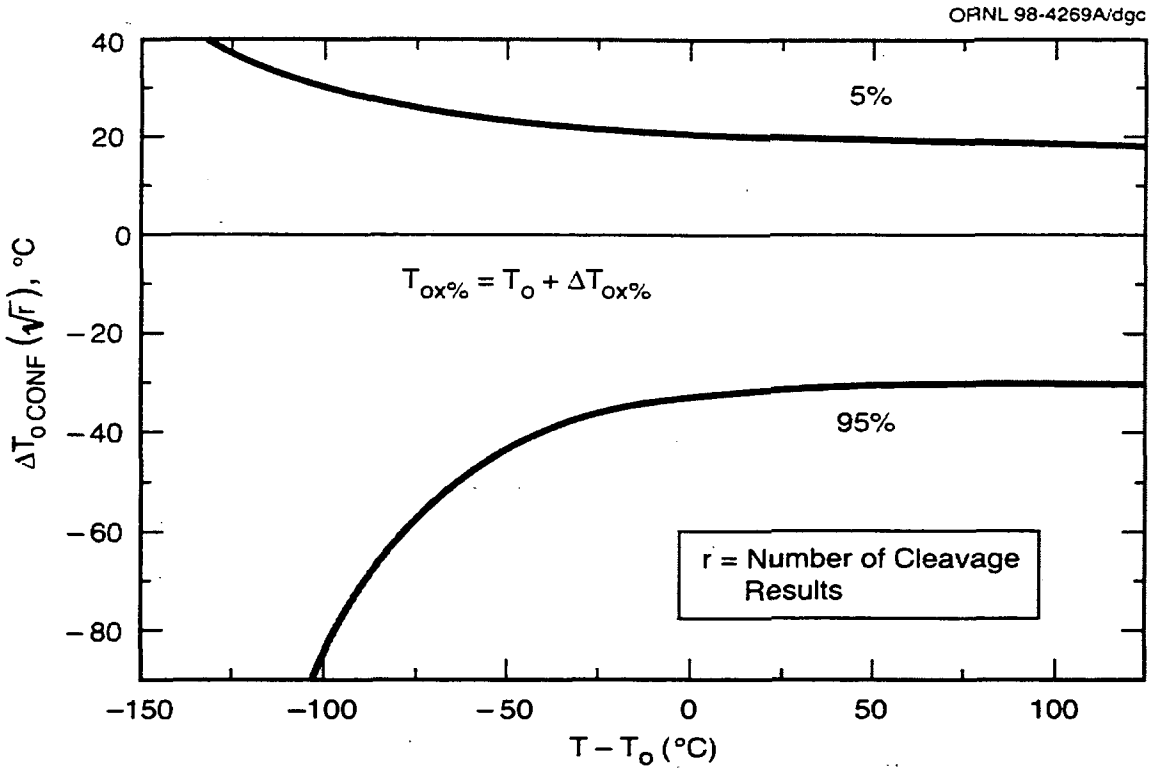

Fig. 5.4. Confidence bounds of 5 and 95% for maximum likelihood estimate of K_0 expressed in terms of corrections to the calculated value of T_0.

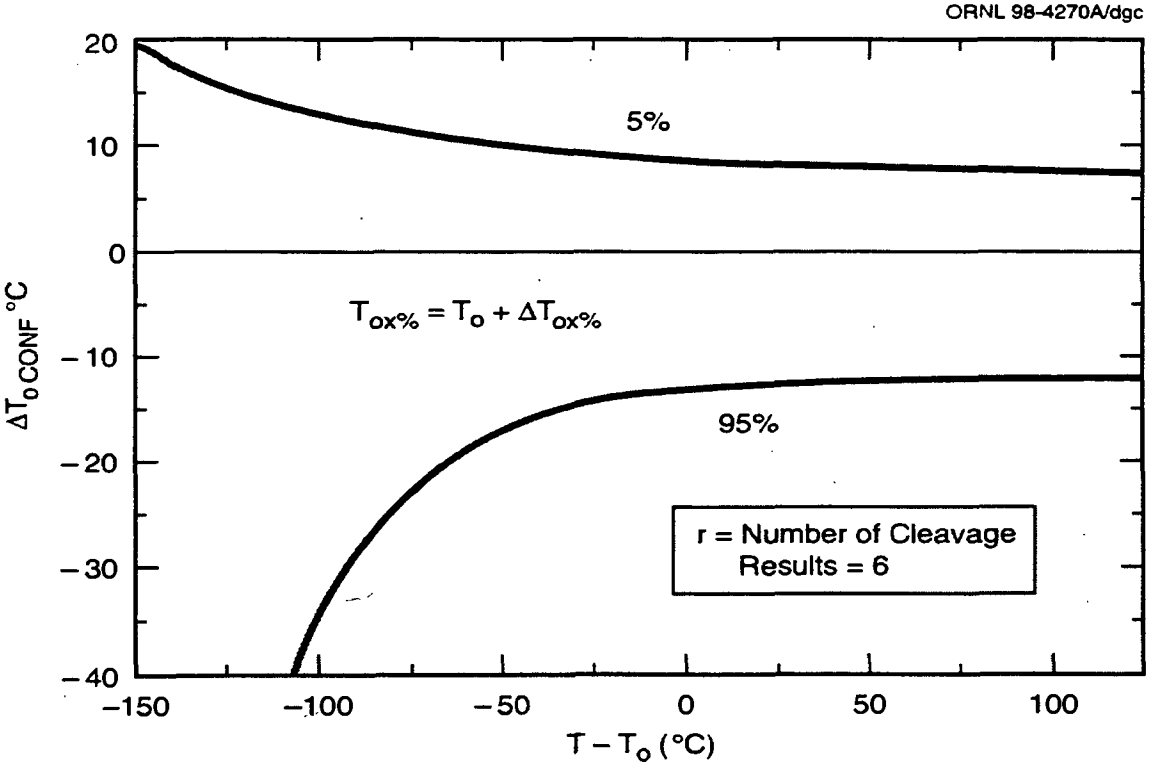

Fig. 5.5. Confidence bounds of 5 and 95% for maximum likelihood estimate of K_0, expressed in terms of corrections to the calculated value of T_0, for r = 6.

figures show that the inaccuracy in T_0 is greater on the conservative side; i.e., unduly high T_0 values may be estimated when testing at too low temperatures.

Figures 5.4 and 5.5 are derived for a case where the material obeys the master curve temperature dependence exactly. The master curve temperature dependence is only an empirical approximation of the whole ductile to brittle transition behavior. Inaccuracies due to the approximate nature of the temperature dependence are usually not significant in the temperature region T_0–50°C... T_0+50°C, but close to the lower shelf, the resulting additional, error in T_0 may be considerable.

If the master curve temperature dependence ($K_0 = 31 + 77 \cdot \exp\{0.019 \cdot (T - T_0)\}$) is inserted into Eq. (5.19), solving for $\partial \ln(L)/\partial T_0 = 0$ gives the randomly censored maximum likelihood estimate of T_0 as[4]

$$\sum_{i=1}^{n} \frac{\delta_i \cdot \exp\{0.019 \cdot [T_i - T_0]\}}{11 + 77 \cdot \exp\{0.019 \cdot [T_i - T_0]\}} - \sum_{i=1}^{n} \frac{(K_{IC_i} - 20)^4 \cdot \exp\{0.019 \cdot [T_i - T_0]\}}{(11 + 77 \cdot \exp\{0.019 [T_i - T_0]\})^5} = 0 \ , \quad (5.23)$$

from which T_0 can be solved by iteration. Eq. (5.20) is actually only a special case of the more general Eq. (5.23). If all data correspond to a single test temperature, Eq. (5.23) reduces essentially to Eq. (5.20).

It should be emphasized that all the estimation procedures require the use of a single "specimen size"; i.e., all fracture toughness values must have been size-adjusted to a single crack front length and, specifically in the case of Eq. (5.23), the adjustment must be to 25-mm the normalization size. This does not mean that data from different size specimens could not be used together; it only means that the data must be size adjusted to a single size for the estimation.

Similar to Eq. (5.20), Eq. (5.23) will produce a slightly biased estimate of T_0 for a small number of "valid" data (r), but for test temperatures above T_0–50°C and for $r \geq 6$, the bias, based on the curve in Fig. 5.6, will be of the order of 1°C or less. The bias of T_0 shown in Fig. 5.6 was estimated with the help of Monte Carlo simulation.

The advantage of the multiple temperature testing according to Eq. (5.23) comes for materials that do not exactly follow the master curve temperature dependence. Doing tests in the temperature region of primary interest for the application enables the master curve procedure to give an adequately accurate description of the material's temperature dependence, even for materials for which the overall temperature dependence does not follow the

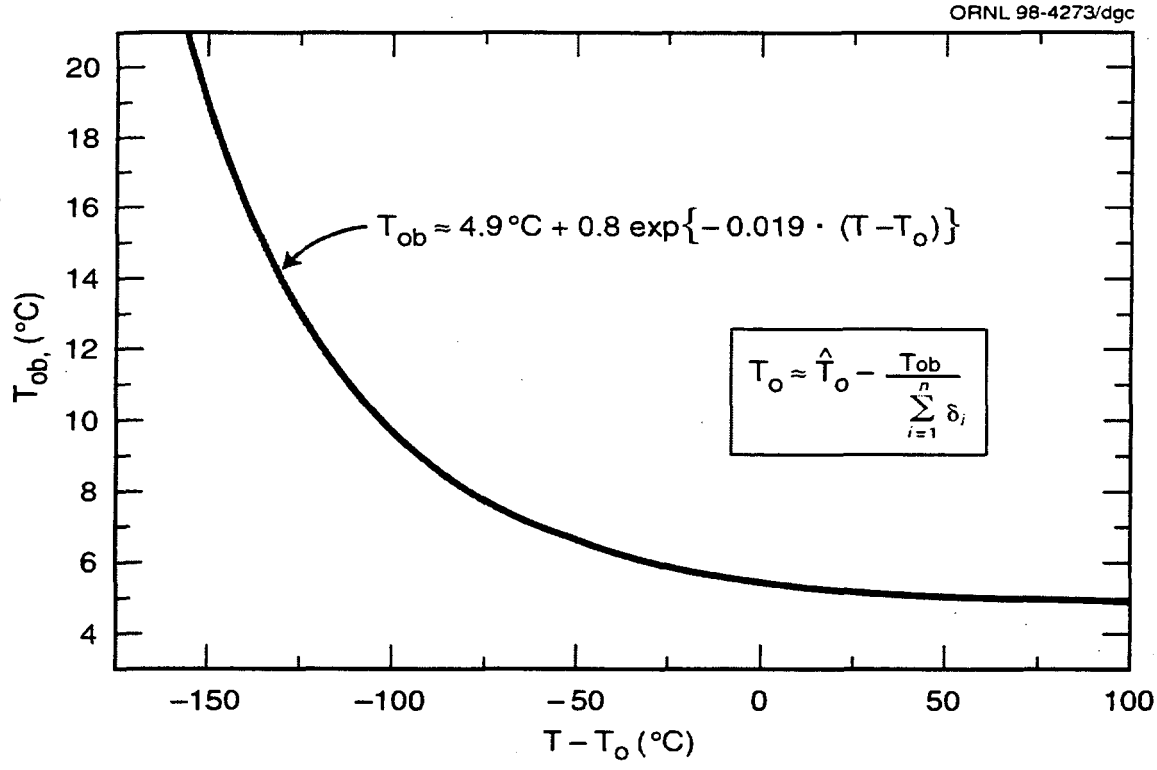

Fig. 5.6. Bias correction for maximum likelihood estimate of T_0.

master curve assumption. For materials that follow the master curve temperature dependence, there should be no difference between the results of single or multiple temperature testing.

5.6 References

1. D. Stienstra, "Stochastic Micromechanical Modeling of Cleavage Fracture in the Ductile-Brittle Transition Region," Ph.D. dissertation, Texas A&M University, 252, 1990.

2. K. Wallin, "Optimized Estimation of the Weibull Distribution Parameters," pp. 1–17 in *Espoo 1989, Research Reports 604*, Technical Research Centre of Finland.

3. R. Moscowic, "Statistical Analysis of Censored Fracture Toughness Data in the Ductile to Brittle Transition Temperature Region 1," *Engng. Fracture Mech.* **44**(1), 21–41, 1994.

4. K. Wallin, "Validity of Small Specimen Fracture Toughness Estimates Neglecting Constraint Corrections," pp. 519–37 in *Constraint Effects in Fracture: Theory and Applications*, ed. Kirk and Bakker, ASTM STP 1244, 1994.

6. PRECISION AND BIAS

6.1 Weibull Parameters

Two key technical breakthroughs were needed to give purpose to the development of a test standard. The first was the observation that data scatter characteristics of steels in the transition range are amenable to statistical modeling.[1] The second was that median fracture toughness versus test temperature trends for ferritic steels tend to follow one universal curve shape.[2]

Three-parameter Weibull modeling of data scatter has been found to tend to a nearly fixed slope of 4, provided that one of the three parameters in the model, namely, K_{min}, is used as a deterministic parameter of the model, set at 20 MPa√m. Early empirical evidence (shown in Fig. 6.1) was used to demonstrate that true population slopes cannot be accurately established using just a few data.[2] This allows the perspective to argue that widely varied Weibull slopes observed in small data sets cannot be regarded as significant experimental evidence. Hence, two of the three Weibull parameters that also happen to be impractical to recommend for experimental determination in a test standard have been predetermined. The third parameter in the Weibull model is the scale parameter, K_o, and, fortunately, this parameter can be determined to sufficient accuracy with modest replicate tests. Monte Carlo

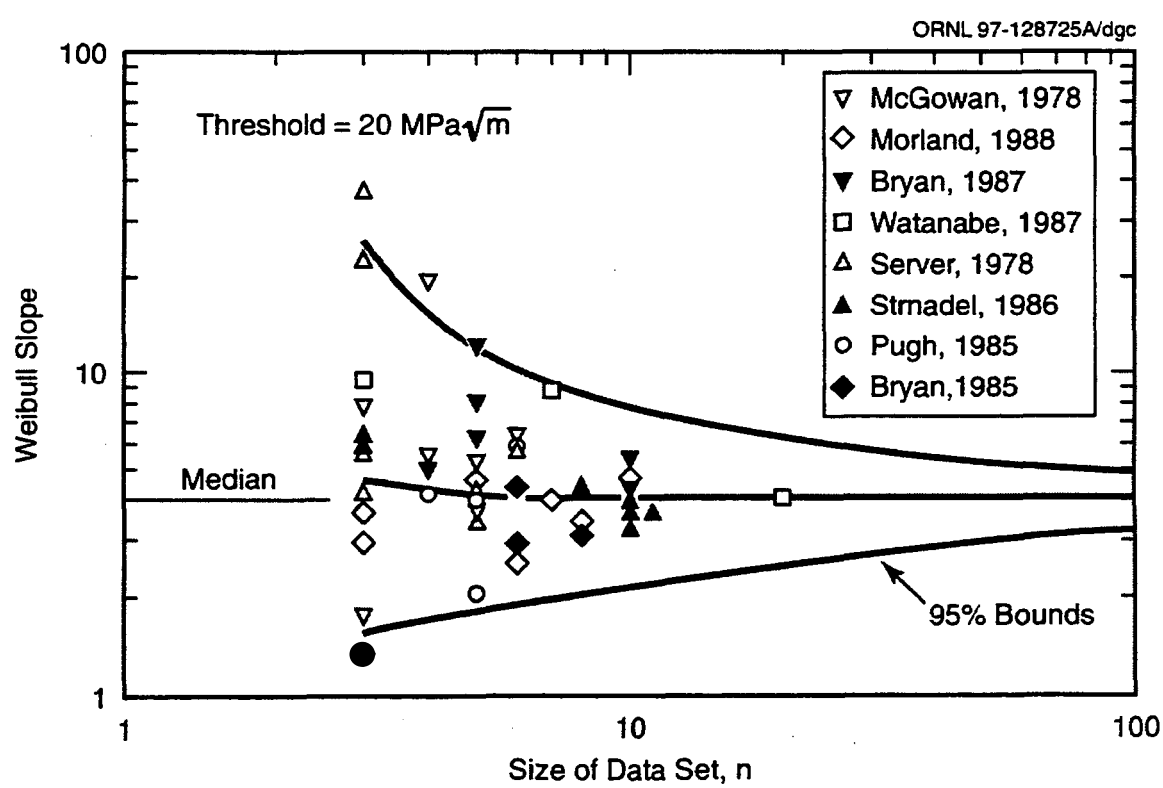

Fig. 6.1. Comparison of the distribution of Weibull slopes calculated from small data sets. Monte Carlo predicted confidence limits when K_{min} is set at 20 MPa√m.

simulations have established that workable accuracy can be assured with six replicate tests. These developments have provided the necessary elements to proceed with the development of a practical standard practice.

The MPC/JSPS round robin mentioned in Section 4 has provided the test method evaluation data that was needed to establish precision and accuracy of the method. Eighteen laboratories representing four countries, namely, Japan, Germany, the United Kingdom, and the United States, had participated. The material used was A 508 class 3. Compact specimens of 1T size were sampled at the 1/4t and 3/4t positions in 255-mm-thick (10-in.) plate. The participants could select from three test temperatures: -50, -75, and -100°C. The number of temperatures chosen was optional and five specimens were provided for each test temperature selected, with the goal of testing 50 specimens at each of the three temperatures. This goal might have been achieved except that one of the participants tested all 15 of their specimens at -75°C.

Table 6.1 summarizes the results of this round robin after these data were analyzed by the maximum likelihood statistical procedure of the present E 1921 test method. The one obvious departure is that the minimum requirement of six replicate tests was not followed. However, this can be explained by the fact that the round robin had been conducted well before work was started on the proposed ASTM standard. Nevertheless, the value of the round-robin data to the standard was hardly diminished as a precision and accuracy evaluation tool. The standard deviation on each T_o determination is calculated by:

$$\sigma = 18/\sqrt{N} \cong 8°C \ . \tag{6.1}$$

Using the standard normal deviate for two-tail distribution, $Z_{85} = 1.44$, indicates that 85% of the T_o determinations are likely to be inside of the temperature range of -118 to -95°C. Twenty-four of the 28 results were inside of these limits.

To make a point about Weibull slope variability, Appendix X1.0 of the proposed standard method was used to least-squares fit the five data of each laboratory. In the analysis, K_{min} is fixed at 20 MPa√m. Figure 6.1 was consulted to establish the 95% confidence limits on slopes at n = 5. The Monte Carlo simulation used to establish the limits indicated a Weibull slope range of 2 to 12. This agrees well with the outcome of the round-robin evaluations. Figure 6.1 used data generated before 1983. During this time, few investigators considered data scatter problems and the need for more than just a few replicates was not appreciated. An additional evaluation of Fig. 6.1 is made with Table 6.2.[3-7] The data in Table 6.2 are from more recent publications where replicates number 20 or more, and the objective here was to check these slopes against the 95% confidence limit spread of

Table 6.1. Analysis of MPC/JSPS round-robin data by linear regression for best slope,[a] maximum likelihood for K_o and T_o

Laboratory	T_o (°C)	Best slope	K_o (MPa√m)
	–50°C test temperature		
B	–115	3.0	294
C	–113	4.1	284
E	–103	2.6	241
H	–111	4.3	277
J	–83	12.6	177
O	–93	1.8	205
P	–87	6.0	187
Q	–108	3.5	262
R	–101	3.8	233
Total	–105	3.75	250
	–75°C test temperature		
A	–111	2.8	184
C	–105	3.7	168
D	–103	8.8	161
H	–101	5.8	156
J	–97	5.5	148
K	–109	7.1	177
N	–104	3.9	163
Q	–114	5.1	192
R	–98	6.5	150
Total	–105	5.8	166
	–100°C test temperature		
A	–107	5.0	118
C	–112	3.0	127
E	–114	4.0	132
F	–108	5.4	120
G	–101	5.6	109
H	–104	5.1	114
L	–120	11.3	143
M	–95	3.4	101
Q	–118	3.9	139
R	–104	2.8	114
Total	–109	4.3	123

[a]95% confidence limits on slope (Fig. 6.1) are 11.8 to 1.8.
95% confidence limits on K_o are listed below.

T (°C)	Upper	Lower
–50		
–75	191	141
–100	139	105

Table 6.2. Best slopes for data sets with 20 or more duplicate tests (K_{min} set at 20 MPa√m)

Material source	Material	Test temperature (°C)	Specimen size	Specimen Number	Best fit slope	"T_o" by maximum (°C)
MPC-JSPS round robin[a]	A508 class 3	−50	1T	47	3.75	−105
		−75	1T	55	5.80	−105
		−100	1T	50	4.30	−109
Ando, 1992[b]	SM41C	−70	1.2T	20	3.40	−126
Faucher[c]	ALgoma LT60	−120	0.4T	23	3.30	−126
ORNL[d]	A533 grade B	−75	1T	25	3.00	−77
	HSSI Plate 13A	−75	1/2T	20	5.20	−79
Iwadate, 1991[e]	A508 class 3	−60	1/2T	30	4.55	−44
		−20	1/2T	28	3.44	−41
	A470	−100	1/2T	27	4.58	−90
		−60		26	3.82	−74

[a]W. A. Van Der Sluys and M. T. Miglin, "Results of MPC/JSPS Cooperative Testing Program in the Brittle-to-Ductile Transition Region," pp. 308-324 in *Fracture Mechanics: Twenty-Fourth Volume, ASTM STP 1207*, J. D. Landes, D. E. McCabe, and J. A. M. Boulet, Eds., American Society for Testing and Materials, 1994.

[b]K. Ando, K. Mogami, and K. Tuji, "Probabilistic Aspects of Cleavage Crack Initiation Sites and Fracture Toughness," pp. 1171–1184 in *Fatigue and Fracture of Engineering Materials and Structures*, Vol. 15, No. 12, 1992.

[c]B. Faucher and W. R. Tyson, "A Statistical Description of the Effect of Strain Rate, Thickness, and Temperature on the Brittle Fracture Toughness of an Arctic Grade of Steel" pp. 1077–1082 in *Proceedings of the 8th International Conference on the Strength of Metals and Alloys*, Tampere, Finland, August 1988.

[d]D. E. McCabe, *A Comparison of Weibull and β_{Ic} Analysis of Transition Range Fracture Toughness Data*, USNRC Report NUREG/CR-5788 (ORNL/TM-11959), January 1992.

[e]T. Iwadate, Y. Tanaka, S. Ono, and J. Watanabe, "An Analysis of Elastic-Plastic Fracture Toughness Behavior for J_{Ic} Measurement in the Transition Region," pp. 531–561 in *Elastic-Plastic Fracture: Second Symposium, Volume II - Fracture Resistance Curves and Engineering Applications, ASTM STP 803*, American Society for Testing and Materials, 1983.

Fig. 6.1. For 20 replicates, the confidence level spread in Fig. 6.1 covers Weibull slopes from 2.5 to 6. The experimental results in Table 6.2 gave slopes from 3.0 to 5.8 confirm the suggested replication slope spread of Fig. 6.1.

The statements in the precision and bias section of the standard method have been essentially verified with experimental data.

6.2 References

1. J. D. Landes and D. H. Shaffer, "Statistical Characterization of Fracture in the Transition Region," pp. 368–382 in *Fracture Mechanics: Twelfth Conference. ASTM STP 700*, American Society for Testing and Materials, 1980.

2. K. Wallin, "The Scatter in K_{Ic} Results," *Engineering Fracture Mechanics*, **19**(6), 1085–93 (1984).

3. W. A. Van Der Sluys and M. T. Miglin, "Results of MPC/JSPS Cooperative Testing Program in the Brittle-to-Ductile Transition Region," pp. 308–24 in *Fracture Mechanics: Twenty-Fourth Volume, ASTM STP 1207*, ed. J. D. Landes, D. E. McCabe, and J. A. M. Boulet, American Society for Testing and Materials, 1994.

4. K. Ando, K. Mogami, and K. Tuji, "Probabilistic Aspects of Cleavage Crack Initiation Sites and Fracture Toughness," *Fatigue and Fracture of Engineering Materials and Structures* **15**(12), 1171–84 (1992).

5. B. Faucher and W. R. Tyson, "A Statistical Description of the Effect of Strain Rate, Thickness, and Temperature on the Brittle Fracture Toughness of an Arctic Grade of Steel" pp. 1077–82 in *Proceedings of the 8th International Conference on the Strength of Metals and Alloys*, Tampere, Finland, August 1988.

6. D. E. McCabe, *A Comparison of Weibull and β_{Ic} Analysis of Transition Range Fracture Toughness Data*, USNRC Report NUREG/CR-5788 (ORNL/TM-11959), January 1992.

7. T. Iwadate, Y. Tanaka, S. Ono, and J. Watanabe, "An Analysis of Elastic-Plastic Fracture Toughness Behavior for J_{Ic} Measurement in the Transition Region," pp. 531–61 in *Elastic-Plastic Fracture: Second Symposium, Volume II—Fracture Resistance Curves and Engineering Applications*, ASTM STP 803, American Society for Testing and Materials, 1983.

7. CONSIDERATIONS FOR APPLICATION OF THE MASTER CURVE APPROACH

The experimental, statistical, and empirical procedures discussed in this report, collectively called the master-curve approach, are considered to be an improvement over present code procedures for estimating static-initiation fracture toughness, mainly for two reasons. First, the new procedures are experimentally direct, because the specimens being tested are sharp-cracked, statically loaded, fracture mechanics specimens, whereas the existing code procedures are indirect, being based on data obtained from blunt-notched, impact-loaded, transition-temperature specimens. A somewhat extreme example of the potential improvement in the accuracy of estimates of static initiation fracture toughness obtainable by employing T_0 as the characterizing temperature instead of RT_{NDT} is illustrated in Fig. 7.1.

For reasons unknown, the value of RT_{NDT} for Heat-Treated Plate 14 was unreasonably high,[1] resulting in a grossly conservative lower bound static initiation fracture toughness by the present ASME Code procedure. This error is substantially reduced or eliminated by the use of the master curve approach,[2] based on T_0, and an associated

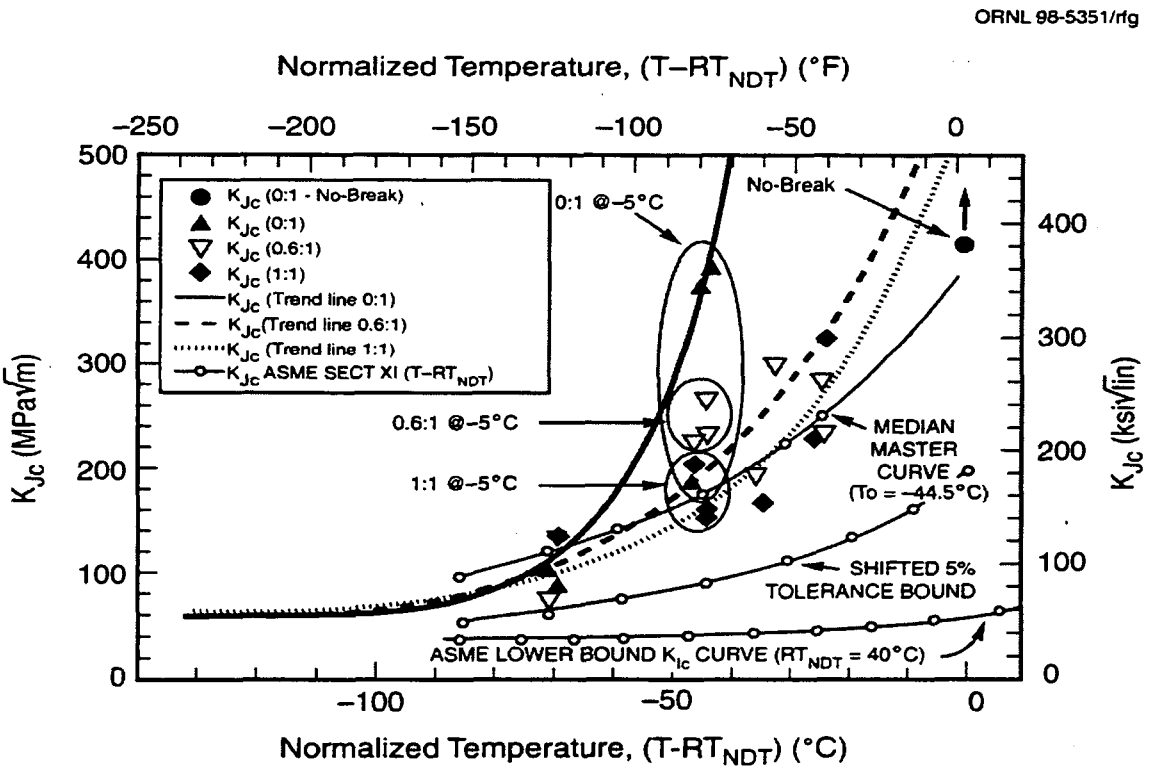

Fig 7.1. Comparison of fracture toughness data from shallow-cracked, biaxial specimen tests, a/W = 0.1, of Heat-Treated Plate 14 with master curve for the material, an associated estimated lower tolerance bound curve shifted for margin, and the ASME lower-bound K_{IC} curve.

lower tolerance bound curve including an upward temperature shift of 10°C to provide for uncertainty in the value of T_0, as also shown in Fig. 7.1. Another example of an apparently ultra-high value of RT_{NDT} with respect to static initiation fracture toughness data[3] is illustrated in Fig. 7.2.

In addition, a plot showing the generally uncertain correlation[4] between RT_{NDT} and T_0, is shown in Fig. 7.3.

Figure 7.3 shows that Heat-Treated Plate 14 is the most prominent, but not the only, example of a material with a high value of RT_{NDT} relative to T_0, and Fig. 7.1 shows that for such materials estimates of static-initiation fracture toughness based on RT_{NDT} are likely to be low. Basing the characterizing temperature, T_0, directly on fracture mechanics test data is intended to prevent such occurrences. Secondly, the new procedures recognize the inherently random variability of the fracture toughness of ferritic steels in the transition regime[5,6], and incorporate a rational, physically based, statistical analysis for quantifying this variability. Doing so provides a basis for improved statistical input for probabilistic safety analyses, as well as a basis for estimating fracture toughness versus temperature curves that have explicit statistical significance, for use in deterministic safety analyses.

The end product of the transition-range standard, ASTM E1921, is a characterizing temperature, T_0, which is an indexing temperature for a curve of median static initiation fracture toughness, K_{JC}, for a 1T specimen, for the

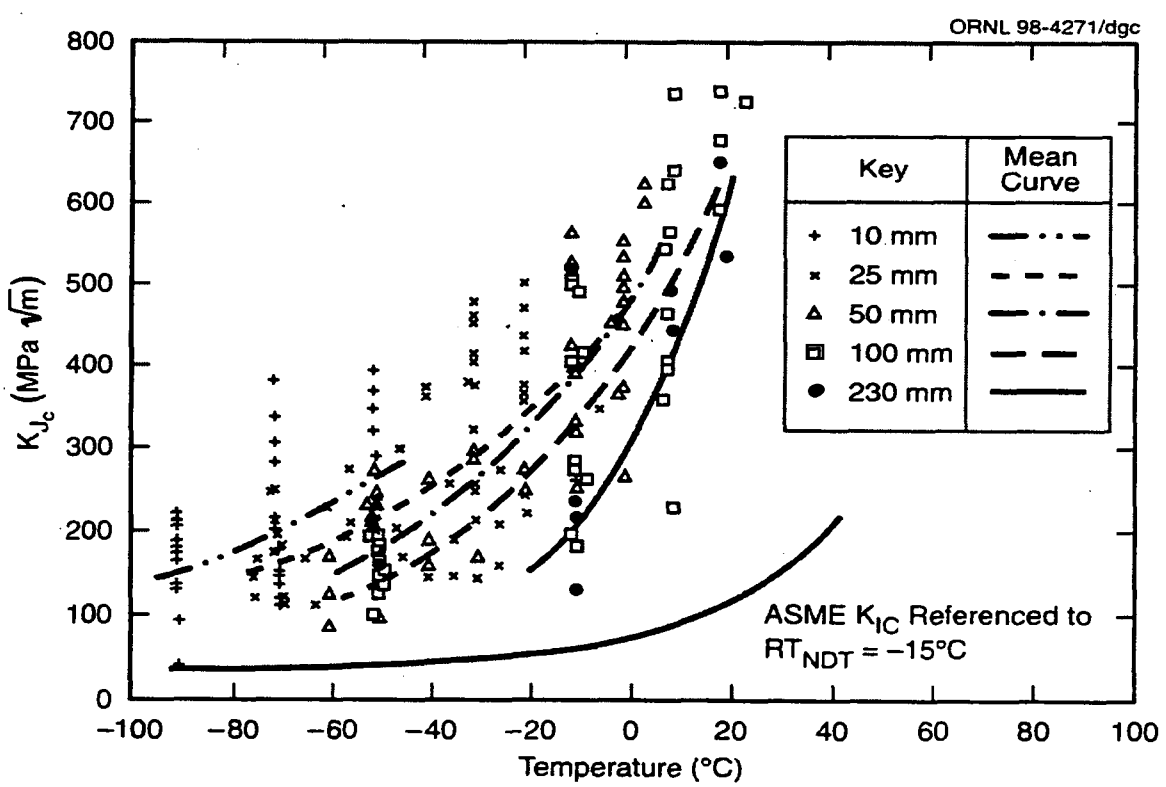

Fig. 7.2. Comparison of fracture toughness data from specimens of various sizes for an A533B, Class 1, steel with the ASME lower-bound K_{IC} curve.

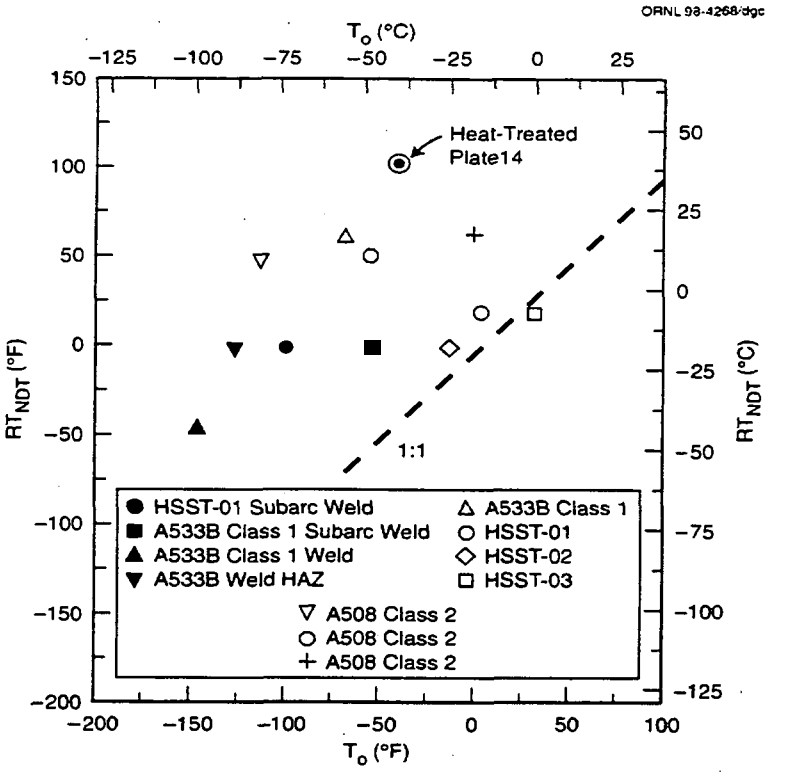

Fig. 7.3. Plot of RT_{NDT} versus T_0 for various steels and weld metals, showing the uncertainty in the relationship between the two parameters.

material tested. The toughness-versus-temperature curve has a known empirical equation, and is therefore termed a master curve. The temperature T_0 is the temperature at which the master curve indicates a median static initiation fracture toughness for a 1T specimen of 100 MPa √m. The reason for stipulating that the master curve characterizes the toughness for a particular size of specimen is the known existence of size effects, consideration of which is basic to the analyses prescribed in the standard. Two types of size effects appear to exist in fracture toughness data for ferritic steels. The first are statistical in nature, depending mainly on crack-front length, and the second are physical, termed constraint effects, depending mainly on a still incompletely defined interaction between toughness, yield stress, strain hardening, crack depth, and remaining-ligament dimensions. The toughness given by the master curve is labeled K_{JC}, rather than K_{IC}, partly to draw attention to the fact that the toughness given by the master curve is obtained using elastic-plastic fracture mechanics analysis methods. The indexing temperature, T_0, is viewed as a material characteristic, sensitive to thermal treatment and environment and as a consequence is believed to yield accurate measures of embrittlement. In the standard, statistical size effects are modeled mathematically by means of the three-parameter Weibull distribution. Constraint effects are considered only for the limited purpose of preventing excessive loss of constraint near the upper end of the range of toughness values measured. Although the three-parameter Weibull distribution implies, mathematically, that the toughness governing the extension of an infinitely long crack at any temperature is K_{min}, this estimate is not believed to be physically important. The empirical value of K_{min} = 20 MPa√m is viewed as a statistical fitting

parameter the value of which preserves the accuracy of the Weibull distribution with a slope of 4 for the majority of data, despite the fact that the actual physical minimum toughness value increases with temperature, thus contracting the lower tail of the real distribution.[7] Thus the Weibull size effect is not believed to persist to an infinite crack length. Although a consensus does not yet exist on how to estimate the minimum toughness at the end of Weibull size effects, a few reasonable estimating procedures have been proposed. However, application of these procedures is beyond the scope of the present standard.

One of the main areas of application of the transition-range standard, E1921, is the estimation of fracture toughness values for the safety analysis of nuclear pressure vessels, according to both the ASME Code, and to Nuclear Regulatory Commission (NRC) guidelines and regulations. However, at present, the physical bases for safety margins in the ASME Code involve more factors than those considered explicitly by the present standard, and there are also some differences in detail. The ASME Code uses the fracture toughness for crack arrest as well as the fracture toughness for static initiation in the procedures specified for safety evaluations. Standard E1921 presently addresses only the fracture toughness at static initiation. Therefore, if Standard E1921 is to be used in conjunction with the ASME Code, experimentally based and analytically sound extensions of the standard relating to dynamic crack initiation and crack arrest will need to be developed. Several sets of experimental data have already been analyzed with this objective in mind. As shown in Fig. 7.4, data for A515 steel obtained by

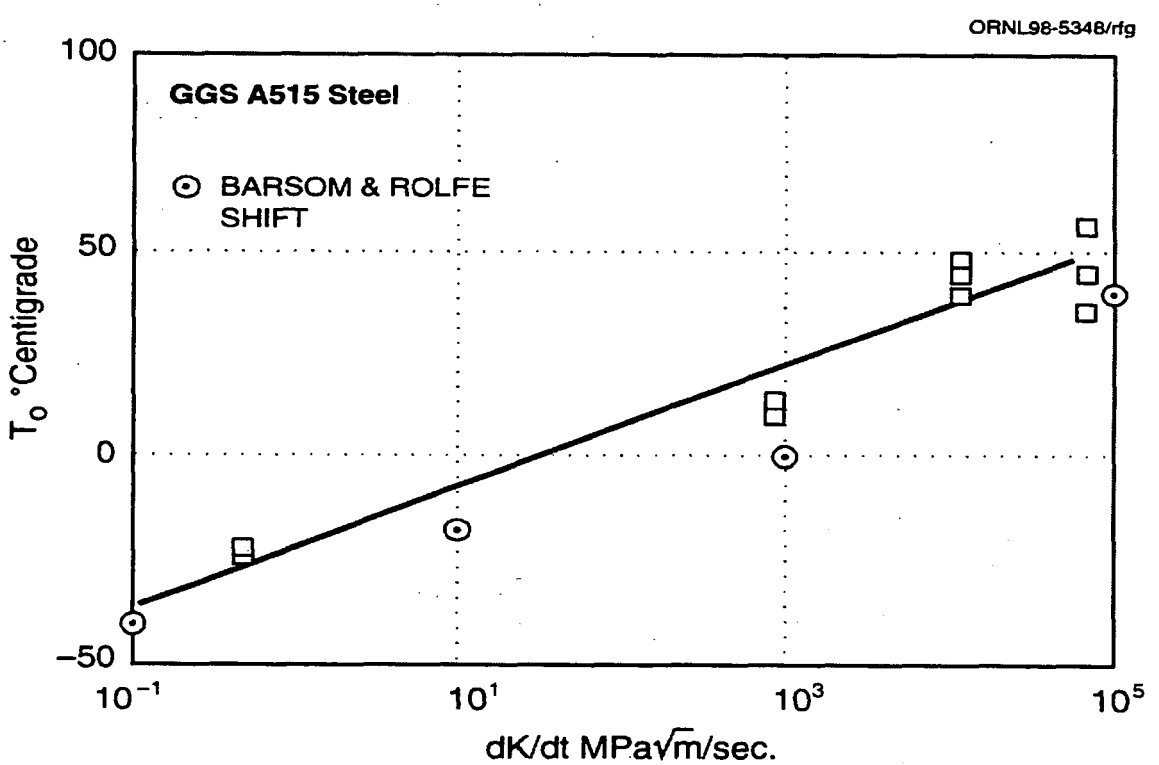

Fig. 7.4. Experimentally determined values of T_o versus loading rate for A515 steel, and values estimated by Barsom's method.

Joyce[8] with precracked Charpy specimens define a consistent trend of increased shift of T_0 with increased loading rate.

In addition, as shown by the round points added[a] to Fig. 7.4, the temperature shifts measured by Joyce are close to those estimated by a method proposed by Barsom.[9] Barsom's estimate depends only on the estimated strain rate at the forward boundary of the crack-tip plastic zone, and the static yield stress. Wallin, by analyzing existing dynamic and static data for several steels, has developed another procedure for estimating the shift of T_0 due to loading rate, using the Zener-Holloman rate-temperature equation in which the calibrating constant depends on both the static yield stress and the static value of T_0. Loading rate does not appear to affect the shape of the master curve.[10] Results obtained by Wallin[10] for HSST Plate 02 are shown in Fig. 7.5. Further research on this subject will be needed, but prospects for the development and validation of a reliable method for estimating loading rate-induced shifts of T_0 appear to be good.

There are two issues related to the shape of fracture toughness versus temperature curves to be addressed in employing ASTM Standard E1921 in conjunction with the ASME Code. The first pertains to the differences in shape between the master curve, or its associated tolerance bound curves, and the ASME lower bound K_{IC} curve. The latter curve has a steeper slope in the upper transition range. The second issue relates to the possible effects of irradiation, and Charpy upper shelf impact energy, on the shape of the master curve. The latter portion of this issue is discussed in Section 4.3 of this report. Present interim proposals for using ASTM Standard E1921 in conjunction with the ASME Code deal indirectly with both the issue of curve shape and the issue of strain-rate effects by using T_0 only to redefine the temperature indexing of the present ASME lower bound K_{IC} and K_{IR} curves, with the relationship between the two curves remaining unchanged. This approach does not deal directly with either the curve-shape issue or the known decreasing temperature shift between static initiation and dynamic initiation fracture toughness curves with increasing yield stress. The question of whether or not irradiation affects the shape of the master curve has been addressed by Wallin,[11] and by Sokolov and McCabe.[b] Figure 7.6, plotted by Sokolov and McCabe, shows that for a large collection of data, irradiation has no significant effect on the shape of the master curve or its tolerance bounds.

Although Standard E1921 was not intended for detecting or measuring local variations of toughness within weldments, some preliminary investigations of this nature have been conducted with specimens of reduced

---

[a]W. A. Van Der Sluys, Babcock & Wilcox Research Center, Alliance, Ohio, "Visual Aids for Effect of Strain Rate Discussion," Attachment 11 in Minutes of the PVRC Task Group on the Toughness Master Curve meeting held on February 7, 1997, in Reno, Nevada.

[b]D. E. McCabe, Oak Ridge National Laboratory, Oak Ridge, Tenn., "Experimental Evidence on Issues Raised at the Westinghouse Meeting, August 2, 1996," Presentation at PVRC Task Group on the Master Curve, Columbus, Ohio, October 7, 1996.

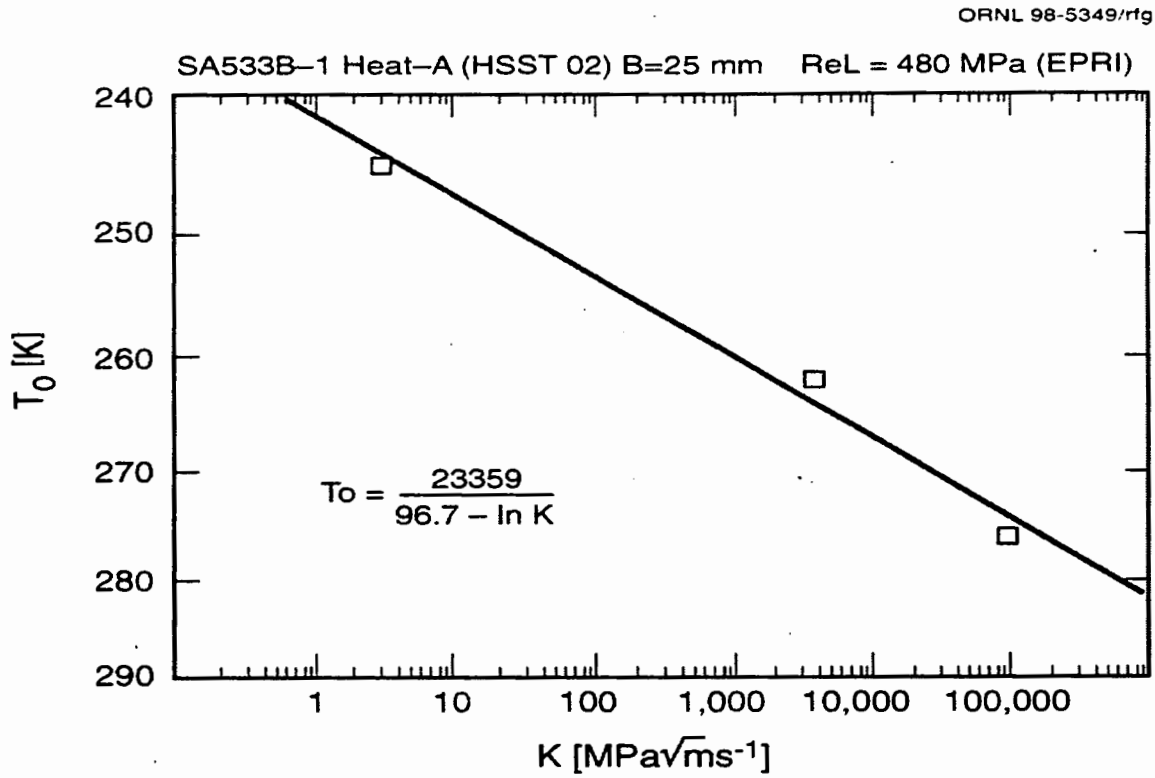

Fig. 7.5. Experimentally based values of T_o versus loading rate for A533B steel, and fitted line representing values estimated by Wallin's method.

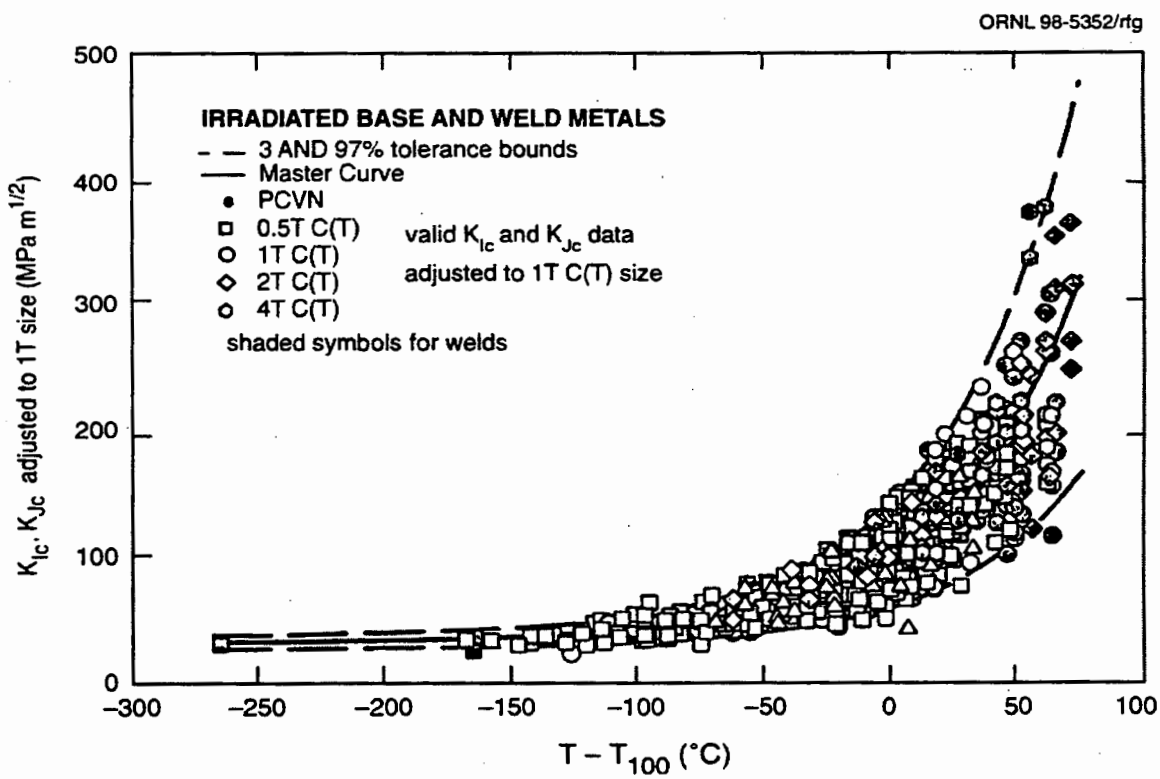

Fig. 7.6. Comparison of fracture toughness data, adjusted to 1T specimen size, for several irradiated base and weld metals, with the master curve and its estimated 3 and 97 percent tolerance bounds, showing that irradiation has no significant effect on the shape of the master curve or its tolerance bounds.

thickness relative to their planar dimensions, producing results that could be significant. Specifically, the value of T_0 for specimens obtained from the clad-to-weld heat-affected zone of a circumferential weldment in a vessel of a canceled nuclear plant was approximately 20°C above that for the remaining weld metal, with initiation points found by metallography to have been located in a narrow transverse region of coarse, columnar grains.[c] The same type of admonition also applies to plate material because values of T_0 for materials of inhomogeneous toughness, particularly thick quenched-and-tempered plate, are subject to some spatial variability.

In order to minimize effects of crack growth and attendant constraint loss on measured values of fracture toughness, Standard E1921 recommends testing at temperatures at which $K_{JC(med)}$ is expected to be close to 100 MPa √m. At these temperatures, ductile tearing prior to cleavage is expected to be minimal. Therefore, the toughness calculations in Standard E1921 do not correct for the amount of prior ductile tearing. A specimen-validity limit on ductile tearing is also included in the standard. The Weibull size effect relationship incorporated in Standard E1921 is assumed to apply above the temperature at which $K_{Jc(med)}$ equals 50 MPa √m. However, in the upper transition regime, beyond the expected range of test temperatures, ductile tearing may become significant in amount, and it may cause an effect of specimen size on measured fracture toughness values and loss of constraint in small specimens.[12] This could tend to increase the implied toughness for large specimens in the upper transition regime, consideration of which might help to explain the differences in slope between the upper parts of the master curve and the ASME lower bound K_{IC} curve. Experimental and analytical evidence on this subject is sparse, but it is not sufficiently resolved for the subject to be considered in writing the standard, and there may not be a strong need to know in applications as well.

It is frequently the case that only pre-cracked Charpy specimens are available for fracture mechanics testing. Thus there is considerable interest in validating the application of Standard E1921 to specimens of that size. The methods employed in the standard for selecting the number of specimens to be tested, and the testing temperature, for precracked Charpy specimens, considering the opposite variations with test temperature of the probable need for censoring and the uncertainty in the estimate of T_0 for a fixed number of specimens, are discussed in Section 3.4 and Appendix D of this report. As shown in Fig. 7.7, it has been experimentally demonstrated by Sokolov et al.[13] with data from HSST Plate 02 that precracked Charpy specimens are capable of producing master-curve data that agree with LEFM data obtained from large specimens that are valid according to ASTM E399.

---

[c]W. E. Pennell, Oak Ridge National Laboratory, Oak Ridge, TN, "Systematic T_o Variation in a RPV Structural Weld." presentation to ASME Joint SC III/XI Task Group on Master Curve Fracture Toughness, Reno, NV, December 8, 1997.

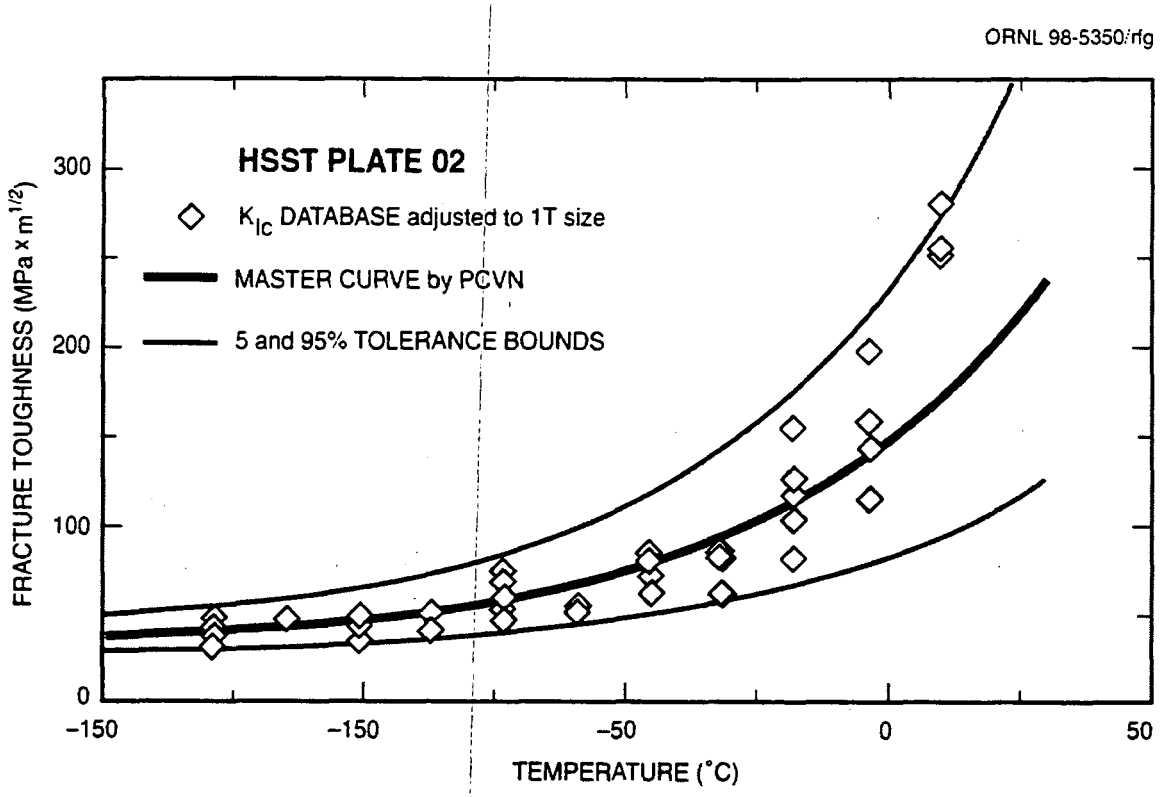

Fig. 7.7. Comparison of the master curve based on data from precracked Charpy specimens of HSST Plate 02, and the associated estimated 5 and 95 percent tolerance bounds, with the ASME K_{IC} database adjusted to 1T specimen size.

Additional data obtained by Wallin[14] with precracked Charpy specimens of A533B, class 1 steel (JRQ material), both unirradiated and irradiated to a fluence of 1.64×10^{19} n/cm^2, show that the temperature shift of static initiation fracture toughness exceeds that of the dynamic initiation fracture toughness, the latter agreeing with the shift of the standard Charpy impact energy curve at the 28J impact-energy level. Consequently, irradiation decreases the temperature difference between the curves of static and dynamic initiation fracture toughness versus temperature, which for the material tested becomes nil for a fluence of 1.64×10^{19} n/cm^2. Especially because of the comparison between the temperature shifts due to irradiation of the static initiation fracture toughness curve and the standard Charpy impact energy curve, these results need to be considered in the development of application procedures for the master-curve approach.

Because calculated values of T_0 are based on small samples of data, there is unavoidably some uncertainty associated with using these values as estimates of the true value of T_0, and with the values of fracture toughness given by the master curve. There are two provisions offered in Appendix X3.0 of Standard E1921 for dealing with these uncertainties. The first provision is margin shift of the calculated value of T_0, the confidence level of which can be chosen by the user. Sample size and the value of $K_{Jc(med)}$ are the variables that influence the uncertainty in the estimate of T_0. The second provision is the use of an estimated lower tolerance bound curve,

again margin-adjusted by the user, as the reference fracture toughness curve, to further reduce the probability of overestimating the fracture toughness.

In some cases, there may be no samples available from what could be the governing material in a structure, and resort must be made to either testing "surrogate" materials believed to be closely similar to the material of interest, or the use of generic estimates based on data bases for the same class of material.[15] Extreme uncertainties arise in the latter case, and corresponding additional margins on T_0 need to be considered as compensation. This situation is not unique to the master-curve approach. It applies to any method of estimating a characterizing temperature. Nevertheless, developing procedures for using data from surrogate specimens, and for applying generic data, possibly from other types of specimens such as Charpy impact specimens, by correlation requires informed judgment and considerable caution.

Taking all the above considerations into account, application of the master-curve approach has the potential for significantly improving the accuracy of structural integrity evaluations in the transition range.

7.1 References

1. W. J. McAfee, "Constraint Effects Analytical Development and Validation," pp. 7–23 in *Heavy Section Steel Technology Program Semiannual Progress Report for October 1995–March 1996*, NUREG/CR-4219, Vol. 13(1) (ORNL/TM-9593/V13), Oak Ridge National Laboratory, Oak Ridge, Tenn., September 1996.

2. W. J. McAfee, "Constraint Effects Analytical Development and Validation," in *Heavy-Section Steel Technology Program Semiannual Progress Report for October 1996–March 1997*, NUREG/CR-4219, Vol. 14(1) (ORNL/TM-9593/V14), Oak Ridge National Laboratory, Oak Ridge, Tenn. (1996).

3. T. Ingham, N. Knee, I. Milne and, E. Morland, *Fracture Toughness in the Transition Regime for A533B-1 Steel: Prediction of Large Specimen Results from Specimen Tests*, ND-R-1354(R), Risley Nuclear Power Development Establishment, United Kingdom Atomic Energy Authority, Risley, Warrington, July 1987.

4. M. A. Sokolov, "Statistical Analysis of the ASME K_{IC} Database," *Journal of Pressure Vessel Technology* **120** 24–28 (February 1998).

5. J. D. Landes and D. H. Shaffer, "Statistical Characterization of Fracture in the Transition Region," pp. 368–82 in *Fracture Mechanics: Proceedings of the Twelfth National Symposium on Fracture Mechanics*, ASTM STP 700, American Society for Testing and Materials, Philadelphia, 1980.

6. J. D. Landes and D. E. McCabe, "Effect of Section Size on Transition Temperature Behavior of Structural Steels", pp. 378–92 in *Fracture Mechanics: Fifteenth Symposium*, ASTM STP 833, American Society for Testing and Materials, Philadelphia, 1984.

7. D. E. McCabe, J. G. Merkle, and R. K. Nanstad, "A Perspective on Transition Temperature and K_{JC} Data Characterization," pp. 215–32 in *Fracture Mechanics: Twenty-Fourth Volume*, ASTM STP 1207, ed. John D. Landes, Donald E. McCabe, and J. A. M. Boulet, American Society for Testing and Materials, Philadelphia, 1994.

8. J. A. Joyce, "On The Utilization of High Rate Charpy Test Results and the Master Curve To Obtain Accurate Lower Bound Toughness Predictions in the Ductile-to-Brittle Transition," *Small Specimen Test Techniques*, ASTM STP 1329, ed. W. R. Corwin, S. T. Rosinski, and E. van Walle, American Society for Testing and Materials, 1998.

9. J. M. Barsom and S. T. Rolfe, *Fracture & Fatigue Control in Structures: Applications of Fracture Mechanics*, Second Edition, Prentice-Hall, Englewood Cliffs, New Jersey, 1987.

10. K. Wallin, "Loading Rate Effect on the Master Curve T_0," Document IIW-X-1403-97, International Institute of Welding, VTT Manufacturing Technology, Espoo, Finland, August 1997.

11. K. Wallin, "Irradiation Damage Effects on the Fracture Toughness Transition Curve Shape for Reactor Pressure Vessel Steels," *Int. J. Pres. Ves. & Piping* **55**, 61–79 (1993).

12. J. G. Merkle, "Consideration of Prior Ductile Tearing in Estimating K_{IC} from Small-Specimen Fracture-Toughness Data in the Transition Regime," pp. 57–66 in *Heavy-Section Steel Technology Program Semiannual Progress Report for April–September 1995*, NUREG /CR-4219, Vol. 12(2) (ORNL/TM-9593/V12), Oak Ridge National Laboratory, Oak Ridge, Tenn., January 1997.

13. M. A. Sokolov, K. Wallin and, D. E. McCabe, "Application of Small Specimens to Fracture Mechanics Characterization of Irradiated Pressure Vessel Steels," pp. 263–79 in *Fatigue and Fracture Mechanics,*

28th Volume, ASTM STP 1321, ed. J. H. Undersood, B. D. Macdonald and M. R. Mitchell, American Society for Testing and Materials, 1997.

14. K. Wallin, M. Valo, R. Rintamaa, and R. Ahlstrand, "The Effect of Loading Rate Upon Irradiation Embrittlement Measured by Fracture Mechanical Properties," in *Effects of Radiation on Materials: 16th. International Symposium*, ASTM STP 1175, ed. Arvind. S. Kumar, David S. Gelles, and Randy K. Nanstad, American Society for Testing and Materials, Philadelphia, 1993.

15. M. E. Mayfield, M. G. Vassilaros, E. M. Hackett, M. A. Mitchell, K. R. Wichman, J. R. Strosnider, and L. C. Shao, "Application of Revised Fracture Toughness Curves in Pressure Vessel Integrity Analysis," *Transactions of the 14th International Conference on Structural Mechanics in Reactor Technology (SMIRT)*, Paper G01/2, Lyon, France, August 17–22, 1997.

APPENDIX A

Appendix A

Eleven data sets are presented that give confirming evidence of the shape of the master curve.

T_o temperatures have been determined; these are reported in Chapter 2, Table 2.1. Master curves are plotted with test temperature referenced to T_o on the abscissa. The data points for K_{Jc} on the coordinate axis are, for the most part, median values determined by Weibull fitting data from at least six replicate tests. If the number of replicate tests was less than six, average K_{Jc} values were used.

The dashed horizontal lines cross the master curve at temperature T_o. This line visually separates tests made above temperature T_o from those made below T_o.

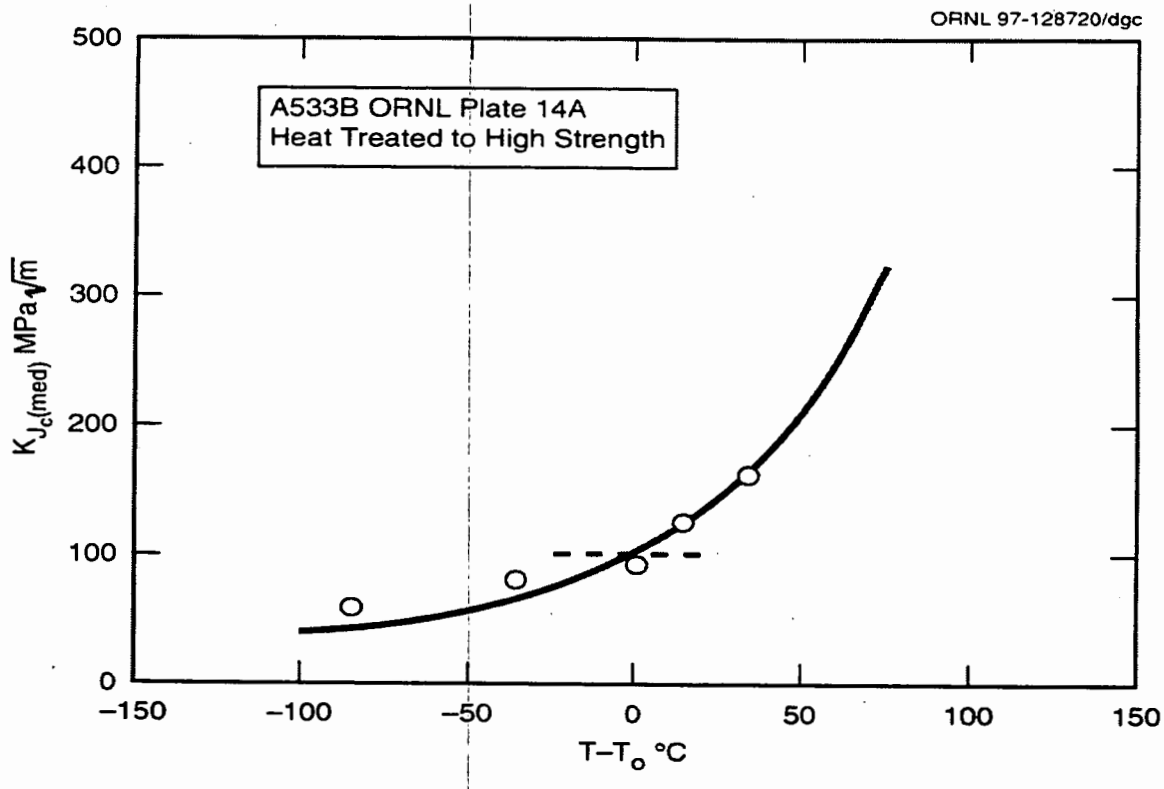

Fig. A.1. ORNL HSST Plate 14A, A 533 grade B (heat treated).

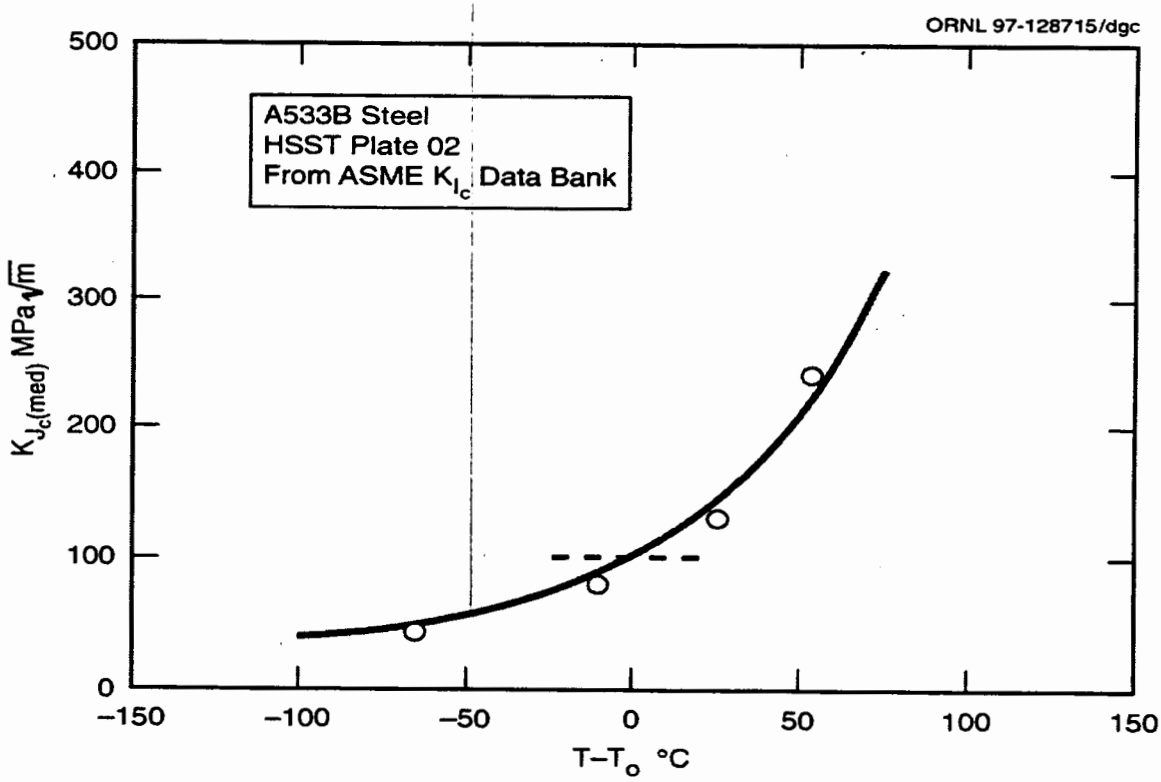

Fig. A.2. ORNL HSST Plate 02, A 533 grade B.

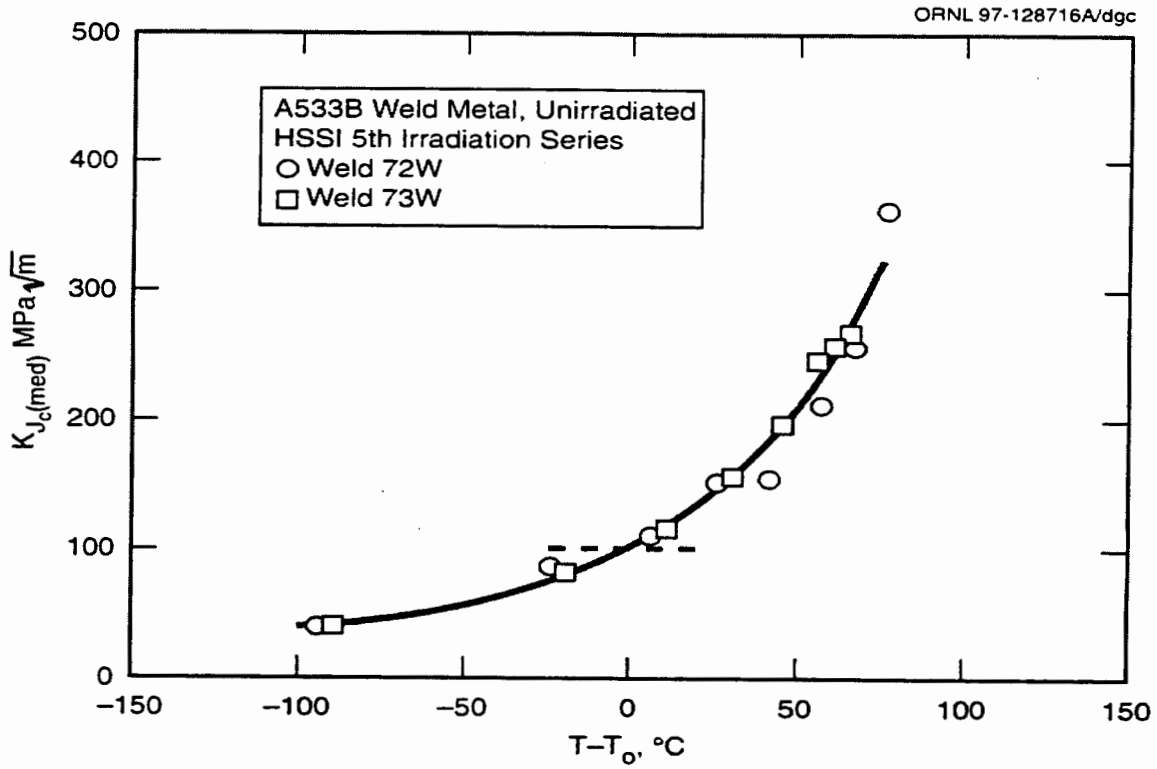

Fig. A.3. ORNL HSSI Fifth Irradiation Series, submerged-arc Welds 72W and 73W.

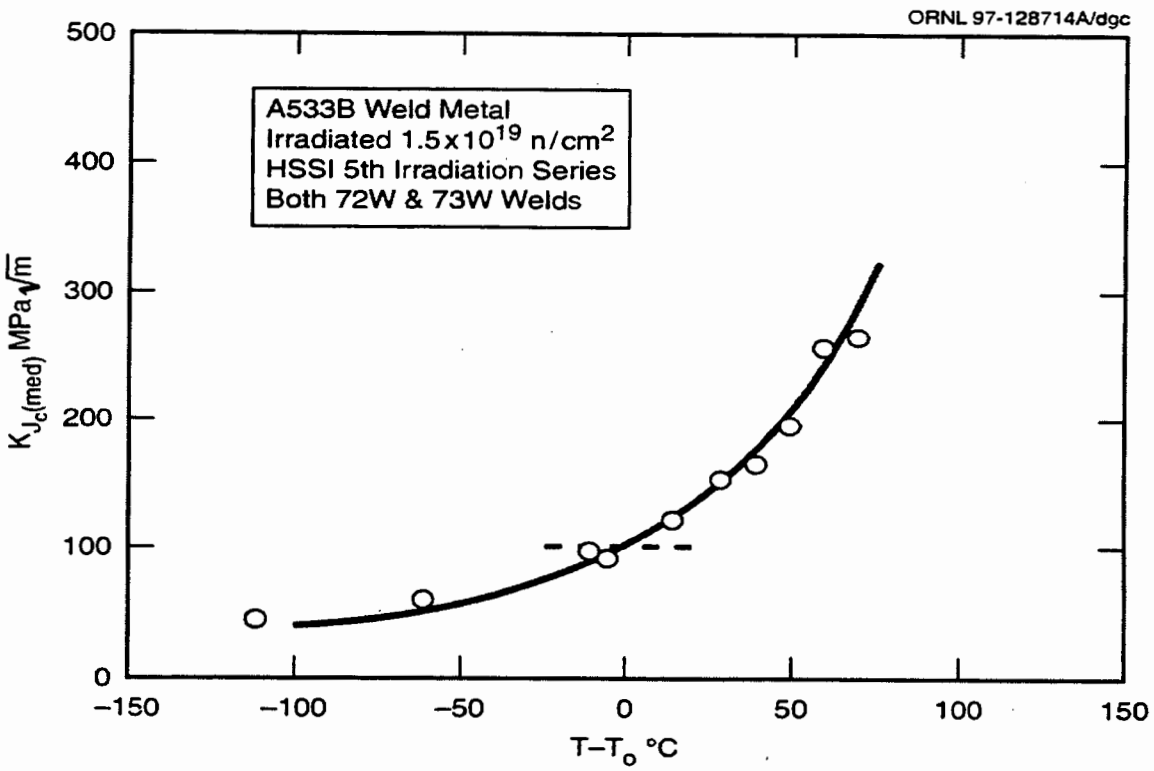

Fig. A.4. ORNL HSSI Fifth Irradiation Series, irradiated submerged-arc Welds 72W and 73W.

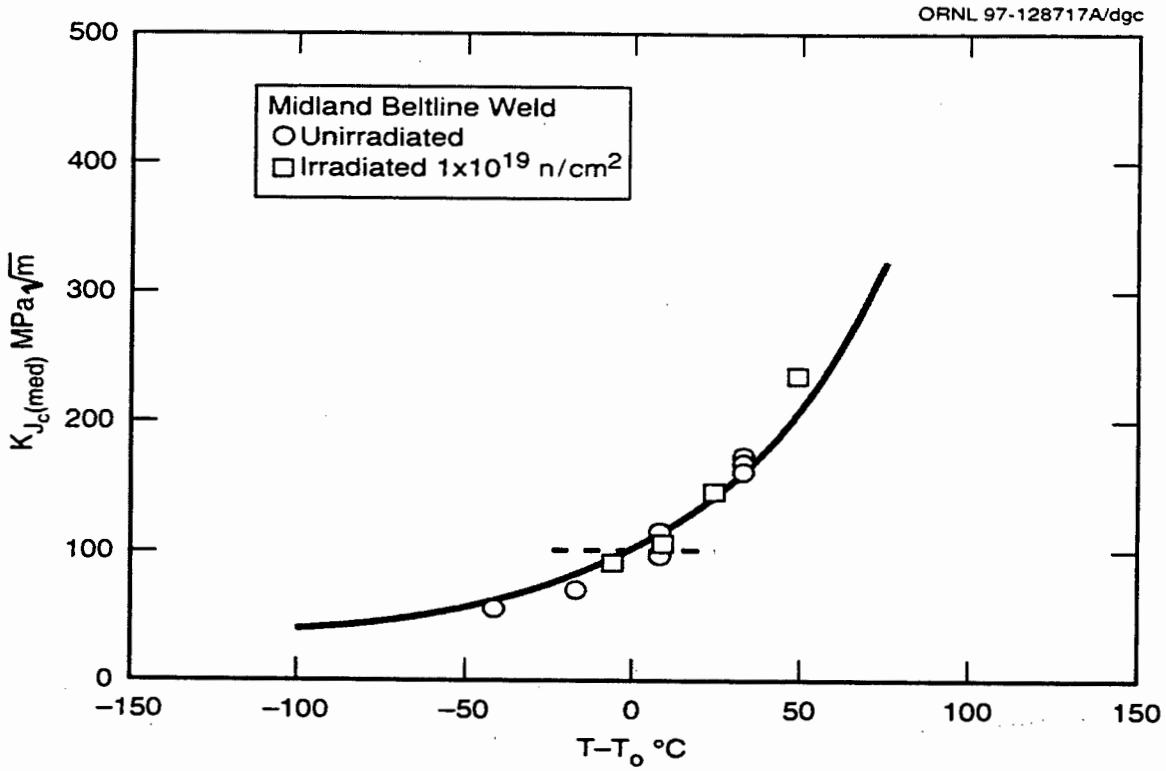

Fig. A.5. ORNL HSSI Tenth Irradiation Series, Weld WF-70 (No. 1) and irradiated WF-70 (No. 1).

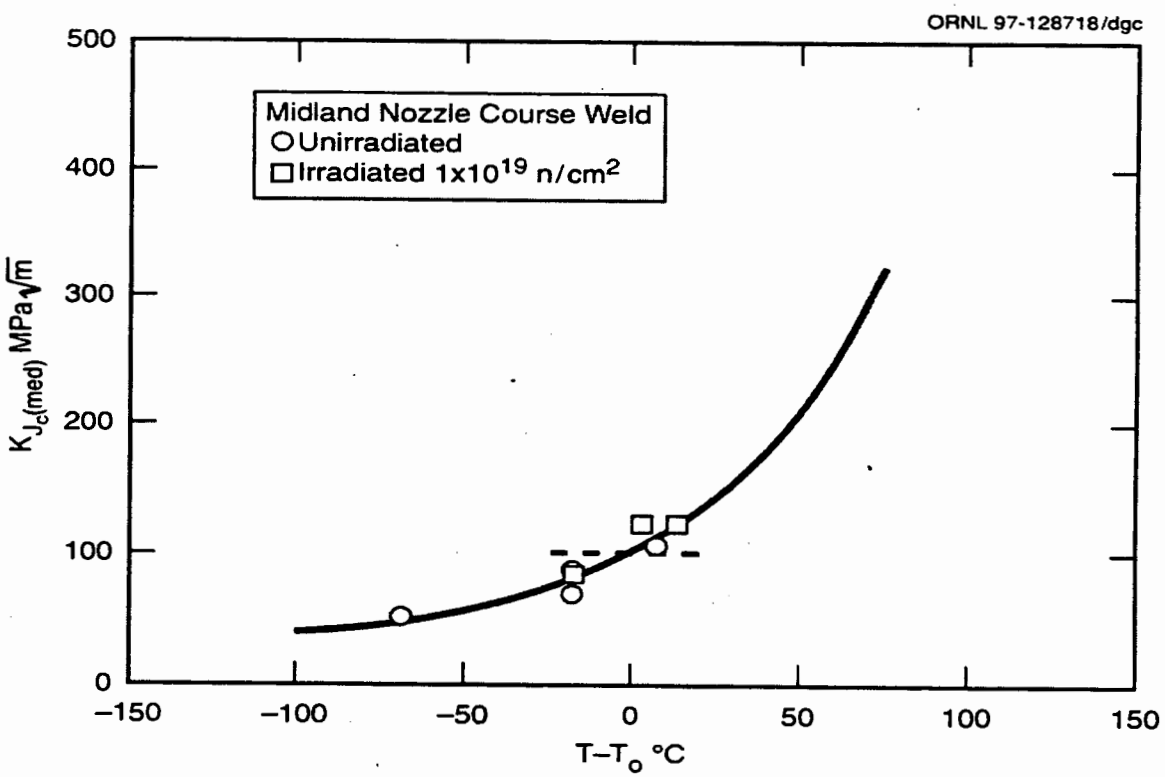

Fig. A.6. ORNL HSSI Tenth Irradiation Series, Weld WF-70 (No. 2) and irradiated WF-70 (No. 2).

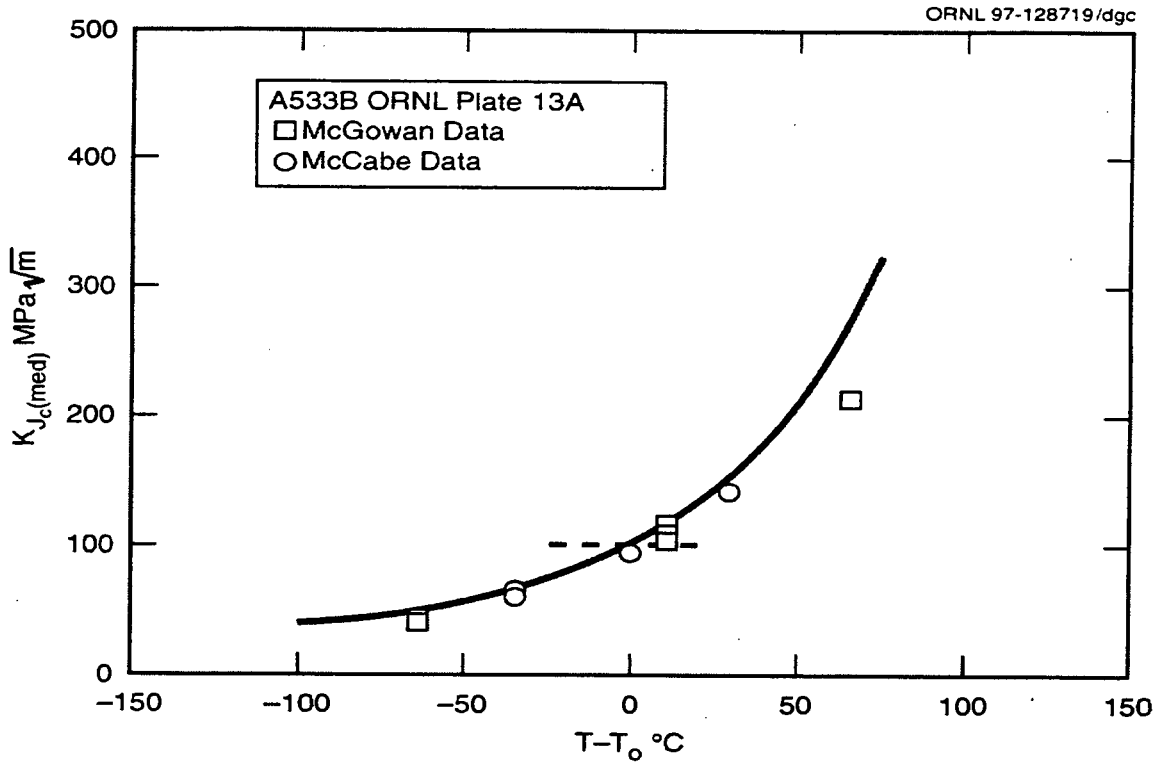

Fig. A.7. ORNL HSST Plate 13A, A 533 grade B.

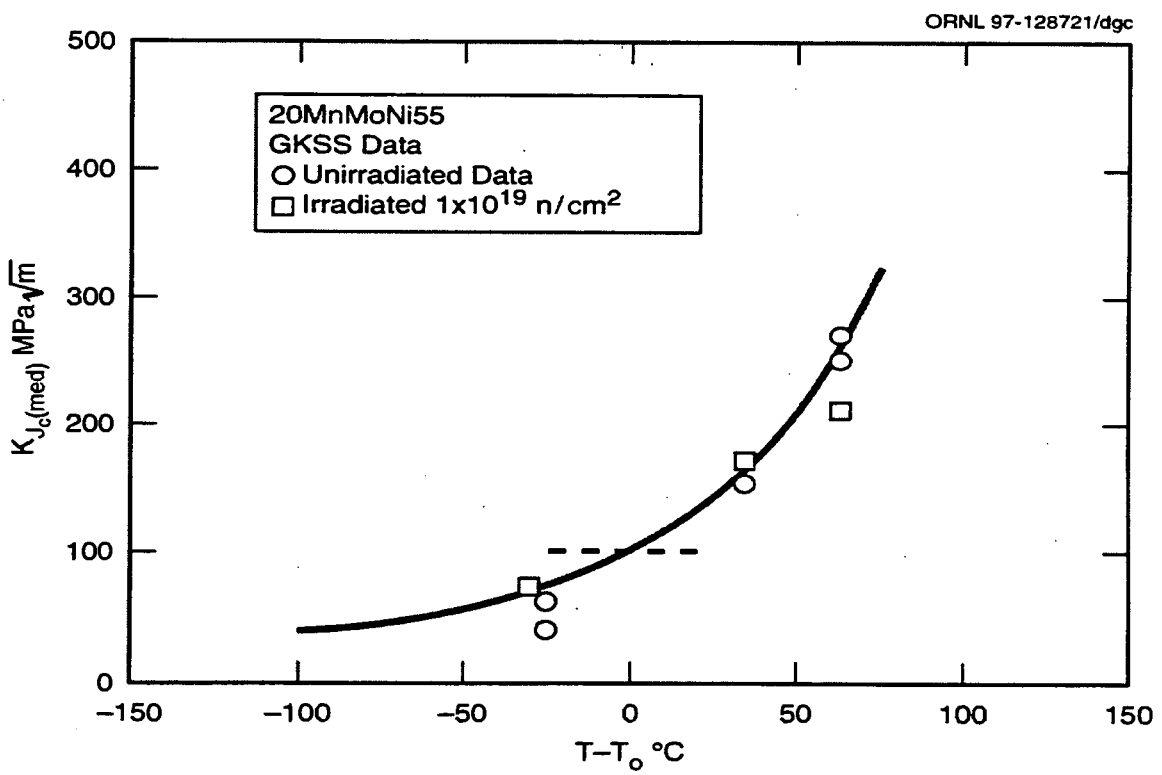

Fig. A.8. GKSS Report 93/E/81, 20MnMoNi55 and irradiated 20MnMoNi55.

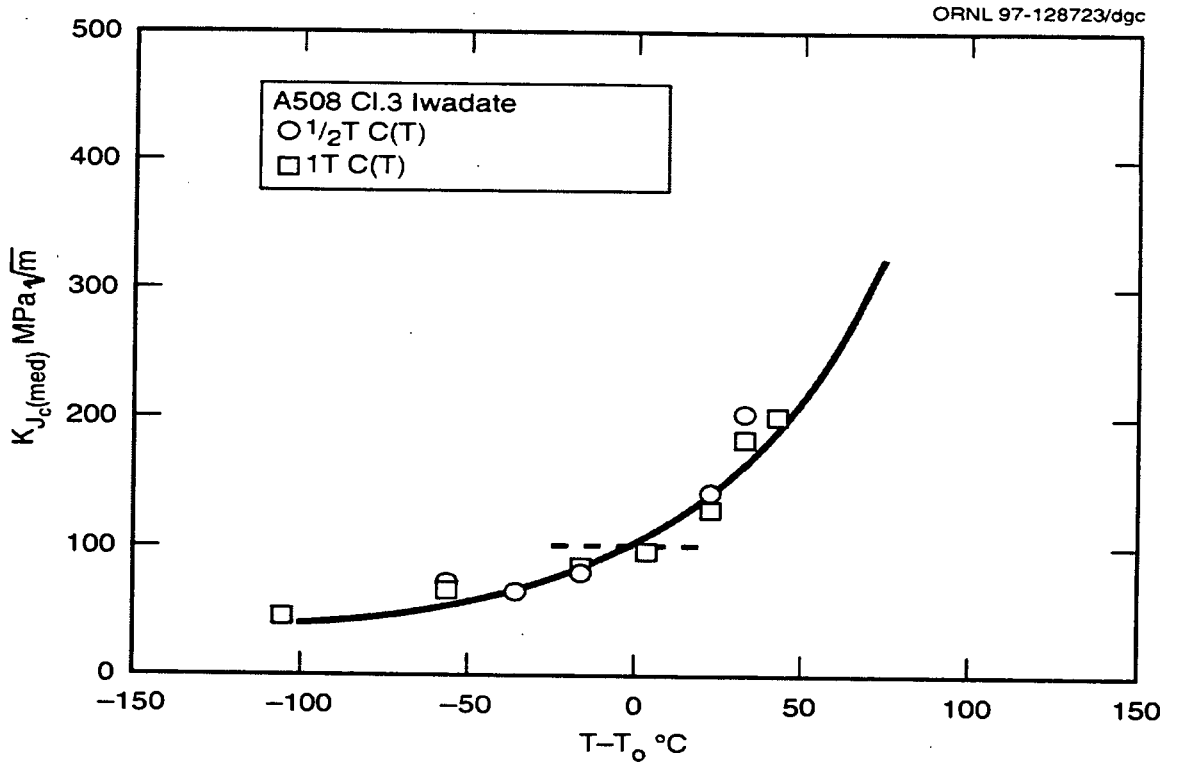

Fig. A.9. Iwadate (ASTM STP 803, Vol. II), A 508 class 3.

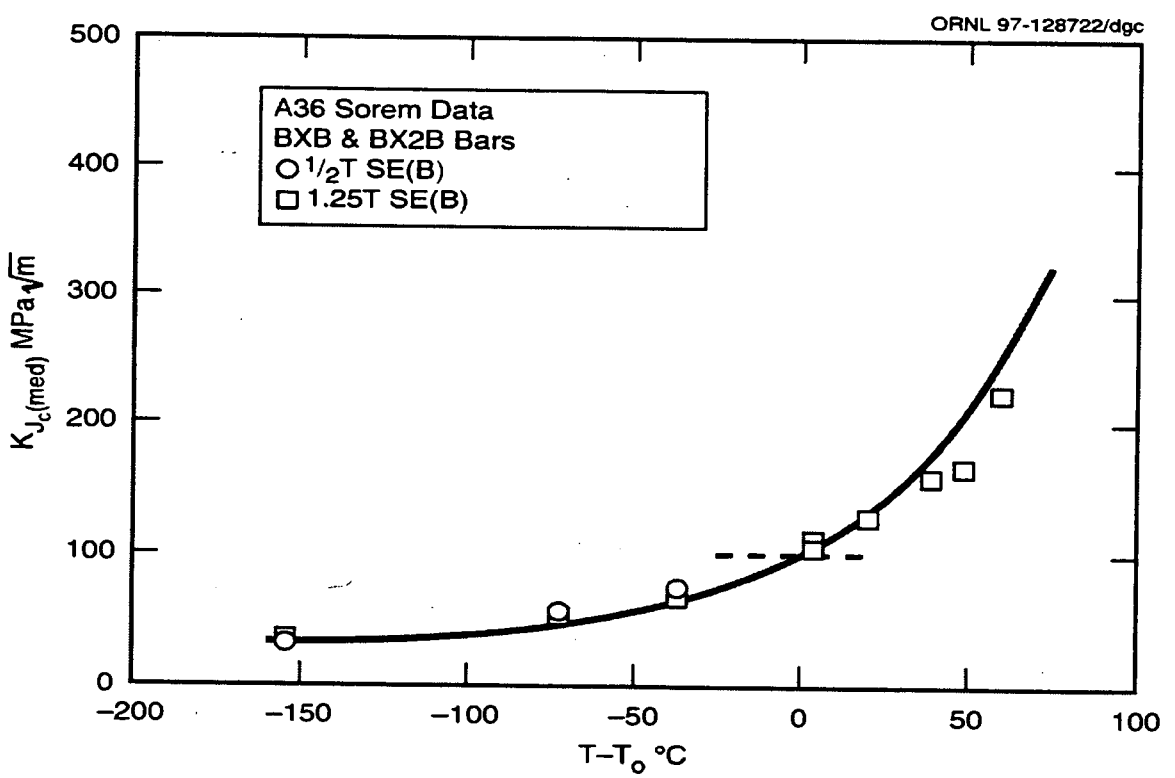

Fig. A.10. Sorem (WRC Bulletin 351), A 36 steel.

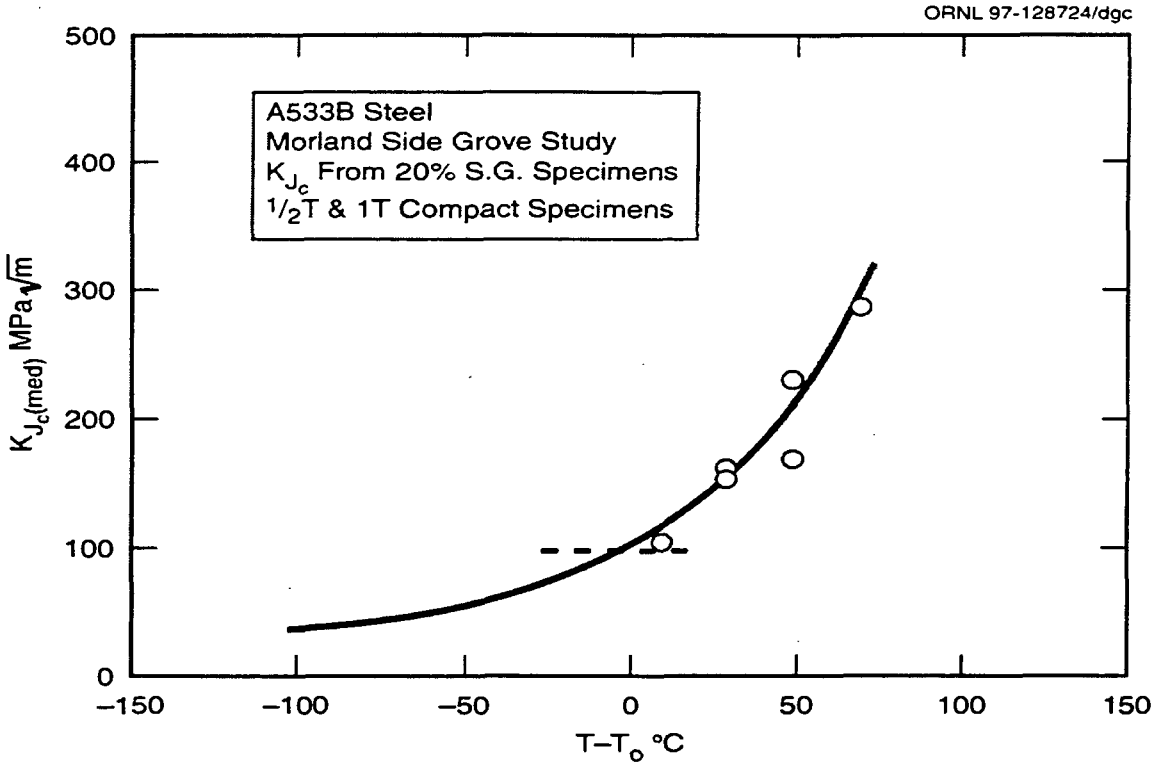

Fig. A.11. Morland [NRL-R-1006(R)], A 533 grade B class 1.

APPENDIX B

Appendix B

B.1 Standard Deviation on K_{Jc} Data

The standard deviation on a known Weibull distribution is a mathematical function of the Weibull slope, $K_{Jc(med)}$, and K_{min}. The following gamma function is used:

$$\sigma = \theta\sqrt{\Gamma(1 + 2/b) - \Gamma^2(1 + 1/b)} , \tag{B.1}$$

where

$$\begin{aligned} b &= \text{Weibull slope,} \\ F(x) &= 1 - e^{-(x/\theta)^b}, \\ \theta &= K_o - K_{min}, \text{ and} \\ &= (K_{Jc(med)} - K_{min})/[\ln(2)]^{1/4}. \end{aligned}$$

For a Weibull slope of four (b = 4),

$$\begin{aligned} \Gamma(1.5) &= 0.88623 , \\ \Gamma^2(1.25) &= 0.82156 , \\ \theta &= (K_{Jc(med)} - K_{min})/[\ln(2)]^{1/4} \end{aligned} \tag{B.2}$$

$$\begin{aligned} \sigma &= 0.2543 \left[\frac{K_{Jc(med)} - K_{min}}{0.9124}\right] \\ &= 0.28\ (K_{Jc(med)} - K_{min}) . \end{aligned} \tag{B.3}$$

Weibull slopes commonly observed in data sets with less than 10 replicates may vary between 2 and 12 and the coefficient in Eq. (B.3) if applied on an individual determination basis could vary between 0.35 to 0.20. Such independent evaluations are not encouraged since population slopes cannot be accurately defined with less than 50 replications.

B.2 Tolerance Bound Determination

Equation (B.3), plus the master curve, and standard normal deviates from statistical tables compiled for normal distributions are employed to develop tolerance bounds on K_{Jc} data.

The lower and upper tolerance bounds (TB) are determined as follows:

$$K_{(TB)} = K_{Jc(med)} \pm \Delta K_{tb} \ , \tag{B.4}$$

where

ΔK_{tb} = $z*\sigma$ (z is the standard normal deviate),

σ = $0.28\ (K_{Jc(med)} - 20)$ MPa√m,

K_{min} = 20 MPa√m.

$$\begin{aligned} K_{(TB)} &= K_{Jc(med)} \pm z*\sigma \ , \\ &= K_{Jc(med)} \pm 0.28z\ (K_{Jc(med)} - 20) \ , \\ &= K_{Jc(med)}\ (1 \pm 0.28z) \pm 5.6z \ . \end{aligned} \tag{B.5}$$

Given:

$$\begin{aligned} K_{Jc(med)} &= 30 + 70\ \exp[0.019(T - T_o)] \\ K_{TB} &= (30 \pm 2.8z) + (70 \pm 19.6z)\ \exp[0.19(T - T_o)]\ \text{MPa}\sqrt{\text{m}} \ . \end{aligned} \tag{B.6}$$

B.3 Lower-Bound $K_{(TB)}$

Let D1 = (30 - 2.8z),

D2 = (70 - 19.6z),

Then K_{TB} = D1 + D2 exp [0.019 (T - T_o)] .

B.4 Upper-Bound $K_{(TB)}$

Let D1 = (30 + 2.8z),

D2 = (70 + 19.6z),

$$K_{TB} = D1 + D2 \exp[0.19(T - T_o)] \text{ MPa}\sqrt{m} . \tag{B.7}$$

Table B.1. Table of coefficients from Eqs. (B.7) and (B.8)

Tolerance bound (%)	Standard normal deviate[a]	D1	D2
1	2.32	23.5	24.5
2	2.05	24.3	29.8
3	1.88	24.7	33.2
4	1.75	25.1	35.7
5	1.64	25.4	37.8
10	1.18	26.7	46.9
90	1.18	33.3	93.1
95	1.64	34.6	102.1
96	1.75	34.9	104.3
97	1.88	35.3	106.8
98	2.05	35.7	110.2
99	2.32	36.5	115.5

[a]One tail of distribution.

B.5 Margin Adjustment

For convenience in the following material, let K_m represent $K_{Jc(med)}$. The master curve is rearranged into the following working form:

$$T_o = T - \frac{1}{0.019} \ln\left[\frac{K_m - 30}{70}\right] . \tag{B.8}$$

Assume an error range on $K_m \pm \Delta K_m$; then

$$T_o = T - \frac{1}{0.019} \ln \left[(K_m \pm \Delta K_m - 30) - \ln 70 \right] . \tag{B.9}$$

For replicate tests at temperature T, ΔT_o is given by

$$\begin{aligned} \Delta T_o &= \frac{1}{0.019} \left[\ln (K_m \pm \Delta K_m - 30) - \ln (K_m - 30) \right] \\ &= \frac{1}{0.019} \ln \left[\frac{(K_m \pm \Delta K_m - 30)}{K_m - 30} \right] . \end{aligned} \tag{B.10}$$

Error in K_m is expressed in units of standard deviation determined from the following:

$$\sigma = \frac{0.28 (K_m - 20)}{\sqrt{N}} . \tag{B.11}$$

Confidence limits are quantified in units of standard deviation using standard normal deviates, z:

$$\Delta K_m = z\sigma = \frac{0.28 z}{\sqrt{N}} (K_m - 20) . \tag{B.12}$$

Let:

$$\lambda_N = \frac{0.28 z}{\sqrt{N}} .$$

Then:

$$\Delta T_o = \frac{1}{0.019} \ln \left[1 \pm \frac{\lambda(1 - 20/K_m)}{(1 - 30/K_m)} \right] . \tag{B.13}$$

Solving Eq. (B.13) for N = 6 and K_m = 100 MPa√m and setting z = 1 produces the standard deviation on T_o; namely ΔT_o = +6.3° and –7.4°C.

Hence, for lower bound:

$$\begin{aligned} \sigma_{To} &= -7.4 = \beta/\sqrt{N} \\ \beta &= 18°C . \end{aligned} \tag{B.14}$$

B.6 Maintaining Equivalent Accuracy in T_o Determinations as Lower-Bound Temperatures are Approached

At T_o temperature, K_m = 100 MPa√m. When T << T_o, how many specimens would be needed to recover equivalent ΔT_o error as otherwise obtained with six specimens at temperature T_o. Let K_m^1 represent the median value at test temperature T. Then establish an equality using Eqs. (B.11) and (B. 13):

$$\lambda_N \frac{(1 - 20/K_m^1)}{(1 - 30/K_m^1)} = \lambda_6 \frac{(1 - 20/100)}{(1 - 30/100)} .$$

$$\sqrt{N} = \sqrt{6} \left[\frac{7}{8} \frac{(K_m^1 - 20)}{(K_m^1 - 30)} \right] . \tag{B.15}$$

Table B.2. Tabulation of modifications for test temperatures that approach lower shelf

Replicates required (N)	N range	Equation (B.16) K_m^I range (MPa√m)	Margin coefficients[a] β in Equation (B.15)
6	6	100	18
7	6.5 to 7.5	83 to 66	18.8
8	7.5 to 8.5	66 to 58	20.1
9	8.5 to 9.5	58 to 53	21.4
10	9.5 to 10.5	53 to 49	22.7

[a]Based on the lowest K_m of the range listed.

B.7 Charpy Specimen Requirements

Because of their small size, Charpy specimens must be tested at temperatures well below temperature T_o. As the lower shelf of fracture toughness is approached, more test specimens are needed to maintain equivalent accuracy. Problems will develop with unknown numbers of test results being declared invalid, causing difficulties in planning test programs. To assist with such problems, a table is given in paragraph 8.5 of the method.

Unpublished results from a Monte Carlo simulation by Ruggeri and Dodds were used to develop part of the tabulated information. The study included predictions of fractional numbers of invalid K_{Jc} data that could result at certain K_m toughness levels. The following parameters apply:

1. Precracked Charpy specimens.
2. $a/W = 0.5$.
3. $\sigma_o/E = 500$ (σ_o = proportional limit stress).
4. $n = 10$ (Ramberg-Osgood hardening exponent).
5. $M = 30$ (validity criterion).

Each Monte Carlo simulation had 10,000 samplings: for sample size ($r = 6$). That is, sampling was continued until six valid K_{Jc} data were obtained.

Table B.3. Precracked Charpy specimen requirements

K_m (MPa√m)[a] (MPa√m)	Test temperature offset $(T_o - T)^{LSV}$	K_m (1T)[b] equivalent by $(T_o - T)$	Average[c] additional data (N - r)	Recommended extra N
73.8	39.9	62.8	0	*d*
82.2	30.1	69.5	0	*d*
91.0	21.5	76.5	0.4	1
99.7	14.2	83.4	1.4	3
108.3	7.9	90.2	3.0	3
116.7	2.4	96.9	5.6	*d*

[a]K_{Jc} obtained from precracked Charpy V-notch specimens before size adjustment.
[b]Calculated from $K_m = 30 + 70 \exp [0.019 (T - T_o)]$.
[c]Average fractional number of invalid K_{Jc} $[N = 6 + (N - r)]$.
[d]Not applicable.

APPENDIX C

Appendix C

Three finite-element-based plastic eta value solutions for the crack mouth position on three-point loaded SE(B) specimens will be presented: (1) Dodds/Nevalainen, (2) Kirk/Dodds, and (3) Electric Power Research Institute (EPRI) Elastic Plastic Handbook (EPRI NP-1931).

C.1 Dodds/Nevalainen

Tabulated values from three-dimensional analysis, SE(B), L = 4W, W/B = 2, a/W = 0.5.

Table C.1. Ramburg Osgood work-hardening exponents, n

n	η_p
5	2.64
10	2.59
20	2.57

C.2 Kirk/Dodds (NUREG/CR-5969)

$$\eta_p = 3.785 - 3.10\,(a/W) + 2.018\,(a/W)^2 \,. \tag{C.1}$$

Two-dimensional finite element. Good for n = 4 to 50 and $0.15 \le a/W \le 0.70$.

C.3 EPRI Elastic Plastic Handbook (EPRI NP-1931)

"Engineering Approach for Elastic-Plastic Fracture Analysis," by Kumar, German, Shih. SE(B), W/B = 2, L = 2W

$$\eta_p = \frac{L}{a}\,\frac{h_1}{h_2}\,\frac{(N+1)}{0.728} = \frac{2}{(a/w)}\,\frac{h_1}{h_2}\,\frac{(N+1)}{0.728} \,.$$

Two-dimensional finite element, N = 1/n.

C.4 Example Comparisons

Table C.2. η_p solutions for a/W = 0.5, W/B = 2
Ramburg Osgood work-hardening exponents, n

Source	Variable n		
	5	10	20
Dodds/Nevalainen	2.64	2.59	2.57
Kirk/Dodds	2.74	2.74	2.74
EPRI Handbook	2.63	2.59	2.59

Table C.3. η_p solutions for n = 10, variable a/W

	0.5	0.625	0.75
Kirk/Dodds	2.74	2.63	2.59
EPRI Handbook	2.59	2.38	2.27

APPENDIX D

APPENDIX D. INTEGRATION OF RESULTS: ESTIMATION OF THE MASTER-CURVE PARAMETERS K_o AND T_o BY THE METHOD OF MAXIMUM LIKELIHOOD

J. G. Merkle

D.1 Introduction

One of the most important aspects of the draft ASTM standard on the fracture toughness of ferritic steels in the transition range is the mathematical basis for calculating the characterizing temperature, T_o. Subject to the assumed accuracy of a semiempirical formula for estimating the cumulative probabilities associated with ordered individual data points, it is possible to use the method of least squares to determine the scale-parameter and median toughness values, K_o and $K_{jc(med)}$, from a linearized cumulative probability plot of data all taken at the same temperature, and to then use the value of $K_{jc(med)}$, to determine T_o. However, an important practical situation likely to arise in the acquisition and interpretation of small-specimen fracture toughness data in the transition temperature range is that of data taken at several different temperatures. Because of the nonlinearity of the master curve as a function of temperature, the method of least squares is not easily applied in this case. Fortunately, an alternative procedure, known as the Method of Maximum Likelihood (MML), is applicable both when data are taken at a single temperature and when they are taken at multiple temperatures. This method does not require the assumption of an auxiliary formula for estimating cumulative probabilities, but instead uses the equation of the postulated probability density curve, applied to a discrete variable with arbitrarily small intervals, to construct an expression for the joint probability of occurrence of exactly the combination of values actually measured. This expression is known as the Likelihood Function. The logarithm of the Likelihood Function is a sum of logarithms, and setting its partial derivative, with respect to the parameter of interest, equal to zero produces an equation for the parameter being sought. Equations for the maximum likelihood estimators (MLEs), for both single and multi-temperature data, have been published by Wallin.[1] However, no derivation was published by Wallin for the case of multi-temperature data and, mainly for this reason, the MML procedure for multi-temperature data is presently not included in the draft standard. However, following unpublished notes received from Wallin,[a] the MML equation for T_o for multi-temperature data has been rederived at ORNL, thus clearing the way, in terms of theory, for this case to be added to the draft standard. Because this addition would be a major

[a]K. Wallin, "Derivation of Maximum Likelihood (MML) Algorithm for Wallin/Master Curve," unpublished notes received from K. Wallin on March 27, 1995.

change to the draft standard, which is now close to its initial acceptance as a standard, it is planned to propose the addition of the multi-temperature MML procedure after the initial acceptance of the present draft standard.

D.2 Concept of the Likelihood Function

If values of x are drawn at random from an infinitely large true population, it is well known that a definite cumulative probability, P(x), is associated with each value of x, giving the fraction of all values of x which are equal to or less than a particular value. It is also well known that there is no such thing as the probability of obtaining exactly a given value of x. However, this problem can be circumvented by returning to the concept of a frequency histogram, to which the curve of the probability density function, f(x), which equals dP(x)/dx, is fit. The histogram defines the fraction of all numbers expected to fall within given arbitrarily small ranges of the stated variable, or within given joint sets of ranges of multiple variables. Thus the probability of a value of x falling within the range between x and x + dx is f(x) dx. The above reasoning can be extended one step farther to consider the probability of a set of physically independent events occurring together. Such a joint probability is the product of the individual probabilities of each of the events occurring separately. Thus the joint probability of obtaining a particular set of N values of x, each within its individual interval dx, is

$$P_J = [f(x_1)dx]\ [f(x_2)dx].....[f(x_N)dx]\ . \tag{D.1}$$

The joint-probability function defined by Eq. (D.1) is called the Likelihood Function, L. Thus,

$$L \equiv P_J\ . \tag{D.2}$$

Frequently, the expression for L is written in compact notation, by using the symbol $\prod_{i=1}^{N}$, which means, "the product of all factors of the form.....". Thus,

$$L = \prod_{i=1}^{N} f(x_i)\ . \tag{D.3}$$

D.3 DETERMINATION OF K_O FOR TESTS PERFORMED ALL AT THE SAME TEMPERATURE

The three-parameter Weibull cumulative probability function is

$$P = 1 - e^{-\left(\frac{x}{\alpha}\right)^{\beta}} , \tag{D.4}$$

where

$$x = K_i - K_{min} , \tag{D.5}$$

$$\alpha = K_o - K_{min} , \tag{D.6}$$

and, for the case of toughness data in the transition range,

$$\beta = 4 . \tag{D.7}$$

The probability density function is given by

$$f(x) = \frac{dP}{dx} = \frac{\beta x^{\beta-1}}{\alpha^{\beta}} e^{-\left(\frac{x}{\alpha}\right)^{\beta}} , \tag{D.8}$$

so that, from Eq. (D.3), the Likelihood Function is

$$L = \prod_{i=1}^{N} \left(\beta x_i^{\beta-1}\right) \alpha^{-\beta} e^{-\left(\frac{x_i}{\alpha}\right)^{\beta}} . \tag{D.9}$$

Since the first factor in parenthesis in Eq. (D.9) is not a function of α, setting

$$\frac{\partial \ln L}{\partial \alpha} = 0 \tag{D.10}$$

gives

$$\sum_{i=1}^{N} \left[-\frac{\beta}{\alpha} + \beta x_i^{\beta} \alpha^{-(\beta+1)} \right] = 0 . \tag{D.11}$$

Eq. (D.11) can be rewritten as

$$-N \beta \alpha^{-1} + \sum_{i=1}^{N} \beta x_i^{\beta} \alpha^{-(\beta+1)} = 0 . \tag{D.12}$$

which, by rearrangement and the use of Eqs. (D.5) through (D.7), leads to

$$K_o = \left[\frac{\sum_{i=1}^{N} (K_i - K_{min})^4}{N} \right]^{1/4} + K_{min} . \tag{D.13}$$

Equation (D.13) is the equation for K_o presently appearing in the draft standard, except for the relatively small bias correction subtracted from the denominator of the term in brackets in the draft standard, by replacing N with (N – 0.3068).

D.4 DETERMINATION OF T_O FOR TESTS PERFORMED AT MULTIPLE TEMPERATURES

For tests performed at multiple temperatures, K_o and therefore α become functions of temperature, making it necessary to define the unknown quantity for this case as T_o. By the chain rule, and using Eq. (D.6),

$$\frac{\partial \ln L}{\partial T_o} = \frac{\partial \ln L}{\partial \alpha} \cdot \frac{\partial K_o}{\partial T_o} = 0 \ . \tag{D.14}$$

The cumulative probability corresponding to K_{med} is 1/2, using Eqs. (D.4) through (D.7) gives

$$K_o = \frac{K_{med} - K_{min}}{(\ln 2)^{1/4}} + K_{min} \ . \tag{D.15}$$

Therefore, by using the equation of the master curve, which is

$$K_{med} = 30 + 70\ e^{0.019(T-T_o)} \ , \tag{D.16}$$

Eq. (D.15) becomes

$$K_o = a + be^{c(T-T_o)} \ , \tag{D.17}$$

where, for

$$K_{min} = 20 \text{ MPa} \sqrt{m} \ , \tag{D.18}$$

a, b, and c are given by

$$a = \frac{10}{(\ln 2)^{1/4}} + 20 = 31 \text{MPa} \sqrt{m} \ , \tag{D.19}$$

$$b = \frac{70}{(\ln 2)^{1/4}} = 77 \text{MPa} \sqrt{m} \ , \tag{D.20}$$

and

$$c = 0.019\ ^{\circ}C^{-1}\ . \tag{D.21}$$

For multi-temperature testing, the frequency distribution of the true population of toughness data is three-dimensional, with every cross section of the distribution perpendicular to the temperature axis having the shape of the three-parameter Weibull probability density function. Since the volume of every slice through the distribution of thickness dT is the same, the fraction of data contained in every slice of thickness dT is dT/T_{RANGE}, where T_{RANGE} is the range of temperatures over which data are taken. Therefore,

$$L = \prod_{i=1}^{N} \left(\beta x_i^{\beta-1} \frac{dT}{T_{RANGE}} \right) \alpha^{-\beta}\, e^{-\left(\frac{x_i}{\alpha}\right)^{\beta}}\ , \tag{D.22}$$

in which the first term in parenthesis is not a function of T_o. Therefore, applying Eq. (D.14), in which, from Eq. (D.17),

$$\frac{\partial K_o}{\partial T_o} = -bce^{c(T-T_o)}\ , \tag{D.23}$$

gives

$$\frac{\partial \ln L}{\partial T_o} = \sum_{i=1}^{N} -\left[-\frac{\beta}{\alpha_i} + \beta x_i^{\beta} \alpha_i^{-(\beta+1)} \right] bce^{c(T-T_o)} = 0\ . \tag{D.24}$$

By rearrangement and by using Eqs. (D.5), (D.6), (D.7), and (D.17), Eq. (D.24) becomes

$$\sum_{i=1}^{N} \left\{ \frac{e^{c(T_i-T_o)}}{a + be^{c(T_i-T_o)} - K_{min}} - \frac{(K_i - K_{min})^4 e^{c(T_i-T_o)}}{\left[a + be^{c(T_i-T_o)} - K_{min}\right]^5} \right\} = 0\ , \tag{D.25}$$

which agrees with ref. 1 for cases not involving censoring. Eq. (D.25) must be solved iteratively to determine T_o.

D.5 REFERENCE

1. K. Wallin, "Validity of Small Specimen Fracture Toughness Estimates Neglecting Constraint Corrections," pp. 519–37 in *Constraint Effects in Fracture, Theory and Applications: Second Volume*, ASTM STP 1244, ed. Mark Kirk and Al Bakker, American Society For Testing and Materials, Philadelphia, 1995.

NRC FORM 335 (2-89) NRCM 1102, 3201, 3202

U.S. NUCLEAR REGULATORY COMMISSION

BIBLIOGRAPHIC DATA SHEET

(See instructions on the reverse)

1. REPORT NUMBER (Assigned by NRC, Add Vol., Supp., Rev., and Addendum Numbers, if any.)

NUREG/CR-5504
ORNL/TM-13631

2. TITLE AND SUBTITLE

Technical Basis for an ASTM Standard on Determining the Reference Temperature, T_o, for Ferritic Steels in the Transition Range

3. DATE REPORT PUBLISHED

MONTH	YEAR
November	1998

4. FIN OR GRANT NUMBER

B0119

5. AUTHOR(S)

J.G. Merkle, K. Wallin, D.E. McCabe

6. TYPE OF REPORT

Technical

7. PERIOD COVERED *(Inclusive Dates)*

8. PERFORMING ORGANIZATION - NAME AND ADDRESS *(If NRC, provide Division, Office or Region, U.S. Nuclear Regulatory Commission, and mailing address; if contractor, provide name and mailing address.)*

Oak Ridge National Laboratory
Oak Ridge, TN 37831-6151

9. SPONSORING ORGANIZATION - NAME AND ADDRESS *(If NRC, type "Same as above"; if contractor, provide NRC Division, Office or Region, U.S. Nuclear Regulatory Commission, and mailing address.)*

Division of Engineering Technology
Office of Nuclear Regulatory Research
U.S. Nuclear Regulatory Research
Washington, DC 20555-0001

10. SUPPLEMENTARY NOTES

S.N. Malik, NRC Project Manager

11. ABSTRACT *(200 words or less)*

This report provides both the theoretical basis and supporting data development that has made possible the development of the American Society for Testing and Materials (ASTM) E 1921-97, Test Method for the Determination of Reference Temperature, T_o, for Ferritic Steels in the Transition Range. The background theory, using a weakest-link model to explain why fracture toughness data for ferritic steels have rather substantial data scatter when tested in the transition range, is developed. Justification is provided for the use of a three parameter Weilbull model to represent the observed data scatter. Development of the master curve concept keyed to the scale parameter of the three-parameter Weilbull model, K_{02} is described. The rationale is presented that explains why the master curve shape tends to be relatively independent of material strength; and as such, behaves as a universal curve for a wide range of steels and covers material-hardening mechanisms. The rational used to arrive at certain test practice requirements are described. T_o reference temperatures are determined for 26 steels of varying types and conditions of embrittlement.

12. KEY WORDS/DESCRIPTORS *(List words or phrases that will assist researchers in locating the report.)*

Fracture toughness, testing, transition range, data scatter, master curve, T_o, Weibull model

13. AVAILABILITY STATEMENT

unlimited

14. SECURITY CLASSIFICATION

(This Page)

unclassified

(This Report)

unclassified

15. NUMBER OF PAGES

16. PRICE